Universidad Autónoma de Madrid

Departamento de Bioquímica

Sequential Notch activation regulates ventricular chamber development

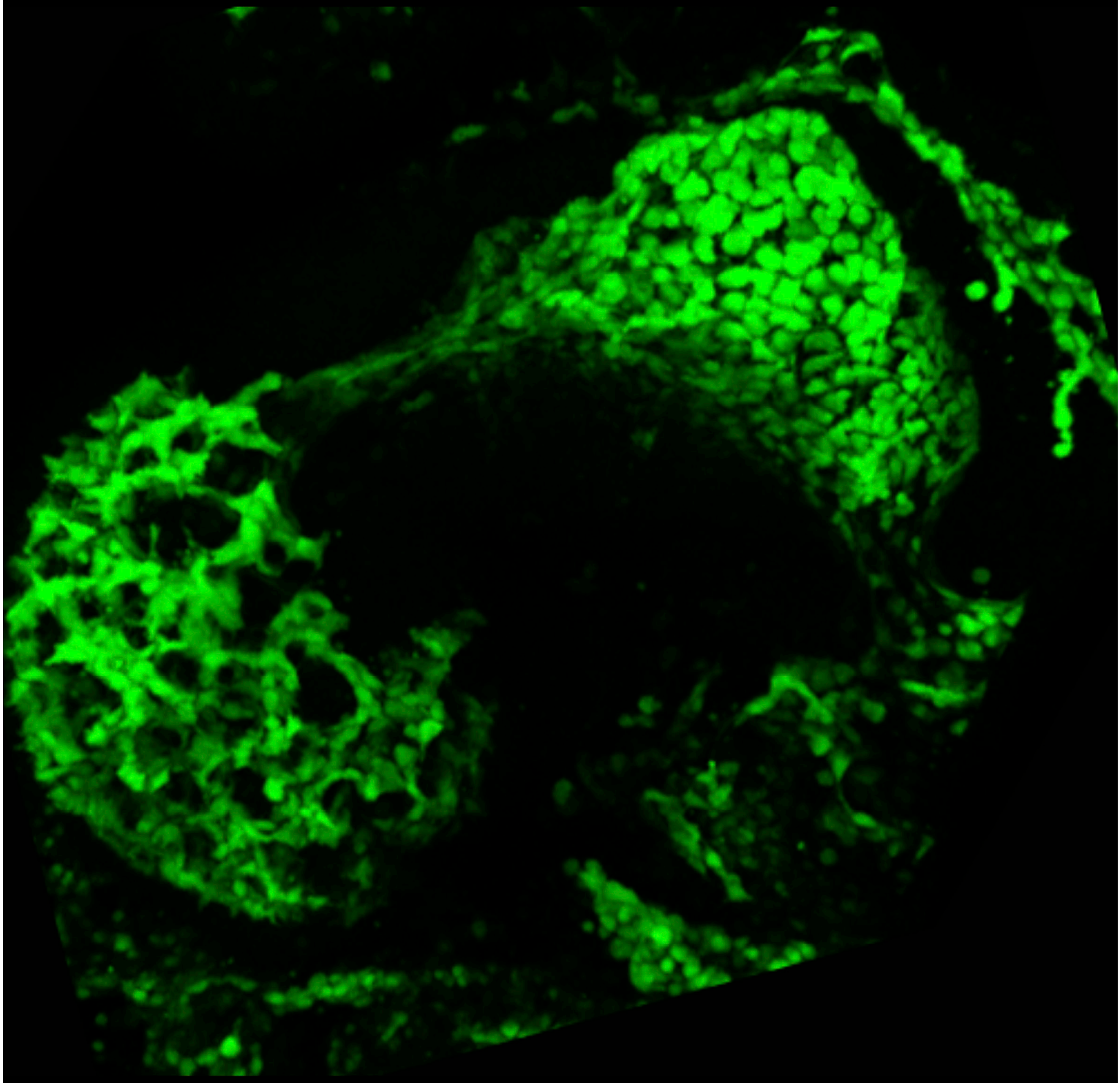

Gaetano D'Amato

Madrid, 2015

Departamento de Bioquímica

Facultad de Medicina

Universidad Autónoma de Madrid

Sequential Notch activation regulates ventricular chamber development

Doctoral thesis

Gaetano D'Amato

Graduated in Biology

Madrid, 2015

Director: José Luis de la Pompa Mínguez

Centro Nacional de Investigaciones Cardiovasculares (CNIC)

Alla mia famiglia

“Volli, e volli sempre, e fortissimamente volli”

Vittorio Alfieri

This work was performed in Dr. José Luis de la Pompa´s laboratory in the Cardiovascular Developmental Biology and Repair Department at the Centro Nacional de Investigaciones Cardiovasculares (CNIC) in Madrid.

This study was funded by grants SAF2010-17555, SAF2013-45543-R, RD12/0042/0005 (RIC) and RD12/0019/0003 (TERCEL) from the Spanish Ministry of Economy and Competitiveness (MINECO), grant FP7-ITN 215761 (NotchIT) from the European Commission and a grant from the BBVA Foundation for Research in Biomedicine (2014)

Gaetano D'Amato holds a PhD fellowship linked to grant FP7-ITN 215761 (NotchIT).

ACKNOWLEDGMENT

Acknowledgments

Antes de una "*lectio magistralis*" sobre el fabuloso mundo de Notch y desarrollo del corazón, quiero dar las gracias a todas las personas que me han apoyando de manera incondicionada en estos últimos años. Ante todo quisiera agradecer a José Luis de la Pompa: my mentor. Por haber confiado en mi dándome la oportunidad de desarrollar mi proyecto de tesis en su laboratorio. En todos estos años su apoyo y su ayuda han sido constantes. A él debo todos mis logros profesionales y en mis etapas futuras siempre llevaré conmigo sus enseñanzas: mejorarse siempre y ser prácticos. De momento estos consejos los estoy aplicando con gran éxito al golf, ¡espero conseguirlos también en la ciencia!

Un ringraziamoento speciale a Paolo Sordino. Capo e amico durante l'indimentcabile anno trascorso nel suo laboratorio presso Napoli. Di lui ricorderó sempre la sua capacitá di trasmettermi la passione per questo lavaro e i suoi valorosi consigli. Grazie per aver creduto in me aiutandomi ad ottenere ciò che piú desideravo.

Quiero agradecer a todos mis compañeros de la factoría de la Pompa, nuevos y antiguos. Desde el momento que pisé el CNIC me habéis hecho sentir parte de este grupo. Al Dott. Luna, el hombre que transformó un ventrículo en un canal, el hombre que me enseñó todos los trucos de las ISH y de la movida madrileña, a Alvarete el biólogo super-cool!, a Gonzalito para haber tenido mucha paciencia conmigo y por haberme enseñado todos los secretos de las IHC. Muchas gracias a Jesusito, fantástico compañero de bench, a Guillermino, el mago de Illustrator, siempre disponible para ayudarme o tomarse una buena cerveza. Gracias a Bea por su total implicación en enseñarme todos los truquillos de las células, a Belenuccia y sus protocolos, a la que he recurrido en cada momento difícil y que me alegra cada mañana invitándome a un buen café. Gracias a Meri y Mauro por haber aguantado todas mis tonterías y por ser tan "fashion", a Vane, la filósofa del grupo que se apunta también un bombardeo, a Patty por haberme ayudado muchísimo en las gestiones de mis ratoncitos y por compartir conmigo los "gossip" del CNIC. Gracias a Dimitri(os) por "obligarme" a practicar el inglés, a super Lao y Marcos, por avisarme de todas las new entries del CNIC, a Paula y sus colores, a Saretta por sus fantásticas PCR y a Abelón por ser tan paciente conmigo y mis "cruces", a mis niños Rebuccuccia y Álex "el cachas". Un gracias especial a Tania, por tener que aguantarme cada día a su lado, por compartir conmigo sus proyectos y por su English revision. A Juli, desde el día que me rescató en el aeropuerto hasta a los últimos días de mi tesis. Jamás olvidaré sus consejos o sus citas (7:27 am en el hall del hotel). Sin duda alguna la pre-doc mas rigurosa y talentosa que he conocido en mi vida. Todo un ejemplo a seguir. Muchísimas gracias al "Prof." Donal Macgrogan (Donnie) por animar nuestros lab-meeting con toda su sabiduría, por darme siempre buenos consejos no solo científicos, por confiar en mi demostrándose un verdadero amigo.

I would also like to thank all the collaborators that made this work possible. Anna-Katerina Hadjantonakis from the Sloan-Kettering Institute in New York, Matthew S. Bochter and Susan Cole from Ohio State University in Columubus, Akiyoshi Uemura and Y. Fukushima Nagoya City University in Nagoya. Un agradecimiento especial a Luis J. Jiménez-Borreguero y su grupo del CNIC por haberme ayudado muchísimo con las imágenes y con los análisis en los experimentos de ecocardiografía, a Jesús Ruíz-Cabello y a su grupo con los experimentos de NMR. Muchísimas gracias a Carlos Torroja por su completa disponibilidad y profesionalidad a la hora de analizar "unos cuantos" RNAseq y a Fernando Martinez por su excelente trabajo *in silico* y por las estimulantes conversaciones sobre la bioquímica de Notch. Gracias a Roisin Doohan por sus sabios consejos de histopatología, al grupo de genómica y de microscopía y Beatriz Ferreiro por su increíble profesionalidad gestionando nuestros papeleos.

Agradezco a toda la 3 norte por haber aguantado mis gritos y mis tonterías desde el primer día que entré en el CNIC. Ha sido un sitio fantástico en el que trabajar, compartiendo protocolos, truquillos experimentales y muchas risas. A Teresuccia Casaseca capaz de regalarme una sonrisa en los momentos más duros. A los " Beneditos" con lo que compartimos una "pasión" en común , a Paco, a Nines y a la hora del café. Un gracias muy especial a la Doctora Cañón demostrándose una verdadera amiga en la que siempre podré confiar.

Sono quasi sei anni che ho lasciato la mia Salerno, i miei cari amici e soprattutto la mia amata famiglia. Senza l'appoggio incondizionato dei miei genitori, il raggiungimento di tale traguardo sarebbe stato oltremodo impossibile. Sono stati un esempio costante durante tutta la mia vita, insegnandomi che i sacrifici e l'impegno sempre pagano. A loro devo tutto e in ogni momento della mia vita sarò loro riconoscente. Un grazie speciale a mia sorella, sempre al mio fianco, aiutandomi in ogni istante della mia vita e a Peppe per avermi regalato due incredibili gioielli: il piccolo Ale e la piccolissima Ginevra. Mi mancate tanto.

En ces dernières années de thèse plus que laborieuses, il y a cette personne qui parmi toutes m'a toujours épaulé et ce de manière inconditionnelle. Milles merci à toi Laurane pour avoir été si patiente et compréhensive pendant cette étape de ma vie, pour avoir eu foi en moi et cru en mes efforts. J'espère pouvoir rattraper aussitôt que possible tout ce temps que je n'ai pu passer à tes côtés et rattraper ces weekends passés loin de toi. Ce que je désire maintenant plus que tout au monde et qui me donne énormément de force aujourd'hui c'est de savoir qu'une nouvelle page de ma vie s'ouvre dans laquelle tu seras à mes côtés.

SUMMARY/ RESUMEN

Ventricular chamber morphogenesis is a beautiful example of tissue interactions orchestrating a precise gene regulatory network essential for tissue patterning, cellular proliferation and differentiation that ultimately lead to a fully compacted and functional adult ventricle.

The Notch signaling pathway is a crucial regulator of the processes leading to the adult ventricular chamber: trabeculation, coronary vessel formation and trabecular compaction. Its alteration may lead to disease in the form of cardiomyopathy. Despite its pivotal role, the exact mechanisms that regulate endocardial-endothelial Notch activity during chamber development remain unclear.

In this work, using loss- and gain-of-function mouse models of different Notch elements we have tried to shed light on the spatio-temporal activation of endocardial Notch1 during ventricular morphogenesis.

We found that in the early mouse ventricle the glycosyltransferase Manic Fringe favors the Dll4-Notch1 signaling in the endocardium that is essential for trabeculation. The functional relationship between the Fringe-modified Notch receptor and its ligand Dll4 was also observed during coronary vessel formation. In this tissue, the Dll4-Fringe-Notch signaling axis is necessary for triggering Notch activity in the endothelium of developing coronary vessels. In endocardial cells, at later stages of chamber development, Manic Fringe and Dll4 expression is down-regulated allowing myocardial Jag1 and Jag2 signaling to Notch1 throughout the ventricular endocardium and leading to a fully compacted heart. Forced expression of Manic Fringe in the endocardium disrupts chamber maturation and compaction, causing a phenotype reminiscent of LVNC, presumably by blocking Jag1 and Jag2 signaling to Notch1. In the absence of Manic Fringe, Dll4, Jag1 and Jag2 activate Notch to similar levels, whereas in the presence of Manic Fringe, Dll4 becomes a superactivator.

Comparative transcriptome profiling revealed Gpr126 as a crucial Notch-dependent signal that connects chamber endocardium and myocardium, sustaining cardiomyocyte proliferation, trabeculation, ventricular patterning and compaction. Further analysis showed that the Jag1 and Jag2 ligands from the myocardium play a non-redundant role in activating Notch1 during chamber compaction and maturation.

The post-translational modifications on the Notch1 receptor mediated by Manic Fringe, in combination with the differential expression patterns of the ligands Dll4, Jag1 and Jag2 determine a spatio-temporal specificity of endocardial Notch1. Perturbation of this signaling equilibrium severely disrupts heart chamber formation.

El desarrollo de los ventrículos en el corazón es un claro ejemplo de interacción entre distintos tejidos. Esta interacción requiere una regulación génica precisa y indispensable para los procesos de proliferación y diferenciación celular y la formación del patrón tisular que finalmente darán lugar a la formación de un ventrículo compacto y completamente funcional.

La vía de señalización Notch juega un papel fundamental en la regulación de los procesos que conducen al desarrollo de la pared ventricular en el corazón adulto: la trabeculación, la formación de los vasos coronarios y la compactación de las trabéculas. La alteración de la correcta activación de la vía produce diferentes cardiomiopatías. A pesar de este papel fundamental, los mecanismos moleculares que regulan la actividad de Notch en el endocardio y en el endotelio coronario durante el desarrollo de la cámaras siguen siendo desconocidos.

En este trabajo, utilizando modelos murinos de perdida y ganancia de función de los distintos elementos de la vía de señalización de Notch, hemos estudiado la activación espacio-temporal de Notch1 durante la morfogénesis ventricular.

Observamos que en el comienzo del desarrollo ventricular, la glicosiltransferasa Manic Fringe favorece la interacción entre el ligando Dll4 y el receptor Notch1 en el endocardio. La actividad de Notch1 es fundamental en el proceso de trabeculación. Esta misma señalización, Dll4-Notch1, se requiere para la formación de los vasos coronarios. En el endotelio coronario, Dll4 interactúa y activa al receptor Notch previamente modificado por Fringe. En las células del endocardio, en etapas posteriores del desarrollo de las cámaras, la expresión de *Manic Fringe* y de *Dll4* se reduce drásticamente. Esto permite a los ligandos expresados en el miocardio, Jag1 y Jag2, activar a Notch1 en todo el endocardio ventricular. La actividad de Notch1 mediada por Jag1 y Jag2 es necesaria para el proceso de compactación trabecular. La expresión ectópica de Manic Fringe en el endocardio durante el proceso de compactación produce un fenotipo similar a la miocardiopatía no compactada. Presumiblemente esto se deba a que se bloquea la activación de Notch1 por parte de Jag1 y Jag2. En ausencia de Manic Fringe, Dll4, Jag1 y Jag2 activan Notch de manera similar, mientras que en presencia de Manic Fringe, Dll4 es en un superactivator de Notch.

El análisis del transcriptoma, comparando los distintos mutantes de la vía de Notch, revela que Gpr126 es una diana directa de la vía con un papel crucial en la comunicación entre el encocardio y el miocardio, manteniendo la proliferación de los cardiomiocitos, la trabeculación, determinación del patrón ventricular y compactación. La comparación del transcriptoma de los ratones con perdida de función de Jag1 y Jag2 revela que estos dos ligandos desempeñan funciones no redundantes durante la maduración y compactación de los ventrículos.

Las modificaciones post-traduccionales del receptor Notch1 mediadas por Manic Fringe, en combinación con los diferentes patrones de expresión de los ligandos Dll4 , Jag1 y Jag2 determinan una especificidad espacio-temporal de la actividad del receptor Notch1. La perturbación de este

equilibrio de señalización desde el endocardio y el miocardio perjudica gravemente el desarrollo de las cámaras cardíacas.

Index of contents

Index of figures, tables and videos

Figures

Tables

Supplementary Videos and RNA-seq data are provided in the digital format of the thesis.

Abbreviations

ALGS: Alagille syndrome

ASD: Atrial Septal defect

AVC: Atrio-Ventricular Canal

BAEC: Bovine aortic endothelial cells

BIFC: Bimolecular fluorescence complementation

bHLH: basic-Helix-Loop_Helix

Bmp: Bone morphogenetic protein

CADASIL: Cerebral autosomal dominant arteriophaty with subcortical infarcts and leukoencephalopathy

CBF1: Cp-binding factor 1

CBFRE: CBF (see RBPJK) responsive element

CNC: Cardiac Neural Crest

CR: Cystein-rich domain

CSL: CBF1/Su(H)/Lag-1

Dll4: Delta-like 1/4

Deltex: RING-domain E3 ubiquitin ligasa

DSL: Delta/Serrate/Lin12 domain

DREG: See Gpr126

EGF: Epidermal Growth Factor

EMT: Ephitelial-to mesenchyme transition

EPDC: Epicardial Derived Cells

FHF: First heart field

Gpr126: G protein-coupled receptor 126

HAS2: hyaluronic acid synthetase 2 (HAS2)

HD: Hetero-dimerization Domain

HES: Hairy/Enhancer of split

Hey: Hairy Related genes

HUVEC: Human umbilical vein endothelial cell

IHC: Immunohistochemistry

ISH: *In situ* Hybridization

Ivs: Interventricular septum

Jag1: Jagged1

LFng: Lunatic-Fringe

LNR: Lin/Notch repeats

La: Left atria

Lv: Left ventricle

LVNC: Left Ventricular Non Compaction

LVOT:

Mam: Mastermind

MFng: Manic-Fringe

MF20: Sarcomeric myosin

MEVEC: Mouse embryonic ventricular endocardial cells

Mib1: Mind bomb-1

NECD: Notch Extracellular Domain

Neu: Neuralized

NICD: Notch Intracellular Domain

NLS: Nuclear localization signal

Nrg1: Neuregulin-1

OFT: Outflow tract

PEST: Proline, glutamic acid, serine and treonined enriched-domain

POFUT-1: Protein O-Fucosyltransferase 1

PTA: Persistent truncus arteriosus

qPCR: Quantitative RT-PCR

Ra: Right atria

RBPJ: Recombination Signal-Binding Protein 1 for J-Kappa sequence (CBF1 in mammals)

RBPJKO: Recombination Signal-Binding Protein 1 for J-Kappa mutant

RFng: Radical-Fringe

Rv: Right ventricle

SHF: Secondary Heart Field

SMC: Smooth muscle cell

SMRT: Silencing Mediator of Retinoic and Thyroid hormone receptors

TAD: Transcriptional activation domain

Tgfβ: Transforming Growth Factor-β

TOF: Tetralogy of Fallot

VEGF: Vascular Endothelial Growth Factor

VEGFR2: Vascular Endothelial Growth Factor Receptor 2 (Flk-1)

VSD: Ventricular septal defect

WISH: Whole mount *in situ* hybridization

WT: Wild type

SMA: α-Smooth muscle actin

SU(H): Suppressor of Hairless

SV40: Simian vacuolating virus 40

INTRODUCTION

Heart development

In vertebrates, the heart is the first organ to form during embryogenesis. It arises through a complex series of morphogenetic interactions involving cells from several embryonic origins (Buckingham, Meilhac et al., 2005, Moorman & Christoffels, 2003).

Cardiac progenitors derive from the mesoderm, which emerges from the primitive streak during gastrulation (Buckingham et al., 2005). At E7.0 in mouse embryos (Fig. 1a), in response to endodermal signals, the cardiac precursors start to migrate in an anterior-lateral direction forming a crescent in the cephalo-medial region (de la Pompa & Epstein, 2012, Moorman & Christoffels, 2003). This crescent contains two populations of progenitors: the first heart field (FHF) and the second heart filed (SHF, Fig. 1b). At E8.0 the precardiac cells from the FHF fuse at the midline of the embryo building the primitive heart (Xin, Olson et al., 2013): an endothelial tube surrounded by a single layer of myocardial cells (High & Epstein, 2008). Extracellular matrix, termed cardiac jelly, separates the two layers (Fig. 1c). Subsequently, the primitive heart tube grows by addition of a second group of progenitors that migrate anteriorly (arterial pole) and posteriorly (venous pole) contributing to the future outflow tract (OFT), the right ventricle and portions of the atria (Kelly, Brown et al., 2001, Zaffran, Kelly et al., 2004). Simultaneously, the heart tube undergoes a characteristic rightward looping (R-loop, Fig. 1d). This morphogenetic process changes the initial antero-posterior axis of the primitive heart to a left-right orientation (Moorman & Christoffels, 2003).

During cardiac looping, in defined regions of the myocardium, a specific gene expression program will determine the myocardium of the future chambers (Christoffels, Hoogaars et al., 2004). Just after looping, this myocardium expands and forms the primitive ventricles and atria. As soon as the chamber myocardium is formed, it differentiates in two distinct layers: an outer compact zone and an inner trabecular zone (Sedmera, Pexieder et al., 2000). In the remaining myocardium the T-box family genes *Tbx2* and *Tbx3* repress the chamber-specific genetic program (Christoffels et al., 2004), forming the myocardium of the atrio-ventricular canal (AVC) and the OFT. This non-chamber myocardium is an important source of signals for the adjacent endocardium. Endocardial cells receiving signals from the overlying myocardium undergo an epithelial-to-mesenchyme transition (EMT) forming the endocardial cushions, primordia of the cardiac valves (Eisenberg & Markwald, 1995). In addition, this process contributes to completing the septation of the heart. The E9.5 heart consists of four anatomically and molecularly distinct regions, the atrium, AVC, OFT and ventricle (Fig. 1e), covered by a single layer of epicardial cells. The epicardium develops from a transient structure, the proepicardium, a group of coelomic progenitors located at the venous pole of the embryonic heart (Perez-Pomares & de la Pompa, 2011). Once the epicardial cells have covered the ventricle, the AVC and the OFT, they undergo EMT, forming the epicardial-derived cells (EPDCs).

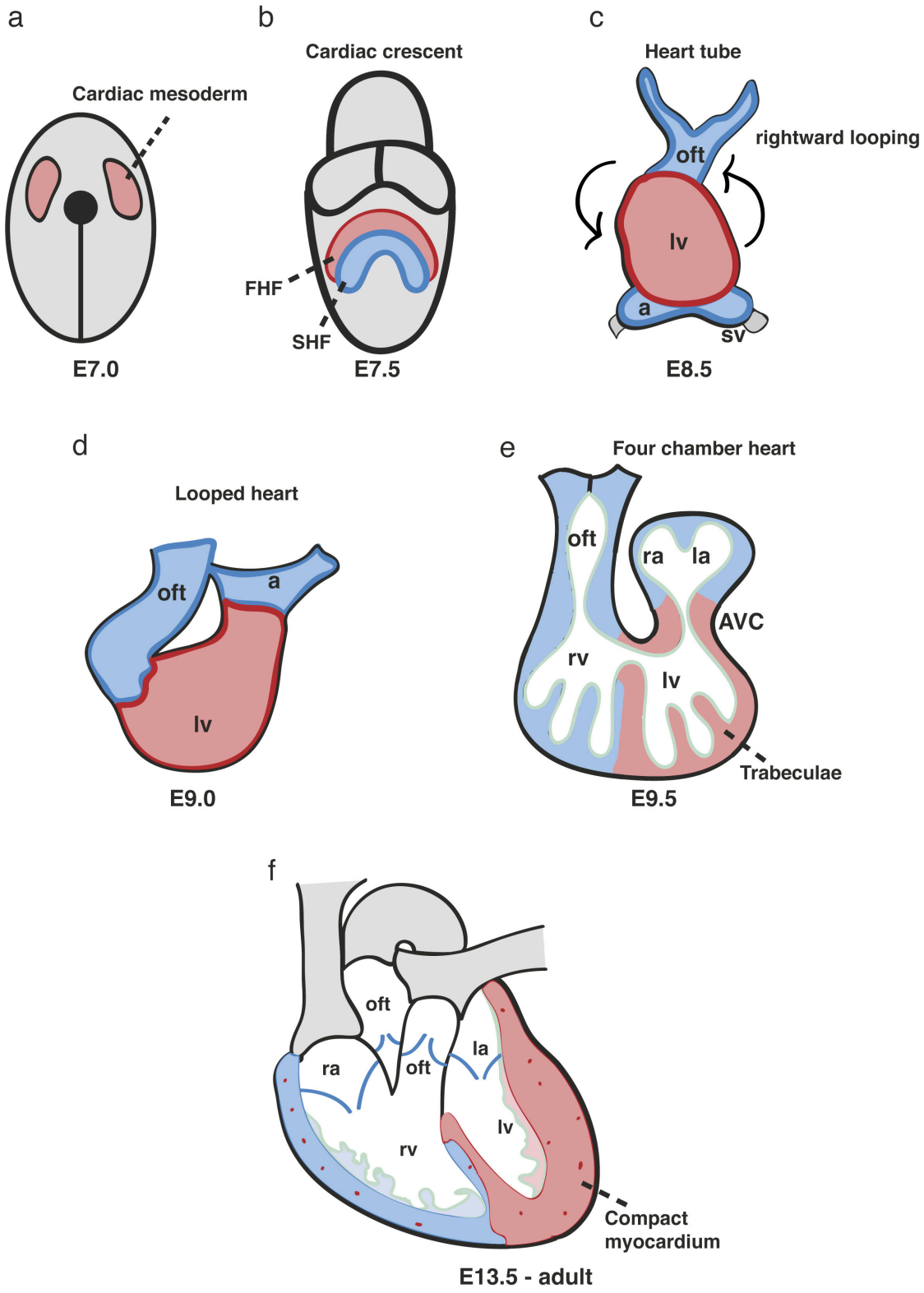

EPDCs invade the sub-epicardium space between myocardium and epicardium and later, they will give rise to different cell types including cardiac fibroblasts, vascular smooth muscle cells (Mikawa & Gourdie, 1996) and a subset of coronary endothelial cells (Perez-Pomares, Carmona et al., 2002).

Figure 1. Heart development.
Ventral view of the developing mouse embryo. At E7.0 (**a**), cardiac progenitors (red) migrate to the center of the embryo to form the cardiac crescent (**b**). At E7.5, two cardiac fields can be distinguished: the first heart field (FHF; red) and the second heart field (SHF; blue) (b). At E8.0-E8.5, the cardiac tube consists of two layers: endocardium and myocardium (**c**). At this stage the heart undergoes a characteristic R-loop to form a looped heart (**d**). Transversal section depicting an E9.5 heart (**e**), which consists of four anatomically distinct regions: atrium, atrioventricular canal (AVC), ventricle and outflow tract (OFT). In the developing ventricle, endocardial cells (green line) delineate the ventricular myocardium (**e**). Longitudinal section of an E13.5 heart. At this stage valve primordia (shown in blue) are remodelled and trabeculae undergo compaction. In the maturing ventricular wall, coronary vessels start to appear (red dots, **f**).

Myocardium, endocardium and epicardium, interacting with each other, generate signals necessary for the proliferation and differentiation of the developing heart (de la Pompa & Epstein, 2012). At E13.5 the main structures of the heart are already formed. Ultimately, via complex morphogenetic processes, these structures are remodelled leading to a fully mature heart.

Endocardium-myocardium crosstalk during early heart development

Formation of the AVC valves starts at E9.0 (Fig. 1e). In this region, non-chamber myocardium emits signals that instruct the adjacent endocardium to undergo EMT. This process will give rise to the endocardial cushions, a structure composed of mesenchymal cells derived by EMT from the overlying endocardium. The OFT cushions develop one day later. Similar to the AVC, the endocardium of the OFT undergoes EMT. In addition, mesenchymal cells derived from migrating cardiac neural crest (CNC) cells contribute to the formation of these cushions (de Lange, Moorman et al., 2004). Valve morphogenesis involves proliferation of the cushion mesenchyme, followed by elongation and remodelling of the valves to form mature, thin, valve leaflets with a characteristic trilaminar structure.

At the molecular level, the key events in the EMT process are the down-regulation of intercellular adhesion junctions within the local endocardium and concomitant expression of EMT-inducing transcription factors in the forming mesenchymal cells (Timmerman, Grego-Bessa et al., 2004). Many signaling pathways have been described as crucial for the initiation of EMT, among them, Tgfβ and Bmp. *Bmp2* is expressed in the myocardium and its deletion completely blocks EMT in the endocardium of the prevalvular region (Ma, Lu et al., 2005, Rivera-Feliciano & Tabin, 2006). Moreover, genetic deletion of the Bmp type 1A receptor, *Bmpr1a*, in the endocardium also results in failed cushion formation, indicating that Bmp2 signals directly to the cushion-forming endocardium to induce EMT (Ma et al., 2005).

The cardiac jelly also plays a pivotal role during EMT. In fact, the absence of hyaluronic acid (HA), a major component of endocardial cushion extracellular matrix (ECM), impairs EMT. HA is synthesized by hyaluronic acid synthetase 2 (HAS2). *Has2* null embryos fail to undergo cushion

EMT, a defect that is rescued in explant cultures by addition of exogenous HA (Camenisch, Spicer et al., 2000). In addition to the myocardium, the endocardial cells are also an important source of signals during EMT (de la Pompa & Epstein, 2012).

The ErbB receptors are critical for heart and valve development and for adult heart function. ErbB2, and ErbB3 are expressed in the endocardium of the developing cushions at the onset of EMT (Camenisch, Schroeder et al., 2002). In *ErbB2*$^{-/-}$ or *ErbB3*$^{-/-}$ null mutants, cushion mesenchymal cells do not form in the heart *in vivo* or in explant cultures *in vitro*. In the endocardium, the Notch signaling pathway is also crucial for the initiation of EMT (Timmerman et al., 2004);(Luna-Zurita, Prados et al., 2010, Wang, Wu et al., 2013). In this tissue, Notch1 promotes the expression of *Snail1* that normally represses vascular endothelial cadherin (*Cdh5*). Abrogation of Notch signaling disrupts EMT due to down-regulation of *Snail1* (Timmerman et al., 2004).

Similarly to cushion EMT, the endocardium-myocardium crosstalk is also essential for the progression of trabeculation in chamber myocardium (Fig. 1e). Cardiac trabeculation is a morphogenetic process by which clusters of ventricular cardiomyocytes extrude and expand into the cardiac jelly to form sheet-like projections (Sedmera et al., 2000). The endocardial cells overlie the growing trabecular myocardium but are separated from it by cardiac jelly. The trabeculae increase the myocardial mass and facilitate oxygen and nutrient exchange in the heart muscle prior to coronary vascularization (Sedmera et al., 2000). These myocardial protrusions are present in all vertebrates and their formation constitutes the first step in chamber development for which endocardial-myocardial signaling is a prerequisite. Although the process of trabeculation is highly conserved (Brutsaert, 2003), the first event by which cardiomyocytes extend into the luminal part of the ventricle remains largely unknown**.** 3D analysis of cell polarity markers in fixed and immunostained mouse embryos reveals that very few cells divide in parallel to the trabeculae. The majority of the cells, deeper or on the luminal side, tend to divide parallel to the heart surface (Le Garrec, Ragni et al., 2013). In contrast, in zebrafish embryos, trabeculation occurs via a process of delamination (Staudt, Liu et al., 2014). Using 3D time-lapse imaging of beating zebrafish hearts, it has been shown that cardiomyocytes constrict their abluminal surface and enter in the trabecular layer. The neighboring cardiomyocytes move into the space left behind to maintain a cohesive compact layer (Staudt et al., 2014).

One of the first evidence that highlighted the existence of an intimate link between endocardium and myocardium was a study performed in the *cloche* mutant zebrafish embryos. In these mutants that lack the inner endocardial tube, the developing outer myocardial layer remains somewhat smaller and dysmorphic and fails to develop trabeculation within the ventricle (Liao, Bisgrove et al., 1997, Stainier, Weinstein et al., 1995). Myocardial VEGF and its receptor VEGFR-2 (Flk-1) represent another excellent example of a signaling pathway connecting endocardium and

myocardium that is required for the initiation of trabeculation. *Flk-1* is expressed at an early stage in all endothelial cells, including the endocardium. As in the *cloche* mutant zebrafish embryo, targeted inactivation of *Flk-1* in the mouse also resulted in the absence of endocardial endothelium, with subsequent failure of myocardial trabeculation (Shalaby, Rossant et al., 1995). In the developing heart, the ligand VEGF is expressed in trabecular cardiomyocytes (Miquerol, Gertsenstein et al., 1999, Sugishita, Takahashi et al., 2000). VEGF binding to its receptor is required for initial differentiation and proliferation of endocardial endothelium, as demonstrated more recently using the *Collagen2a1-Cre* driver. Heterozygous *VEGF-A* conditional mutant embryos died at E10.5 and showed dramatic decrease in the thickness of the myocardium as well as impaired trabeculation (Haigh, Gerber et al., 2000).

As previously described for the EMT in the AVC region, Neuregulin-ErbB signaling is also necessary for the initiation of trabeculation. *Neuregulin1* expression is confined to the endocardial cells. It is secreted from the endocardium and it works as a paracrine factor signaling to ErbB2 and ErbB4 receptors, expressed in nearby cardiomyocytes. Activation of the ErbB2/ErbB4 receptor complex by neuregulin1 is required for trabeculation of the primitive heart. Mutant embryos lacking any of these three genes do not form trabeculae and die *in utero* at an early stage (Kramer, Bucay et al., 1996, Lee, Simon et al., 1995, Meyer & Birchmeier, 1995). During trabeculation, paracrine factors have to traverse the cardiac jelly separating the endocardium and myocardium. Interestingly, both endocardial Neuregulin and myocardial VEGF signals are modified by extracellular matrix components (Camenisch et al., 2002).

The formation of cardiac jelly results critical for appropriate receiption of signals between ventricular myocardium and endocardium not only during EMT, as described before, but also for trabeculation. In agreement with this, *Has2* or *Versican* null mutants do not develop trabeculae (Camenisch et al., 2000, Mjaatvedt, Yamamura et al., 1998). The pivotal role of the cardiac jelly during chamber morphogenesis was recently described by use of conditional endocardial *Brg*1 mutant embryos. Brg1, a chromatin remodeling protein, blocks endocardial expression of *Adamts1*, a secreted matrix metalloproteinase. In E9.5 *Brg1* mutants, de-repressed expression of *Adamts1* induces early extracellular matrix degradation and trabeculation is abrogated. In physiological conditions, as development proceeds, the metalloproteinase starts to be expressed in the endocardium in order to break down cardiac jelly and prevent excessive trabeculation (Stankunas, Hang et al., 2008). This study highlights how the cardiac jelly plays an essential role during the initiation of trabeculation, while at later stages its degradation is required for the compaction of the trabeculae, a morphogenetic process that stars at around E14.5 in the mouse embryo.

Chamber compaction

At later stages of chamber development, as ventricular volume increase, trabeculae become compressed within the ventricular wall resulting in significant increase of proportion and thickness of the compact myocardium. In this process, termed compaction, the majority of trabeculae have become compacted by E14.5 in the mouse contributing to the formation of a thicker, compact ventricular wall (Sedmera et al., 2000). Just after the formation of primitive trabecular ridges, the myocardium undergoes extensive expansion by recruiting cardiomyocytes from the myocardial wall into the trabecular ridges as well as, via cellular proliferation within the trabecular cardiomyocytes. The cellular recruitment mechanism forces the outer myocardial layer to proliferate more than the trabecular myocardium. Such a gradient of proliferation has been recently demonstrated by quantitative 3D proliferation analysis (de Boer, van den Berg et al., 2012). This gradient increases during chamber development reaching its maximum at E13.5, when proliferation within the trabecular cardiomyocytes ceases.

As the myocardium grows and the trabeculae are compacting, a hypoxic environment facilitates the invasion of coronary vessels in the outer myocardial layer. The origin of coronary endothelium is controversial. Chick-quail chimera experiments (Perez-Pomares et al., 2002) and more recently lineage-tracing approaches (Red-Horse, Ueno et al., 2010, Tian, Hu et al., 2013, Wu, Zhang et al., 2012) indicate that different cell types contribute to the assembly of mature vascular coronary endothelium. Despite the controversy in the matter of coronary vessel formation, their function in the heart is very well known. Myocardial growth requires enhanced oxygen delivery triggering an influx of endothelial cells that undergo vasculogenesis to form a capillary plexus (Mikawa & Fischman, 1992). A fully compacted and irrigated ventricular wall is the result of complex morphogenetic processes that come to completion just after birth. Reduced vasculogenesis as well as defects in trabecular remodeling (compaction) during ventricular wall formation, are the causes of different types of human cardiomyopathies such a Left Ventricular Non Compaction (LVNC, OMIM 601493).

Left Ventricular Non Compaction

LVNC is a cardiomyopathy of poorly understood etiology that is characterized by prominent and excessive trabeculation with deep recesses in the ventricular wall (Jenni, Oechslin et al., 2007). It is a cardiomyopathy with developmental bases, caused by the intrauterine arrest of myocardial morphogenesis that leads to the presence of persistent trabeculae (Ritter, Oechslin et al., 1997). The first case of LVNC was diagnosed in 1984, in a 33-year old woman assessed by echocardiography (Engberding & Bender, 1984). LVNC is the third most common cardiomyopathy after dilated and

hypertrophic cardiomyopathy, and its prevalence ranges from 0.05% to 0.3% of the general population (Oechslin, Attenhofer Jost et al., 2000, Ritter et al., 1997, Stollberger & Finsterer, 2004). Although LVNC can manifest as depressed systolic function (Captur & Nihoyannopoulos, 2010), its clinical manifestation and the age of the affected individual at symptom onset are highly variable. Classical complications include systemic embolism, malignant arrhythmias, heart failure and sudden death (Oechslin et al., 2000). LVNC is generally associated to mutations in genes encoding mainly structural proteins of the muscle fibres (Klaassen, Probst et al., 2008), cytoskeletal (Ichida, Tsubata et al., 2001), nuclear-membrane (Hermida-Prieto, Monserrat et al., 2004) and chaperone proteins (Shou, Aghdasi et al., 1998). Familial forms of LVNC are transmitted as an autosomal dominant trait (Captur & Nihoyannopoulos, 2010). Recently, it has been shown that mutations in Mib1, an E3 ubiquitin ligase that regulates the endocytosis of Notch ligands, lead to LVNC (Luxan, Casanova et al., 2013). This work highlights the essential role of endocardial cells during chamber compaction and maturation suggesting that also at later stages of chamber development, endocardium and myocardium are intimately connected.

The NOTCH signaling pathway

Notch is an evolutionary conserved cell-to-cell signaling pathway (Artavanis-Tsakonas, Rand et al., 1999). Notch signals, in a context dependent manner, promote or suppress proliferation, cell death, acquisition of specific cell fates and activation of differentiation programs throughout development and during maintenance of self-renewing adult tissues (Kopan & Ilagan, 2009). Notch signaling regulates many fundamental processes in a wide range of tissues. Thereby it is not surprising that mutations of NOTCH signaling components have been directly linked to multiple human disorders, from developmental syndromes, such as Alagille (Oda, Elkahloun et al., 1997), Tetralogy of Fallot (Krantz, Smith et al., 1999), Familial Aortic Valve Disease (Garg, Muth et al., 2005) and LVNC (Luxan et al., 2013), to adult onset diseases, like CADASIL (Joutel, Corpechot et al., 1996), hematological (Ellisen, Bird et al., 1991) or solid tumors.

Notch receptors are large single pass Type I transmembrane proteins (Fig. 2a). In fly only one Notch receptor exists. Mammals have four Notch paralogues that display both redundant (Krebs, Iwai et al., 2003) and unique functions (Cheng, Kim et al., 2007). The extracellular domain of Notch (NECD) contains 29–36 tandem Epidermal Growth Factor (EGF)-like repeats, required for interactions with the ligands. Repeats 11–12 mediate the binding between the receptor and a ligand expressed in neighboring cells (*trans* interactions), whereas inhibitory interactions with a ligand co-expressed in the same cell (*cis* interactions) are mediated by repeats 24–29 (de Celis & Bray, 2000). Some of the EGF repeats can bind calcium, especially the EGF-repeats in proximity to the ligand binding sites. It has been shown that calcium plays an important role in determining the structure

and affinity of Notch to its ligands (Cordle, Redfieldz et al., 2008b). The EGF repeats are followed by three Lin/Notch repeats (LNR) and a heterodimerization domain (HD), forming a unique negative regulatory region (NRR), adjacent to the cell membrane. The NRR plays a critical role in preventing receptor activation in the absence of ligand (Fig. 2a). The intracellular domain of Notch (NICD) contains a RAM (RBPJK Association Module) domain, seven ankyrin repeats (ANK), a transcription activation domain (TAD) and a PEST domain (Fig. 2a). Both the RAM domain and the ANK repeats have been identified as regions involved in the interaction with CSL transcription factors (Tamura, Taniguchi et al., 1995), RBPJK in mouse. The TAD region is present in Notch-1 and -2 but not in Notch-3 and -4 (Fig. 2a). The C-terminal PEST domain is involved in NICD degradation by proteolysis. Mutations in this region are associated with T-cell leukemias, emphasizing the important functional role of regulated NICD degradation (Weng, Ferrando et al., 2004). The NECD and NICD are synthetized as a single polypeptide, which is directly cleaved after translation by a Furin-convertase in the Golgi. This first (S1) cleavage (Blaumueller et al., 1997, Logeat et al., 1998) is necessary to form the functional heterodimeric receptor that will be translocated to the membrane where the two domains are still associated by Ca^{2+}- dependent non-covalent bonds (Rand et al., 2000).

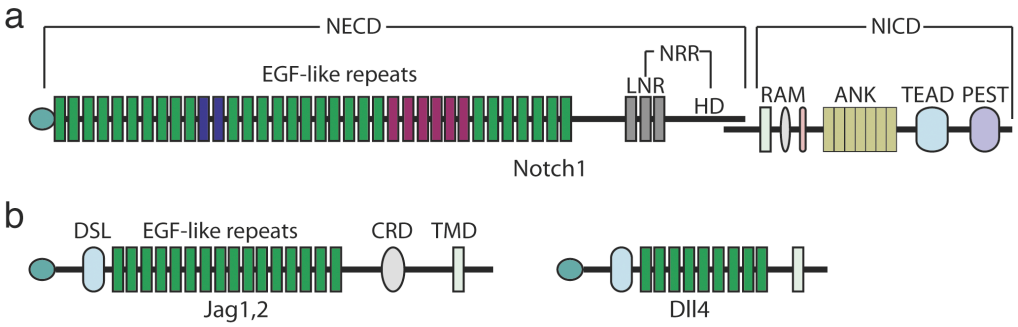

Figure 2.Notch receptors and ligands
In mammals there are four Notch receptors (Notch1-4). Mature Notch proteins reside on the cell surface as heterodimers formed by a transmembrane domain (NECD) and an intracellular domain (NICD) (**a**). The ECD comprise of a variable number of EGF-like repeats. Repeats 11-12 (blue squares) mediate the binding with ligands expressed in the neighbouring cell (trans-activation). Repeats 24-29 (red squares) mediate the binding with ligands expressed in the same cell (cis-interaction.) The EGF-like domain is followed by the Lin/Notch (LNR) repeats and the heterodimerization domain. NICD is formed by a RAM domain, which mediates interaction with several cytosolic and nuclear proteins; the Ankyrin (ANK) domain, which is also important for protein–protein interactions; two nuclear-localization sequences (NLSs); a carboxy-terminal transactivation domain (TAD), which is important for activating transcription; and a PEST (proline-, glutamate-, serine- and threonine-rich) domain, which is important for regulating Notch degradation. Notch receptors interact with two types of ligands (**b**), Delta (Delta1, 3 and 4) and Serrate (Jagged1-2) that are also transmembrane proteins with a long extracellular domain composed of a variable number of EGF-like repeats depending on the ligand and a DSL domain, and a short intracellular domain related with their recycling. The Serrate family also presents a cystein-enriched domain (CR).

In mammals there are two families of Notch ligands, homologous to the ones present in *Drosophila*; the Delta family, composed by Delta-like-1 (Bettenhausen, Hrabe de Angelis et al., 1995), Delta-like-3 (Dunwoodie, Henrique et al., 1997) and Delta-like-4 (Shutter, Scully et al., 2000) and the

Serrate family, composed by Jagged-1 (Lindsell, Shawber et al., 1995) and Jagged-2 (Shawber, Boulter et al., 1996).

As well as the Notch receptor, the ligands are type I transmembrane proteins and all of them present an extracellular domain formed by EGF-like repeats (Fig. 2b). The ECD of the Jagged family contains 16 EGF repeats, whereas the Delta family contains 5–9, followed by a DSL (Delta/Serrate/Lin12) domain. Serrate family ligands also present a cystein-enriched domain (CRD) (Fig 2b). On the cytosolic side, a PDZL domain was identified in some vertebrate ligands (Jagged-1, Delta-like-1, 4). This domain facilitates the interaction with proteins at adherens junctions, promoting cell–cell adhesion and inhibiting cell motility (Mizuhara, Nakatani et al., 2005). The intracellular domain of the DSL ligands interacts with E3 ubiquitin ligases Neuralized (Neurl) (Deblandre, Lai et al., 2001) and Mind bomb (Mib) (Itoh, Kim et al., 2003) to promote ligand ubiquitylation and internalization in the signaling cell (see below).

Post-translational modifications of the ECD Notch receptor tune the amplitude of Notch activity

Many of the EGF modules in the NECD are modified by O-fucose and/or O-glucose glycans (Moloney, Shair et al., 2000). The protein O-fucosyltransferase (Pofut)-1 in mammals (Ofut1 in Drosophila) adds O-fucose to Serine or Tyrosine (Ser/Thr) residues in the consensus sequence C_2-X-X-X-X-(S/T)-C_3 (Fig. 3a). This post-translational modification is essential for optimal Notch signaling in flies and mice (Okajima & Irvine, 2002, Shi & Stanley, 2003). Similarly, O-glucose can also be added to a Ser in the consensus C_1-X-S-X-(P/A)-C_2 by protein O-glucosyltransferase (Poglut). O-glucosylation is also essential for Notch signaling in mouse and Drosophila (Acar, Jafar-Nejad et al., 2008, Fernandez-Valdivia, Takeuchi et al., 2011). The presence of O-fucose can enhance ligand binding by mammalian Notch receptors, whereas O-glucose does not appear to affect ligand binding but a subsequent step before receptor cleavage. Many of the O-fucose monosaccharides on Notch can be extended with GlcNAc by a β-1,3-N-acetylglucosaminyltransferase Fringe (Fig. 3b). The vertebrate fringe family comprises of three members: Lunatic fringe (LFng), Manic fringe (MFng), and Radical fringe (RFng) (Moran, Shifley et al., 2009), each of which affects Notch activity in slightly different ways (Johnston, Rauskolb et al., 1997). The effects of glycosylation on Notch signaling are complex and almost all studies have focused on the role of O-linked glycosylation on the Notch receptor itself. This modification alters the responsiveness of the receptor to different DSL ligands (Fig. 3c). Dynamic expression pattern of Fringe leads to spatial regulation of Notch sensitivity to its different ligands, triggering patterns of Notch activation within a developing tissue. Perhaps the best understood example of Fringe-dependent Notch modulation involves the up-regulation of Notch in a stripe of cells separating the

dorsal and ventral compartments of the Drosophila wing margin (Panin, Papayannopoulos et al., 1997). In the presumptive wing margin tissue, Notch and Delta are widely expressed, but both Fringe and the ligand Serrate are restricted to the dorsal compartment. Expression of Fng allows dorsal cells to respond to Delta, resulting in Notch activation. This leads to transcription of downstream genes, including Serrate. Serrate signals back from dorsal to ventral cells, activating Notch, and leading to the transcription of downstream genes, including Delta. Fng blocks the ability of Serrate to signal to other dorsal cells (Panin et al., 1997).

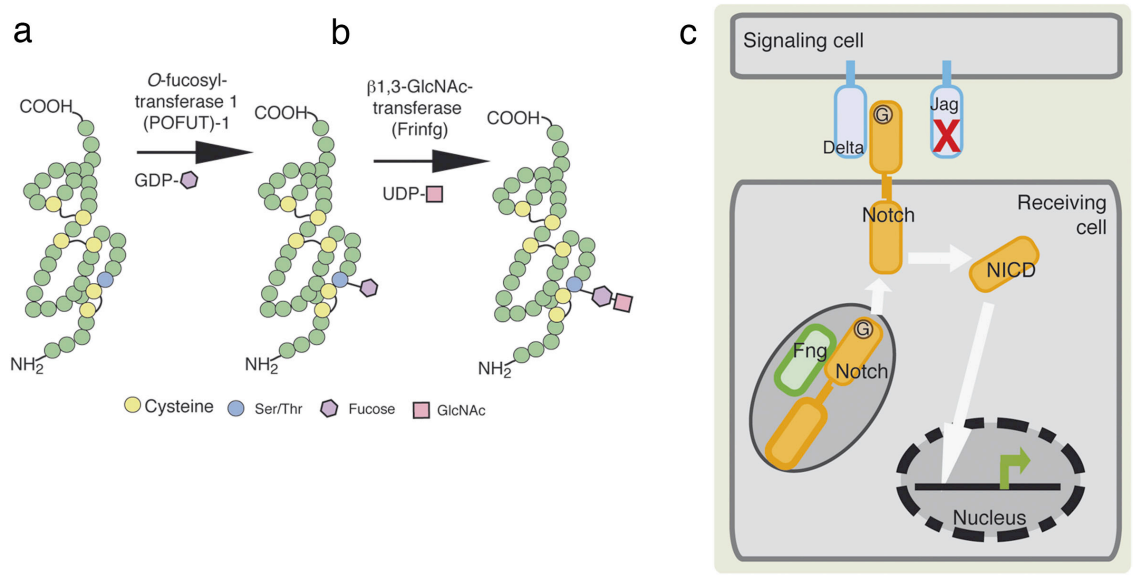

Figure 3. Post-translational modifications of NECD tune ligand-receptor interactions.
A schematic representation of an EGF-like repeat is shown, highlighting the cysteines involved in internal disulfide bonds (black lines). Sugars (coloured symbols, see key) are added in a sequential process by distinct glycosyltransferases. POFUT-1 mediates the fucosylation on the Ser/Thr residues of the EGF domain (**a**) that can be glycosylated by β-1,3-N-acetylglucosaminyltransferase Fringe (**b**). Fringe modification of the ECD of Notch receptors enhances the affinity with Delta ligands and prevents the interaction with Jagged ligands (**c**).

After this pioneer work, the effect of Fringe to shift the activation balance towards Delta ligands at the expense of Jagged has been described in many other biological processes. It has also been demonstrated that in cells expressing both ligands, Jag1 acts as an inhibitor on the Fringe-modified Notch receptor. This is the case of retinal angiogenesis (Benedito, Roca et al., 2009), pancreas development (Golson, Le Lay et al., 2009) or during early hematopoiesis (Van de Walle, De Smet et al., 2011). More recently, X-ray crystallographic analysis has shown that Fringe-mediated elongation of O-fucose on the residue EGF12 of Notch1 effectively enhances the affinity of the Notch/DLL1 complex, but the same modification also increases the binding with Jagged1 (Taylor, Takeuchi et al., 2014). These data explain the Delta-Notch signaling increase in the presence of

Fringe and suggest that the inhibitory effect of the Jagged/Serrate ligands on Notch may be mediated by other regions of the receptor. Interestingly, prior studies have demonstrated that the O-fucose modifications on EGF26 and 27 are both elongated by Fringes and play important roles in ligand-mediated Notch activation (Rampal, Arboleda-Velasquez et al., 2005).

Notch Pathway Activation

In the receiving cell, the ECD of Notch receptor interacts with an exposed ligand in the neighboring cell (signaling cell, Fig. 4b). Ligand-receptor binding induces in the signaling cell, ligand endocytosis mediated by ubiquitin-ligases such as Mib1 (Itoh et al., 2003) and Neuralizad (Neu) (Deblandre et al., 2001, Lai, Deblandre et al., 2001), (Fig. 4b). This process is critical for signaling since its blockage inhibits the proteolytic cleavage required for NICD release in the receiving cell (Itoh et al., 2003). The force generated by the signaling cell during the endocytosis of the ligand bound to NECD produces a conformational change exposing the S2 cleavage site (Parks, Klueg et al., 2000). Once the S2 is exposed, a metalloprotease from the ADAM family cleaves in S2 (Hartmann, de Strooper et al., 2002), and the NECD joined to the ligand is released and is endocytosed by the signaling cell (Fig. 4d). Subsequently, a γ-secretase activity (Okochi, Steiner et al., 2002) mediates the cleavages (S3) in the transmembrane domain (De Strooper, Annaert et al., 1999) producing the release of NICD (Fig. 4e). Once released, the NLS facilitates the nuclear translocation of NICD. In the nucleus, NICD binds to the transcriptional repressor Cp-binding factor 1 (CBF-1) also termed recombination signaling binding protein for immunoglobulin Kappa J region (RBPJ) or Suppressor of Hairless (SU(H)) (Artavanis Tsakonas, 1999) (Fig. 4f). RBPJ is bound to DNA and is associated with transcriptional co-repressors such as SMRT (Silencing Mediator of Retinoic and Thyroid hormone receptors) or Mint (Tanigaki & Honjo, 2007) and Histone-deacetylases (Pursglove & Mackay, 2005) inhibiting gene expression. The interaction between NICD and RBPJK converts the latter from a transcriptional repressor to an activator (Lu & Lux, 1996). In this process the co-repressors will be released and transcriptional, co-activators such as Mastermind (Mam or Master Mind like (MAML) in mammals), will be recruited (Wu, Aster et al., 2000), forming a ternary complex that recruits proteins like p300/PCAF (Kurooka & Honjo, 2000, Wallberg, Pedersen et al., 2002). This protein complex promotes the expression of target genes (Fig. 4f).

There are also intracellular regulators of the pathway such as Deltex (RING-domain E3 ubiquitin ligase) (Matsuno, Ito et al., 2002) or Numb and Numb-like (Campos-Ortega, 1996, Jafar-Nejad, Norga et al., 2002) that will interact with NICD and, depending on the cellular context, they will function as activators or repressors. The spectrum of target genes that are activated by the Notch pathway is very large and it depends on the cellular context.

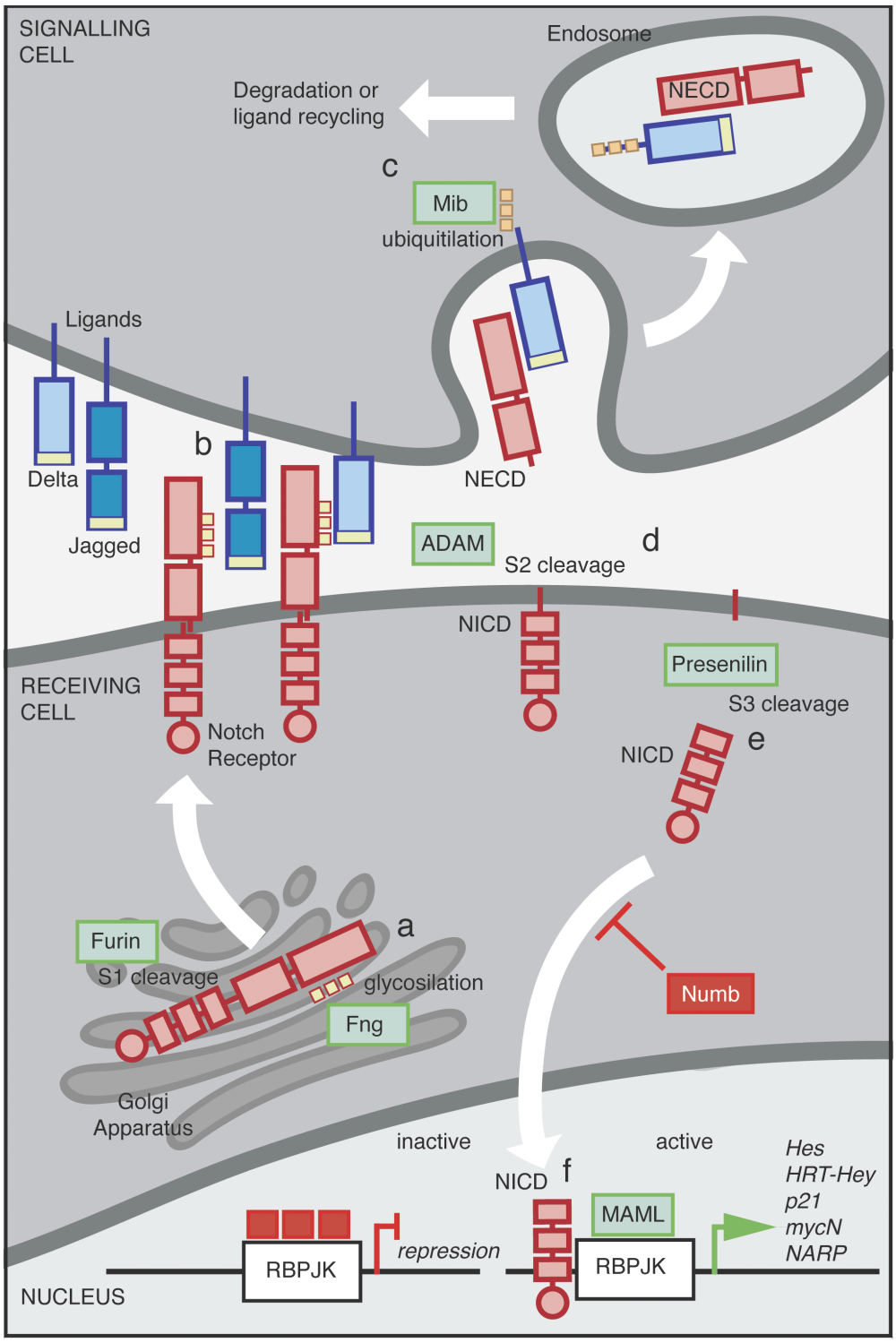

Figure 4. Notch signaling pathway.
Notch proteins are synthesized as a single polypeptide of approximately 300 kDa. In the Golgi, it is cleaved by a furin-like protease at the S1-cleavage site to generate the non-covalently linked Notch heterodimer. The heterodimer can undergo glycosylation by several specific glycosylases, including MFng, LFng and RFng (**a**). Once in the membrane Notch interacts with its ligand expressed in the neighbouring cell (**b**). Upon ligand interaction, Mib1 induces ligand endocytosis (**c**). This produces a conformational change in the NECD that allows the cleavage (S2) by an ADAM metalloproteinase and (S3) by presenilin (**d**), which release the Notch intracellular domain (NICD, **e**). Intracellular Notch then travels to the nucleus, and forms a transcriptional activation complex after binding to Mastermind (MAML) and RBPJk (**f**). This ternary complex activates the transcription of a set of target genes.

The most known targets are the basic helix-loop-helix (bHLH) repressor transcription factors of the *Hes* (Davis & Turner, 2001) (Hairy and enhancer of split) and *Hey* (Iso, Kedes et al., 2003) (HESR) (Hairy and enhancer of split repressor) families. They respond to Notch in the endocardium during embryogenesis, but not in the myocardium where Notch is not active. Others well known targets of Notch are the *Snail1*/*2* transcription factors, implicated in the induction of the EMT process during heart valve development (Timmerman et al., 2004), the cell cycle regulator p21 (Devgan, Mammucari et al., 2005), the *c-Myc* oncogene, described as a Notch target gene promoting cell growth in leukemia (Palomero, Lim et al., 2006, Weng, Millholland et al., 2006) and *EphrinB2/EfnB2* (Grego-Bessa, Luna-Zurita et al., 2007) among others.

Mechanisms of Action

The complex expression pattern of receptors, ligands and modulators of the Notch pathway anticipates the tight regulation of the pathway by its elements during development and adult tissue homeostasis. There are several *modus operandi* (lateral inhibition, lateral induction or cis-inhibition) in which Notch determines cell fate specification, promotes or suppresses proliferation or induces cell death, but the crucial event that triggers Notch activity is the ligand-receptor interaction.

The classical view of Notch-mediated lateral inhibition is based on the pioneering studies of neurogenesis in Drosophila (Artavanis-Tsakonas et al., 1999). In Drosophila, loss of function of either Notch or its ligands, leads to the overproduction of neurons. Lateral inhibition is the process by which a cell that stochastically expresses high levels of ligand becomes a signaling cell. In the neighbouring cells, the Notch pathway is activated and by a negative feedback mechanism ligand expression is inhibited (Heitzler, Bourouis et al., 1996). Thus, cells with high levels of ligand acquire a fate different from cells with lower levels of ligand in which the pathway is active. This mechanism has been described in several developmental processes, including early neurogenesis in frogs (Chitnis, Henrique et al., 1995, de la Pompa, Wakeham et al., 1997) and sensory hair cell formation in the vertebrate inner ear (Eddison, Le Roux et al., 2000, Petrovic, Formosa-Jordan et al., 2014). The Notch pathway can also generate cell clusters with the same fate. In this mechanism, called lateral induction (Lewis, 1998), cells expressing both ligand and receptor, activate the pathway in all neighboring cells. In this mechanism the expression of the ligand is regulated by a positive feedback mechanism. This is the case of Notch signaling during early cardiac valve development (Timmerman et al., 2004) In this context, inactivation of Notch in the endocardium results in decreased ligand expression. Indeed, *RBPJk* and *Notch1* mutants show reduced *Dll4* expression in the endocardium (Grego-Bessa et al., 2007, Timmerman et al., 2004), while Notch gain-of-function expands *Dll4* expression (Luna-Zurita et al., 2010, Rutenberg, Fischer et al., 2006,

Watanabe, Kokubo et al., 2006), suggesting the existence of a Notch-dependent positive feedback loop regulating *Dll4* expression in embryonic endocardium. This mechanism has also been described in processes such as the formation of the wing margin in *Drosophila* (Panin et al., 1997), as well as in the mouse in the induction of proneural domains in the inner ear (Daudet & Lewis, 2005), limb bud margin formation (Irvine & Vogt, 1997) and formation of the edges of somites (Lewis, 1998). Studies performed mostly in *Drosophila* but also in vertebrates indicate that ligand–receptor interactions can also take place within the same cell. These *cis*-interactions reduce the ability of a cell to receive signals from neighboring cells by a process called '*cis*-inhibition' of the receptor by the ligand (del Alamo, Rouault et al., 2011). A recent structural analysis further suggests that Notch may interact with the DSL domain of its ligands via two modes of interaction, referred to as parallel and antiparallel binding. Interaction of Jagged with Notch *in trans* would follow antiparallel binding, leading to activation of Notch, whereas interaction *in cis* would be mediated by parallel binding, resulting in inhibition of Notch (Cordle, Johnson et al., 2008a). Interaction of Notch with its ligands *in cis* may inhibit signaling either by forming complexes that are inactive for signal reception or by regulating a catalytic process that results in Notch inhibition, for instance by promoting the internalization and degradation of Notch whereas ligands are recycled (del Alamo et al., 2011). Lateral inhibition or lateral induction, *cis*-interactions and the glycosylation of NECD mediate the specificity of ligand-receptor interactions and selectively control Notch activity.

Notch signaling during heart development

Endocardial Notch signaling is involved in several morphogenetic processes during cardiac development (de la Pompa & Epstein, 2012, High & Epstein, 2008). The receptor Notch1 is widely expressed in endocardial cells as soon as the primitive heart tube is formed (Grego-Bessa et al., 2007). In contrast Notch activated cells show restricted localization (Del Monte, Grego-Bessa et al., 2007, Grego-Bessa et al., 2007) as a consequence of differential expression of the ligands. During AVC valve development Notch elements are expressed in the endocardium of the valvulogenic region (Del Monte et al., 2007, Timmerman et al., 2004). Targeted inactivation of *Notch1* (or *RBPJ*) results in severely hypoplastic endocardial cushions at E9.5 due to impaired EMT (Timmerman et al., 2004). The endocardial N1ICD-RBPJ complex directly activates the EMT drivers *Snail1/2*, whose expression is severely reduced in the AVC and OFT endocardium of *RBPJk* mutants (Sahlgren, Gustafsson et al., 2008, Timmerman et al., 2004). Loss of *Snail* expression prevents down-regulation of vascular endothelial cadherin (Cdh5)-mediated endocardial cell adhesion and thus EMT is blocked. These *in vivo* observations were confirmed by the defective EMT of AVC and OFT explants of *Notch1 and RBPJ* mutants, or wild type (WT) explants treated with a Notch-signaling inhibitor, cultured *in vitro* on collagen gels, indicating that Notch is essential for this

process (Timmerman et al., 2004). More recently, by using conditional loss-of-function alleles, the role of Notch1 during EMT was confirmed (Wang et al., 2013).

Notch activity also regulates OFT morphogenesis. As aforementioned, the endocardial cushions of the OFT are populated by mesenchymal cells derived from EMT as well as by cells coming from the CNC (High, Zhang et al., 2007). The cross talk between these two populations is essential for OFT septation, formation of the semilunar valves and remodeling of the aortic arch arteries. Deficient CNC investment into the OFT results in persistent truncus arteriosus (PTA) and a perimembranous ventricular septal defect (VSD) (Neeb, Lajiness et al., 2013). Conditional inhibition of Notch signaling using a dominant-negative form of the transcriptional co-activator mastermind (DNMAML; Fig. 4f) induced with the CNC driver lines *Wnt1-Cre* or *Pax3-Cre* resulted in a variety of defects with variable penetrance: pulmonary artery stenosis, VSD, atrial septal defect (ASD), and OFT misalignment similar to the TOF (High et al., 2007).

At E9.5, Notch1 is expressed throughout the endocardium of the developing ventricles, but it is only active at the base of the trabeculae. Systemic or endocardium-specific Notch mutant embryos show defective trabeculation, defective trabecular marker expression and reduced ventricular cardiomyocyte proliferation (de la Pompa & Epstein, 2012, Grego-Bessa et al., 2007, High & Epstein, 2008). Notch signaling abrogation affects the expression of three pathways required for trabeculation: Bmp10, Nrg1/ErbB and EphrinB2. Endocardial *EphrinB2* is a direct transcriptional target of N1ICD/RBPJK (Grego-Bessa et al., 2007) and its expression and activity is abrogated in Notch mutants. In addition, endocardial *Ngr1* or myocardial Bmp10 expression was impaired in Notch mutants. These findings suggest that endocardial Notch1 signaling is required for proliferation and differentiation of chamber myocardium during trabeculation (de la Pompa & Epstein, 2012, Grego-Bessa et al., 2007, High & Epstein, 2008). Furthermore, Notch1 in the endocardium triggers downstream signaling events that sustain normal trabecular patterning, maturation and myocardial compaction at later stage of chamber development (Luxan et al., 2013). Conditional inactivation of myocardial *Mib1* gene causes a phenotype strongly reminiscent of LVNC. In fact, E16.5 *Mib1^{flox};cTnT-Cre* embryos show a dilated heart with a thin compact myocardium and large, non-compacted trabeculae, protruding toward the ventricular lumen (Luxan et al., 2013). These embryonic features are present in newborn and adult mutant mice as revealed by echocardiographic analysis of 6 month-old mice that also show reduced ejection fraction and a ratio of non-compacted to compacted myocardium (non-compaction index) of 2.0, diagnostic of LVNC in humans (Jenni, Oechslin et al., 2001). Analysis of chamber-specific markers in *Mib1^{flox};cTnT-cre* mutant embryos revealed the expansion of compact myocardium markers to the trabeculae and reduced expression of trabecular markers. These observations suggest that trabecular patterning and maturation is impaired after *Mib1* abrogation in the embryonic myocardium.

The data presented above highlight the importance of endocardial Notch signaling and regulation in many aspects of heart development, namely the formation of the valves and the processes of ventricular trabeculation and compaction. Indispensable to these events is the intimate and tightly regulated interaction between endocardium and myocardium.

OBJECTIVES

The Notch1 receptor, shown to be the most relevant Notch receptor in the context of cardiac chamber development, is ubiquitously expressed throughout the endocardium of the forming heart. Endocardial Notch1 activation is crucial for proper ventricular trabeculation and compaction. Its activity is also of pivotal importance in the endothelium of the coronary vessels, affecting their formation but also indirectly contributing to chamber maturation. Published work strongly point towards a tight spatio-temporal regulation of endocardial Notch1 signaling.

The objectives of this thesis were:

- To evaluate the detailed expression pattern of specific Notch components during the process of ventricular chamber development: the three Notch ligands Dll4, Jag1 and Jag2, as well as the three Fringe paralogs (Manic, Radical and Lunatic).
- To generate the corresponding tissue-specific loss- and gain-of-function models in order to decipher the tissues and time points that are important for triggering Notch1 signaling.
- To determine the exact contribution of Fringe modifications in the regulation of Notch1 signaling in the context of chamber development, mediated by changes in the affinity of ligand-receptor interactions.
- To unravel new Notch targets by thorough transcriptome analysis of different mutants with a particular interest in understanding: a) whether different Notch ligands, individually or in combinations, trigger distinct target responses, and b) which Notch-induced molecules could be involved in the communication between endocardium and myocardium that is crucial for proper chamber differentiation, proliferation and maturation.

MATERIAL AND METHODS

Mouse strains and genotyping.

Mouse strains were *CBF:H2B-Venus* (Nowotschin, Xenopoulos et al., 2013), *R26R* (Soriano, 1999), *R26R-YFP* (Srinivas, Watanabe et al., 2001), *Notch1* (Conlon, Reaume et al., 1995), *RBPJk* (Oka, Nakano et al., 1995), *Tie2-Cre* (Kisanuki, Hammer et al., 2001), *Nfatc1pan-Cre* (Wu et al., 2012), *cTnT-Cre* (Jiao, Kulessa et al., 2003), *Cdh5(PAC)-Cre^{ERT2}* (Wang, Nakayama et al., 2010), *Dll4^{flox}* (Koch, Fiorini et al., 2008), *Jag1^{flox}* (Mancini, Mantei et al., 2005), *Jag2^{flox}* (Xu, Krebs et al., 2010), *Notch1^{flox}* (Radtke, Wilson et al., 1999), *Mib1^{flox}* (Koo, Yoon et al., 2007). Fringe mutant strains (*M$^{-/-}$; L$^{-/-}$;R$^{-/-}$*) were bred and maintained as described (Moran et al., 2009). For the generation of *Rosa26-MFng* Tg mice (Acc. No. CDB0917K: http://www.cdb.riken.jp/arg/mutant%20mice%20list.html), a cDNA encoding a native form of murine *MFng* was cloned into a modified version of the *pROSA26-1* vector, preceded by the ubiquitous CAG promoter and a loxP-flanked 'Neo^{R}-STOP' cassette and followed by a frt-flanked IRES-EGFP cassette and a bovine polyadenylation sequence. Gene targeting was done with TT2 ES cells and confirmed by Southern blotting. Mice were generated by injection of targeted ES cells into ICR embryos, and were backcrossed with the C57BL/6 strain. In the case of the different mutants analyzed, the WT embryos were the littermates who did not express the Cre-recombinase. To simplify the nomenclature we used the following names to refer the different mutant and transgenic line.

Name	Genotype
CBF:H2B-Venus	*CBF:H2B-Venus;*WT
CBF:H2B-Venus;Notch1KO	*CBF:H2B-Venus ;Notch1$^{-/-}$*
CBF:H2B-Venus;RbpjKO	*CBF:H2B-Venus;RbpjKO$^{-/-}$*
R26R;Nfatc1-Cre	*R26R$^{/+}$; Nfatc1pan-cre$^{+/-}$*
R26R-YFP;Nfatc1-Cre	*R26R-YFP $^{/+}$; Nfatc1pan-cre$^{+/-}$*
Dll4^{flox};Tie2-Cre	*Dll4$^{flox;flox}$;Tie2-Cre$^{+/-}$*
Dll4^{flox};Nfatc1-Cre	*Dll4$^{flox;flox\ /+}$; Nfatc1pan-cre$^{+/-}$*
Notch1^{flox};Nfatc1-Cre	*Notch1$^{flox;flox}$; Nfatc1pan-cre$^{+/-}$*
Dll4^{flox};Cdh5-Cre	*Dll4$^{flox;flox}$;Cdh5-Cre$^{+/-}$*
Jag1^{flox};cTnT-Cre	*Jag1$^{flox/flox}$;cTnT-cre$^{+/-}$*
Jag2$^{flox;}$cTnT-Cre	*Jag2$^{flox/flox}$;cTnT-cre$^{+/-}$*
Jag1^{flox}; Jag2^{flox}; cTnT-Cre	*Jag1$^{flox/flox}$;Jag2$^{flox/flox}$;cTnT-cre$^{+/-}$*
M$^{-/-}$; L$^{-/-}$;R$^{-/-}$	*MFng$^{-/-}$; LFng$^{-/-}$;RFng$^{-/-}$*
MFng^{tg}; Tie2-Cre	*MFng$^{tg/tg}$;Tie2-Cre$^{+/-}$*
MFng^{tg}; Tie2-Cre	*MFng$^{tg/tg}$;Tie2-Cre$^{+/-}$*

Genotyping of the different genes was performed using the primers listed in Table1.

Table 1. PCR primers and conditions for genotyping

Gene	Oligos 5' to 3'	Annealing Temperature (ºC)	Product
RbpjKO	5′CAGTGGGGAGCATTTTAQCAT 3′	55	415 bp
	5′GAGGAAATTGCATCGCATTGT C 3′		
Notch1KO	5′GATATCGTGGTGCATACCCTCCTG3′	60	400 bp
	5′GTCAGTTTCATAGCCTGAAGAACG3′		
Dll4^{flox}	5′ GTGCTGGGACTGTAGCCACT 3′	60	455 bp -Flox
	5′ TGTTAGGGATGTCGCTCTCC 3′		408 bp -WT
Notch1^{flox}	5′ CTG ACTTAGTAGGGGGAAAAC 3′	60	350 bp -Flox
	5′ AGTGGTCCAGGGTGTGAGTGT 3′		300 bp -WT
Jag1^{flox}	5′ AGGTTGGCCACCTCTAAATC 3′	60	417 bp -Flox
	5′ GCAAGTCTGTCTGCTTTCATC 3′		267 bp -WT
Jag2^{flox}	5′ GGCAGAGTAGCACATCACCA3′	60	453 bp -Flox
	5′ CAAGCGCACAGGTTGAGTAG3′		401 bp -WT
MFng^{tg}	5′ AAAGTCGCTCTGAGTTGTTAT 3′		300 bp -Tg
	5′ GCGAAGAGTTTGTCCTCAACC 3′	60	650 bp -WT
	5′ AGGCTGCAGAAGGAGCGGGA 3′		
Tie2-Cre	5′ GGGAAGTCGCAAAGTTGTGAGTT 3′	60	500 bp -Cre
	5′ CTAGAGCCTGTTTTGCACGTTC 3′		
Nfatc1-Cre	5′ AATAAG CCTGCCGTGGTCACTGG 3′		1000 bp -Cre
	5′ AACCCTGGACGCCTGGGACAC 3′	60	290 bp -WT
	5′ GAAGCAACTCAT CGATTGATTTACG 3′		
cTnt-Cre	5′ TACTCAAGAACTACGGGCTGC 3′	57	350 bp -Cre
	5′ GCACTCCAGCTTGGTTCCCGA 3′		
Cdh5-Cre	5′CTGGGATGCTGAAGGCATCAG 3′	55	760 bp -Cre
	5′ TTGCGAACCTCATCACTCGTT 3		

Tissue Processing.

Embryos were fixed in 4% paraformaldehyde (PFA) at 4ºC. In the case of immunostaining, embryos from E9.5 were fixed for 2 hours whereas older embryos were fixed for 4 hours. For *in situ* hybridization (ISH) studies embryos were fixed overnight. Embedding was performed following a dehydratation using a graded ethanol series, xylene washes, a xylene-paraffin step and a final paraffin-embedding step. Adult hearts were perfused with PBS and fixed overnight in PFA 4%. Neonatal mouse hearts (P1-P3) were dissected and washed in PBS and fixed overnight. Fixed hearts were rinsed 2-3 times in PBS, ethanol/xylene processed and embedded in paraffin.

Histology and *in situ* hybridization.

Hematoxylin/eosin (H&E) staining, *in situ* hybridization (ISH) on sections, and whole-mount ISH were performed as described (de la Pompa et al., 1997, Kanzler, Kuschert et al., 1998).

Whole-mount immunofluorescence

E9.5 *CBF:H2B-Venus* embryos were dissected and fixed for 2h in 4% PFA at 4°C, permeabilized for 1h with 0.5% Triton X-100/PBS and subsequently blocked for 1h in Histoblock solution (5% goat serum, 3% BSA, 0.3% Tween-20 in PBS). Primary and secondary antibodies used are listed in Supplementary Table 2. After several washes in PBS-T (PBS containing 0.1% Tween-20) embryos were mounted in a 60mm petri dish with 1% agar. To detect endogenous GFP, fixed E9.5 *CBF:H2B-Venus; CBF:H2B-Venus;N1KO and CBF:H2B-Venus;RBPJkKO* embryos were imaged with a Zeiss 780 confocal microscope fitted with a 20X objective with a dipping lens. Z-stacks were taken every 5µm. 3D images were reconstructed with IMARIS software (Bitplane Scientific Software).

Immunohistochemistry

Paraffin sections (7µm) were incubated overnight with primary antibodies, followed by 1h incubation with a fluorescent-dye-conjugated secondary antibody. N1ICD, Dll4, Jag1 and p21 staining was performed using Tyramide signal amplification (TSA) (Del Monte, Casanova et al., 2011). All the primary antibodies antibodies used are listed in Table 2.

Proliferation analysis and quantification.

Cell proliferation was analyzed by detection of BrdU incorporation. Pregnant females were intraperitonally injected with 300ul BrdU at 10mg/ml and two hours later embryos were isolated in sterile PBS. Embryos were fixed overnight in PFA 4%. BrdU positive cells were detected following the protocol described in (Del Monte et al., 2007). Total cells and BrdU-positive cells in the compact myocardium were counted in sections (at least five) in three embryos of each genotype. For p21 and N1ICD quantification, positive nuclei were divided by the total number of nuclei counted on sections (≥4) in six embryos of each genotype. Images were processed with ImageJ

software. Statistical significance was assessed by Student's *t*-test.

Table 2. List of primary antibody used for the IHC

Antobody	Cardiac expression	Source Ig	IHC dilution
a-SMA-Cy3	CM/SMc	Mouse	100
BrdU	BrdU	Mouse	50
CD31/Pecam-1	Endo/CV	Rat	100
cTnT	CM	Mouse	200
Dll4	Endo/CV	Rabbit	100
Endomucin	Endo	Rat	200
GFP	GFP expressing cells	Mouse	200
Jag1	CM/CV	Rabbit	100
Myosin Heavy Chain (MF-20)	CM	Mouse	20
Cleaved Notch1 (Val1744)_N1ICD	Endo/CV	Rabbit	100
p21	p21 expressing cells	Goat	100

(**CM**) cardiomyocytes;(**SMc**) Smooth muscle cells; (**Endo**) Endocardium; (**CV**) coronary Vessels; (**PC**)=proliferating cells.

Quantification of compact myocardium thickness and trabecular complexity

The method used was a modification of that described by (Chen, Zhang et al., 2009, Yang, Bucker et al., 2012). Briefly, 7µm paraffin sections from E9.5 WT and mutant hearts were stained with anti-CD31 and anti-MF20 to facilitate visualization of ventricular structures. In E16.5 wild type and mutant hearts endocardial cells were stained with anti-endomucin and myocardium with anti-cTnT. Confocal images were obtained with a NIKON A1R confocal microscope. ImageJ software was used for the measurements. In E16.5 heart sections, left and right ventricles were analysed separately. For each measurement, settings were kept constant for all images using the scale bar recorded in each image as the reference distance. Several measurements were taken in each region and the mean was expressed in µm. The complexity of trabecular myocardium indicates the size of the trabecular mesh of myocardial fibres and is considered a landmark of cardiomyopathy(Captur, Lopes et al., 2014). It was represented as the mean ratio, expressed in µm, obtained by dividing the length of each trabecula by its thickness. The ratio of trabecular area and compact myocardial thickness was measured by dividing the surface occupied by trabeculae in the ventricle (μm^2) by the length of compact myocardium expressed in µm.

Imaging, photography and 3D reconstruction.

E9.5 whole-embryos or hearts were imaged with a Zeiss 780 confocal microscope fitted with a 20X objective with a dipping lens. Z-stacks were taken every 5µm. 3D images were reconstructed with

IMARIS software (Bitplane Scientific Software). WT E9.5 embryos were sectioned at 10μm and stained for Dll4, Jag1 and N1ICD. Images were acquired with a confocal microscope (Leica TCS SPE) taking 10 optical sections per histological section. After acquisition, 3D reconstructions were performed as described(Soufan, van den Berg et al., 2006) and the resulting surfaces were exported to Adobe Acrobat Professional 9 Extended version to generate 3D interactive pdf files (de Boer, Soufan et al., 2011).

Lentiviral production and infection.

Full-length murine *Manic Fringe (MFng)* (Benedito et al., 2009) was subcloned into the lentiviral vector pRLL-IRES-eGFP (Addgene). Concentrated lentiviruses expressing pRLL-IRES-eGFP or pRLL-MFng-IRES-eGFP were obtained as described (Esteban, Mendez-Barbero et al., 2011). Viruses were titrated in Jurkat cells, and infection efficiency (GFP-expressing cells) and cell death (propidium iodide staining) were monitored by flow cytometry.

Isolation and immortalization of MEVEC.

Mouse embryonic ventricular endocardial cells (MEVEC) were obtained from ventricles of E10.5 embryos. Embryos were dissected in PBS and hearts were collected. Atria and the atrioventricular canal were removed and the remaining ventricles were mechanically dissociated. Isolated cells were collected in DMEM containing 20% FBS and centrifuged at 400 x g for 5 min. The cells were finally resuspended in 500 μl culture medium (DMEM, 20% FBS supplemented with penicillin/streptomycin and 100 μg/mL endothelial cell growth supplement (ECGS, Sigma-Aldrich), and seeded into one-well of a MW24 plate pre-treated with collagen type I (4.08 mg/ml) (BD Bioscience). After 1 week, a confluent cobblestone morphology culture was observed and cells were transferred to one gelatinized p60 flask. MEVEC in passage 1 were infected with lentivirus expressing SV40-large T antigen (Fig. 5) in the presence of polybrene (8 μg/ml). Overexpression of SV40-large T antigen was determined by qRT-PCR. MEVEC cultures expressed the chamber endocardial markers *Notch1*, *Dll4*, *Nfatc1, Nrg1* and *Gpr126* (Fig. 19o) and maintained their endocardial phenotype and cobblestone morphology over 20-25 passages.

Cell culture

Human umbilical vein endothelial cells (HUVEC) were purchased from Lonza, and cultured on gelatin-coated dishes until passage 9 in EGM-2 complete medium (Lonza) supplemented with penicillin/streptomycin. For expression analysis by qPCR, HUVEC were pre-treated with 10 μM γ-secretase inhibitor (RO4929097, Selleckchem) or vehicle (DMSO) and stimulated with Notch ligands as described above for MEVEC.

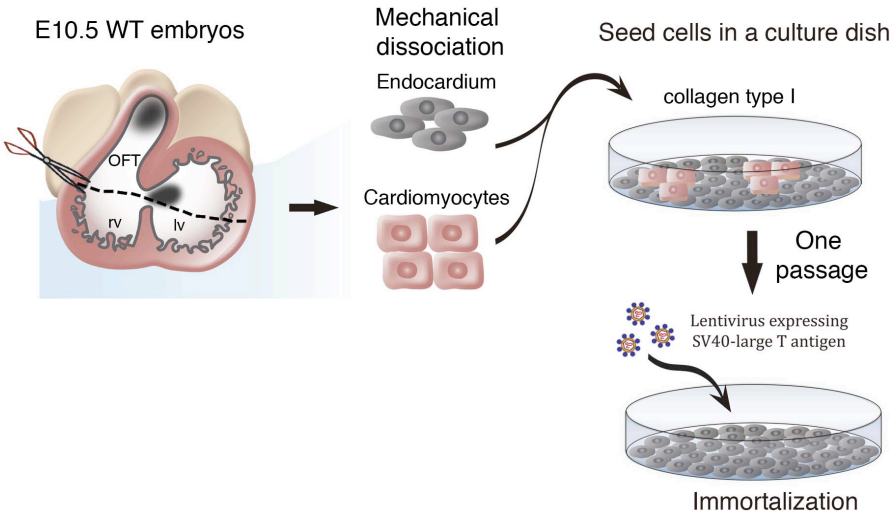

Figure 5. Isolation and immortalization of MEVEC.
Cartoon illustrating the different steps used to obtain MEVEC.

Bovine aortic endothelial cells (BAEC) were purchased from Lonza and cultured in DMEM supplemented with penicillin/streptomycin plus 10%FBS.

Luciferase assays with *Gpr126* genomic DNA fragments

The *Evolutionary Conserved Region* web platform (ECR;http://ecrbrowser.dcode.org/) was used to identify RBPJ motifs in the *Gpr126* gene. Two conserved RBPJ binding sites were found in the intronic region, flanking the 5th and 6th exon of human, monkey, rat and mouse *Gpr126*. In human the conserved RBPJ sites are separated by 445bp. Genomic DNA from HUVEC was used as template to amplify 726bp of *GPR126* containing the two conserved sites and the product was cloned into the KpnI and XhoI sites of pGL3 promoter luciferase plasmid (Promega). The primer sequences were: 5'-ATGCGGTACCATTTATACTTGTTACTGTGC-3' (forward, KpnI site underlined) and 5'- ATCGCTCGAGGGCCAAGAATTATAAAGAATGAG-3' (reverse, XhoI site underlined). For luciferase assays we transiently co-transfected BAEC with the hGPR126 reporter plasmid (pGL3-hGPR126-Luciferase), Renilla plasmid, and increasing amounts of vector expressing the intracellular domain of Notch1 (0-200ng) (pCS2-N1ICD). Twenty-four hours after transfection the cells were lysed, and luciferase activity was measured with the Dual Luciferase Assay System (Promega).

Notch stimulation with recombinant ligands and luciferase assays

For Notch stimulation with recombinant ligands, MW24 plates were incubated with anti-human-IgG-Fc, anti-mouse-IgG2a-Fc (Jackson), anti-His (Zymed), or a 1:1 mixture of antibodies (6.48 mg/ml) for 30 min at 37ºC. After washing with PBS, plates were blocked for 1 hr at 37ºC with 10% FBS in DMEM. Recombinant Dll4 (mouse Dll4-His R&D Systems #1389-D4), Jagged1 (rat Jag1-Fc, R&D Systems #599–JG) or Jagged2 (mouse Jag2-Fc, R&D Systems #4748–JG) were diluted in PBS and added to the dishes individually or in a 1:1 mixture at a final concentration of 18 nM. After 2h at 37ºC, wells were washed and GFP-MEVEC and MFng-MEVEC were incubated on the coated plates at subconfluency overnight. For luciferase assays, stimulated cells were transiently co-transfected with the Notch reporter plasmid pGL3-10xCBF1-Luciferase and pGL3-Renilla luciferase at a 5:1 ratio using Lipofectamine and Plus reagents (Life Technologies). Twenty hours after transfection, luciferase activity was measured with the Dual Luciferase Assay System (Promega). Data are expressed as Firefly/Renilla luciferase ratios. Experiments were performed at least three times, with quadruplicate samples each experiment. Data are presented as mean ± standard deviation. Differences were considered statistically significant at $p<0.05$ (Student's *t* test).

Quantitative RT-PCR

WT and mutant embryos at different stages were dissected in ice-cold PBS. Whole E8.5 hearts, ventricles of E9.5-16.5 embryos and P1 hearts were separated from the rest of the body and RNA was extracted. For RNA extraction from cells stimulated *in vitro* with recombinant Notch ligands, the stimulation protocol was conducted as above in MW6 dishes and RNA was extracted after overnight incubation. Total RNA was purified using Trizol (Invitrogen). cDNA was synthesized with SuperScript III First Strand (Invitrogen), with 1µg total RNA per reaction. Quantitative PCR was performed with Power SYBR Green Master Mix (Applied Biosystems, 4367659). Oligonucleotide sequences for real-time PCR analysis performed in this study are listed in Table 3. Data are presented as mean ± standard deviation. Differences were considered statistically significant at $p<0.05$ (Student's t test).

RNA-Seq

RNA was isolated at E9.5 from whole hearts of WT and *Dll4^{flox};Nfatc1-Cre* embryos (32 per genotype), WT and *Notch1^{flox};Nfatc1-Cre* embryos (24 per genotype), and WT and *Dll4^{flox};Tie2-Cre* embryos (27 per genotype). RNA was pooled into four replicates for the first genotype pairs and three replicates for the last two genotype pairs. For *Jag1^{flox};cTnT-Cre* hearts, RNA was isolated from the ventricles of 12 WT and 12 mutant hearts at E15.5 and then pooled into three replicates. RNA was prepared using the standard Illumina TrueSeq RNASeq library preparation kit. Libraries were sequenced in a GAIIx Illumina sequencer using a 75bp single end elongation protocol. For *Jag2^{flox};cTnT-Cre* and *Jag1^{flox};Jag2^{flox};cTnT-Cre* hearts, RNA was isolated from the ventricles of 8

Table 3. List of primers used for qPCR experiments.

Gene	Forward primer	Reverse primer
mouse-*Notch1*	AGCCTCTCCACCAATACCTT	GGCTGGAGCTGTAAGTTCT
mouse-*Dll4*	GGACTCTATGTACCAATCAG	CCTGCCTTATACCTCTGT
mouse-*Jag1*	ACACAGGGATTGCCCACTTC	AGCCAAAGCCATAGTAGTGGTCAT
mouse-*Jag2*	GACGCCAATGAGTGTGAA	ACAGTAATAGCCGCCAATC
mouse-*Hey1*	CTCTGCCTTCTCATTCATT	TAGTCACAACACATCAATACA
mouse-*Gpr126*	GTCTACAATGCTACCAATAACG	GCCTCAGTCCATCCTCTA
mouse-*Cxcl12*	GAAAGCTTTAAACAAGAGGC	GTGAAAGTACAGCAAAACTG
mouse-*MFng*	TCCAGGATCAGGCAACAGA	GTCTCTCCTGGAGGCGTTC
mouse-*Nrg1*	AACTGGTGAATCAATATGTATCT	GTGTAGTGACTGGTGGAA
mouse-*Nfatc1*	CCAAGTCAGTTTCTATGTCTG	ATAATTGGAACATTGGCAGG
mouse-*Gapdh*	AACTTTGGCATTGTGGAAGG	ACACATTGGGGGTAGGAACA
human-*DLL4*	GTTACACAGTGAAAAGCCAG	CTCTCCTCTGATATCAAACAC
human-*HEY1*	CCGGATCAATAACAGTTTGTC	CTTTTTCTAGCTTAGCAGATCC
human-*HEY2*	GGATTATAGAGAAAAGGCGTC	GTTTTTCAAAAGCAGTTGGC
human-*HEYL*	GTGGGACAGGATTCTTTG	GTTGAGGTGGGAGAGAGAAG
human-*GPR126*	GATGGATTTTGAGAGTGGAC	GGAAAAGTCCAGTTTTGTTG
human-*NRARP*	AAATCCGTGAGTTTTGGAAG	AAAAGGTAACGAAGGTTCAC
human-*GAPDH*	ACAGTTGCCATGTAGACC	TTTTTGGTTGAGCACAGG

WT and 12 mutant hearts at E15.5 and then pooled into two and three replicates respectively. For *MFng*^{tg}*;Tie2-Cre* hearts, RNA was isolated from the ventricles of 16 WT and 16 transgenic hearts at E15.5 and then pooled into four replicates each. RNA was prepared using the NEBNext Ultra RNA Library Prep Kit for Illumina. Libraries were sequenced in a HiSeq2500 Illumina sequencer using a 61bp single end elongation protocol. Sequenced reads were QC and pre-processed using cutadapt v1.6 (Martin, 2011) to remove adaptor contaminants. Resulting reads were aligned and gene expression quantified using RSEM v1.2.3 (Li & Dewey, 2011) over mouse reference GRCm38 and Ensembl genebuild 70. Gene differential expression was analysed using the EdgeR R package(Robinson, McCarthy et al., 2010). Data from *Dll4*^{flox}*;Tie2-Cre* and *Dll4*^{flox}*;Nfatc1-Cre* experiments were analysed together, as were data from and *Dll4*^{flox}*;Nfatc1-Cre* and *Notch1*^{flox}*;Nfatc1-Cre* experiments, by applying batch correction using ComBat (Johnson, Li et al., 2007) to account for experimental differences. For *Jag1*^{flox}-, *Jag2*^{flox}*;cTnT-Cre* and double Jag1^{flox};Jag2^{flox};*cTnT-Cre* experiments, data were analysed together applying batch correction to account for technical differences and adding the genotypes of both alleles as covariates. Genes showing altered expression with adjusted P<0.05 were considered differentially expressed. For the set of differentially expressed genes a functional analysis was performed using Ingenuity Pathway Analysis Software and DAVID (Huang da, Sherman et al., 2009), and some of the enriched processes were selected according to relevant criteria related to the biological process studied.

Unsupervised hierarchical clustering with Genesis Software(Sturn, Quackenbush et al., 2002) was used to group genes according to the similarity of their expression profiles across the different Dll4 and Notch1 deficiency experiments. Using a new R visualization package called GOPlot (Walter, Sanchez-Cabo et al., 2015) a chord plot (Krzywinski, Schein et al., 2009) was generated to better visualize the relationships between genes and the selected enriched processes.

Accession number

Data are deposited in the NCBI GEO database under accession number GSE67889.

Ultrasound

Left ventricle (LV) function and wall thickness were analysed by transthoracic echocardiography in 6-month-old male mice and in the same mice at 9 months of age. Mice were mildly anesthetized by inhalation of isoflurane/oxygen (1-2%/98.75%) adjusted to obtain a target heart rate of 450 ±50 beats per minute and examined with a 30 MHz transthoracic echocardiography probe. Images were obtained with Vevo 2100 (VisualSonics, Toronto, Canada) from *Jag1^{flox};cTnT-Cre, Jag2^{flox};cTnT-Cre* and WT littermates. LV long axis M-Mode views were obtained as described (Cruz-Adalia, Jimenez-Borreguero et al., 2010). From these images, interventricular septum end-diastolic thicknesses was measured, and LV systolic function was assessed by estimating LV shortening fraction (SF) and LV ejection fraction (EF) (Cruz-Adalia et al., 2010).

Cardiac MRI

6-month-old male mice were anaesthetized by inhalation of isoflurane/oxygen (2%) and monitored by ECG and breathing rhythm (Model 1025, S.A. Instruments Inc.) Images were acquired with an Agilent/Varian 7 Tesla system equipped with a DD1 console and an active shielded 205/120 gradient insert coil with 130 mT/m maximum strength and a combination of volume coil/two channel phased-array (Rapid Biomedical GmbH, Rimpar, GermainY) for transmit/receipt. Data were collected in a triggered cine gradient echo sequence with TE=1.45 ms and TR= 7ms, FA 25º, 20 cardiac phases, and NA (number of averages) =3. A total of 13 contiguous slices in short axis view were acquired, with a slice thickness of 0.8 mm. The field of view was 3x3cm, with a 256x256 matrix. Left ventricle (LV) and right ventricle (RV) function, end-diastolic volume, mass and wall thickness of right ventricle were estimated by the Simpson method, which sums the RV end-diastolic areas from the 13 slices in short axis view and multiplies this figure by the 0.8 mm slice thickness. Images were processed using OsiriX (Pixmeo, Geneva, Switzerland) and Medis MASS software (The Netherlands) to calculate every RV area by segmentation of end-diastolic epicardial and endocardial edge (van de Weijer, van Ewijk et al., 2012).

3D structure prediction

In-silico models for the extracellular domain (ECD) of mature Notch1 (N1), Dll4, Jag1 and Jag2 proteins were calculated using a "de novo" prediction method with structural homologue comparison. A partial X-ray or NMR structure was used as template/constrain for each model. The Fasta sequences of the ECD for mature Notch1 (UniProtKB: Q01705,N-term of 1499 aa), Dll4 (UniProtKB: Q9JI71, 506 aa), Jag1 (UniProtKB: Q9QXX0, 1034 aa) and Jag2 (UniProtKB: Q9QYE5, 1059 aa) were used for modeling with local implementation of iTASSER suite. A model template restraint (2rr2 for Notch1 or 2vj2B for DLL4, Jag1 and Jag2) was used for prediction. The PDB model with the best C-score (more stability) compatible with previously established biological and structural properties previously established for each prediction was selected. Notch1 dimer (N1d). To find the region implicated in dimerization, two Fasta sequences of the mature NECD were submitted to the Spring Server (http://zhanglab.ccmb.med.umich.edu/spring). The X-ray structure 3etoA was selected and aligned with two monomers previously modeled with PyMol application v1.6.0.0 (http://www.pymol.org/). The aligned structures were assembled, remodeled and refined in a new final homodimer model using the Backrub application of the Rosseta suite v 3.5 (https://www.rosettacommons.org/). The model with the best score (more stability and smaller free energy) was selected. Docking. The stoichiometry of the Dll4:Notch1 ligand-receptor pair was previously established as 1:1 and we assumed that this stoichiometry holds for all Notch1 ligands. To model ligand-receptor docking, we pre-aligned the Notch1 homodimer (chain A) with one monomer of each ligand close to the interaction-binding site using PyMol v1.6.0.0 (http://www.pymol.org/). Each very preliminary structure was modeled using the docking protocol of the Rosseta suite v 3.5 (https://www.rosettacommons.org/) with the local refinement and energy minimization option selected. For each structure, 1000 models with a side-chain conformer range between 50000 and 100000 (average 70000) were calculated, scored, clustered and filtered by biological, topological and energy properties. The model most compatible with biological and topological properties and with the smallest free energy was selected. To obtain the final models for N1d-2Dll4, N1d-2Jag1, N1d-2Jag2, N1d-Jag1Jag2 and N1d-Jag2Jag1, a second ligand was pre-aligned with the Noch1 B chain of the previous models and the pipeline was repeated.

Statistics.

Statistical analyses were performed using Student's t test inGraph Pad (Prism 5.0). Data are presented as means ± s.d., unless otherwise indicated. Differences were considered statistically significant at $P < 0$.

RESULTS

Endocardial Dll4 and myocardial Jag1 are candidate Notch ligands in the early mouse heart

In the developing ventricle the Notch activity was monitored using a recently described murine transgenic line *CBF1:H2B-Venus*, a bright single-cell resolution Notch reporter activity (Nowotschin et al., 2013). The CBF:H2B-Venus reporter carries human histone H2B fused to the bright yellow fluorescent protein Venus under the control of four RBPJK/CBF1 responsive elements (CBFRE) and the simian virus 40 (SV40) minimal promoter.

From E8.5, the CBF:H2B-Venus reporter was observed in the somites and in the endocardium of the forming heart (Fig. 6a). At E9.5 we detected expression of the reporter in endothelial cells of the dorsal aorta, as well as in the intersomitic vessels and in the pharyngeal arch arteries. In the heart the expression of the reporter was restricted to endocardial cells of the developing ventricle and the AVC (Fig. 6b). To better characterize the expression pattern of *CBF:H2B-Venus* during trabeculation, we performed triple-whole-mount staining of E9.5 *CBF:H2B-Venus* hearts. We used α-smooth muscle actin (SMA) as a marker of myocardium, CD31/Pecam1 to stain endocardial cells and GFP to label the *CBF:H2B-Venus* positive cells. Confocal imaging and 3D reconstruction of E9.5 *CBF:H2B-Venus* hearts revealed colocalization of Venus-positive cells with CD31/Pecam staining confirming Notch reporter activity only in endocardial cells (Fig. 6c-c'' and video 1). The endocardial expression of *CBF:H2B-Venus* throughout chamber endocardium was confirmed with two-photon imaging at E9.5 (Fig. 6d), while its expression was strongly down-regulated in the endocardium of *Notch1* (Fig. 6e) and *RBPJk* (Fig. 6e) null mutant embryos carrying the *CBF1:H2B-Venus* transgene. The finding that the abrogation of *Notch1* dramatically impaired Notch activity in the endocardium suggests Notch1 as the main receptor triggering Notch activity during early chamber development.

To elucidate which ligand was responsible for endocardial Notch activitation during myocardial trabeculation we stained E8.5 and E9.5 *CBF1:H2B-Venus* reporter embryos with antibodies against Dll4 and Jag1. A GFP antibody was used to detect *CBF1:H2B-Venus* expression and myocardium was counterstained with SMA. At E8.5, the ligand Dll4 was preferentially expressed in the endocardium (Fig. 6g-g''), while Jag1 was expressed all over the chamber myocardium with stronger expression in the cardiomyocytes forming the trabeculae (Fig. 6h-h''). At E9.5, Dll4 was strongly detected in the endocardium at the base of the trabeculae and to a lesser extent in interventricular endocardium (Fig. 6i-i''). Jag1 expression remained confined to the developing trabecular myocardium (Fig. 6k-k''). The expression of both ligands was coincident with sites of *CBF:H2B-Venus* activity (Fig. 6g-k'').

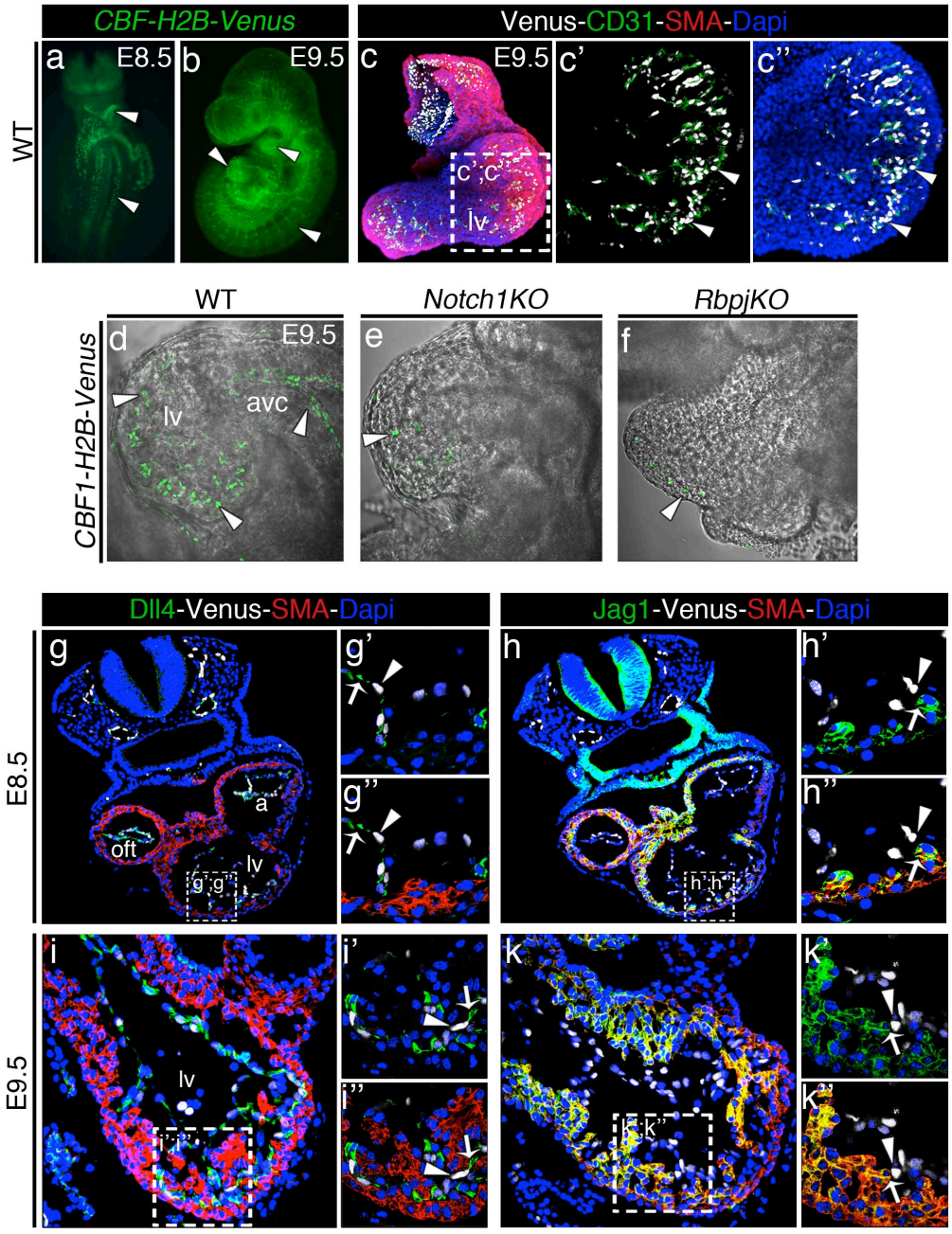

Endocardial Dll4-Notch1 Signaling is necessary for Trabeculation

To determine the role of Dll4 during heart development we crossed mice bearing a conditional *Dll4*^{flox} allele (Koch et al., 2008) with two different *Cre*-lines according to the Dll4 expression pattern. We used the pan-endothelial and pan-endocardial driver line *Tie2-Cre* (Kisanuki et al., 2001). To avoid possible secondary effects due to the lack of Dll4 in the vasculature, where it plays a pivotal role during vasculogenesis (Krebs, Shutter et al., 2004), we also used the pan-endocardial driver line *Nfatc-Cre* (Wu et al., 2012).

Figure 6. Dll4, Jag1 and Notch activity in ventricular endocardium.
(a-b) Stereo widefield image of a frontal view of an E8.5 (a) and later view of E9.5 (b) embryo expressing *CBF:H2B-Venus*. Arrowheads indicate strong expression of the reporter (Notch activity) in endocardial cells and somites (a), intersomitic vessel, pharyngeal arch arteries and endocardium in the looped heart (b). (c-c'') 3D view of triple whole-mount immunohistochemistry (IHC) for smooth-muscle actin (SMA), CD31/PECAM-1 and GFP in a E9.5 WT *CBF:H2B-Venus* heart. In c', note that Notch activity detected by GFP expression (arrowheads) colocalizes with CD31-positive cells (green) in the endocardium. (d-f) Two-Photon whole-mount images of the left ventricle of E9.5 WT *CBF:H2B-Venus* mice (d), *CBF:H2B-Venus;Notch1KO* mice (e) and *CBF:H2B-Venus;RbpjKO* mice (f). Arrowheads indicate endocardial Venus expression in WT mice (d) and the much lower expression in *Notch1KO* and *RbpjKO* mice (e,f). Triple IHC of Dll4, SMA, and GFP in E8.5 (g-g'') and E9.5 (i-i'') WT *CBF:H2B-Venus* paraffin sections. GFP-positive cells (gray, arrowheads) are in contact with cells expressing Dll4 (green, arrows) in the endocardium of the developing chamber (g-g''). At E9.5 a similar expression pattern is observed at the base of the trabeculae (i-i''). (h-k'') Triple IHC of Jag1, SMA, and GFP in E8.5 (h-h'') and E9.5 (k-k'') WT *CBF:H2B* paraffin sections. GFP-positive cells are adjacent to developing trabeculae expressing Jag1 (green, i-k''). In h';k' note that myocardial Jag1 is more strongly expressed in cardyomyocytes forming trabeculae comparing with those delineating the outer layer of the ventricle (i-k''). In (c-c'' and g-k'') nuclei are counterstained with DAPI. a= atrium; lv= left ventricle; avc=atrio-ventricular canal; oft= outflow tract.

Initially, we monitored Cre activity by crossing the *R26R;LacZ* reporter line (Soriano, 1999) with *Nfatc1-Cre*. Whole-mount X-gal staining in E8.5 and E9.0 *Nfatc1-Cre;LacZ* embryos revealed strong expression of the reporter gene in endocardial cells of the developing heart (Fig. 7a-b). At mid-gestation the endocardial-Cre activity was confirmed by *Nfatc1-Cre* transgenic mice bearing the *R26R;YFP* reporter (Srinivas et al., 2001). At E9.5 YFP expression was restricted to the endocardium confirming *Nfatc-1-Cre* line as a perfect tool for the endocardial-specific deletion of *Dll4* (Fig. 7c). In addition, we crossed mice bearing a conditional $Notch1^{flox}$ (Radtke et al., 1999) allele with *Nfatc1-Cre*. Based on previous observations that Notch1 is the main Notch receptor involved in trabeculation, we compared the heart phenotype of this mutant with *Dll4* conditional mutants.

Targeted inactivation of *Dll4* with the *Tie2-Cre* driver caused embryonic lethality at day E10. Conditional deletion of *Dll4* or *Notch1* with *Nfatc1-Cre* delayed embryonic lethality until E11.5-E12.0. To characterize the morphology of the heart, we stained heart sections of E9.5 $Dll4^{flox}$*;Tie2-Cre,* $Dll4^{flox}$*;Nfatc-Cre* and $Notch1^{flox}$*;Nfatc1-Cre* embryos with an antibody against the rod-like tail region of myosin heavy chain protein (MF20) to mark the myocardium and with an antibody against CD31/Pecam1 to delineate the endocardium. The $Dll4^{flox}$*;Tie2-Cre* (Fig. 7e-e') as well as the $Dll4^{flox}$*;Nfatc1-Cre* (Fig. 7e-e') mutant embryos showed hypoplastic ventricles and impaired trabeculation compared to controls (Fig. 7f-f'). In both mutants a strong phenotype was also observed in the AVC, where very few endocardial cells were able to undergo EMT (Fig. 7d-f'). The phenotypes caused by the inactivation of $Dll4^{flox}$ with either of these driver lines were very similar to those observed in the E9.5 $Notch1^{flox}$*;Nfatc1-Cre* mutant embryos (Fig. 7g-g').

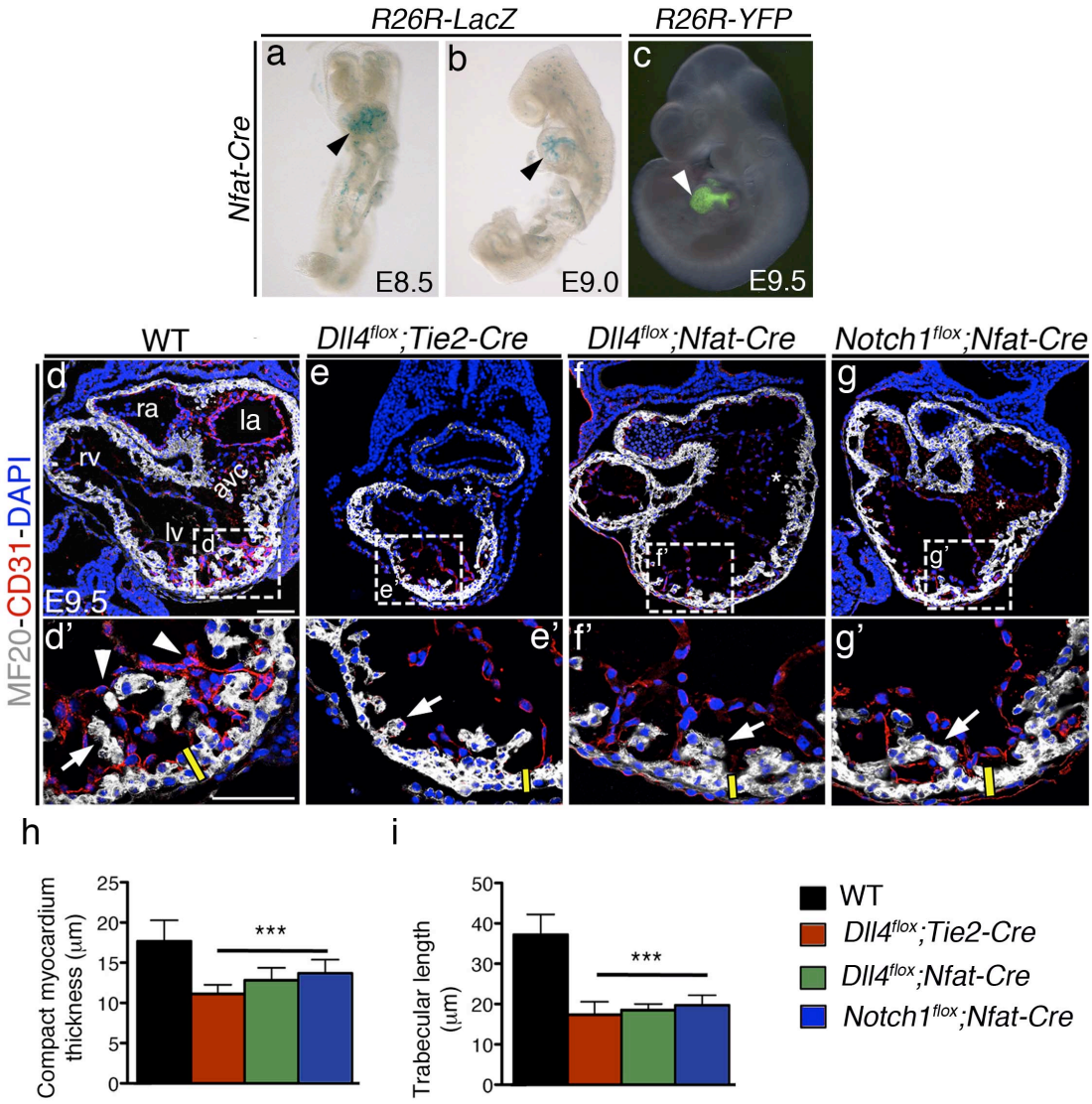

Figure 7. Abrogation of endocardial Dll4-Notch1 signaling disrupts trabeculation.
(**a-b**) LacZ-expressing cells (blue) in *Nfat-Cre;R26R* E8.5 (**a**) and E9.0 (**b**) WT embryos. Arrowheads indicate the strong expression of the reporter gene in the endocardium. (**c**) Stereo widefield image of a lateral view of an E9.5 *Nfat-Cre;YFP* mouse embryo shows YFP-expressing cells (green) only in the endocardium. (**d-g'**) IHC for MF20 (gray) and CD31 (red) in sections from E9.5 WT (**d,d'**), *Dll4^{flox};Tie2-Cre* (**e,e'**), *Dll4^{flox};Nfat-Cre* (**f,f'**) and *Notch1^{flox};Nfat-Cre* embryos (**g,g'**). Arrowheads indicate the endocardium and arrows the trabecular myocardium. Note the absence of mesenchymal cells in the AVC (asterisks) of the mutants (d-g'). The yellow bars indicate the thickness of the nascent compact myocardium. (**h**) Quantification of compact myocardium thickness and (**i**) trabecular length in E9.5 WT, *Dll4^{flox};Tie2-Cre*, *Dll4^{flox};Nfat-Cre* and *Notch1^{flox};Nfat-Cre* embryos. Data are represented as mean ± S.D. (3 WT and 3 mutant embryos of each genotype, ***P < 0.001, determined by Student's *t* test). ra= right atrium; la=left atrium; rv= right ventricle; lv= left ventricle; avc=atrio-ventricular canal. Scale bar=50μm.

Endocardial inactivation of *Notch1* caused hypotrabeculation in the ventricle and reduced EMT in the AVC region. Parameters of ventricular morphology were quantified by measuring the thickness of the primitive compact myocardium (Fig. 7h) and trabecular length (Fig. 7i) of MF20- and CD31/Pecam1-stained E9.5 WT and mutant hearts. Both parameters were significantly reduced in mutant embryos (around 28% and 50% reduction, respectively; Fig. 7h-i). The morphological analysis suggested that from the endocardium Dll4 interacts and activates Notch1. To confirm this hypothesis we performed immunostaining against the activated form of Notch1 (N1ICD) in E9.5 WT and *Dll4* mutant heart sections. In E9.5 WT embryos, in the developing chamber the expression of N1ICD is restricted to the endocardium, particularly in the endocardial cells located at the base of the forming trabecuale (Fig. 8a-a'). The N1ICD expression was almost 50% below normal in E9.5 *Dll4^{flox};Nfatc1-Cre* (Fig. 8b-b' and Fig. 8d). The number of endocardial cells expressing the active form of Notch1 was even lower, reaching 70% of reduction in the *Dll4^{flox};Tie2-Cre* mutant embryos (Fig. 8c-c' and Fig. 8d) comparing with controls. This result confirmed that during early heart development Dll4 is required for Notch1 activation. We then assayed by *in situ* hybridization (ISH) the expression of different cardiac markers implicated in chamber morphogenesis. In the ventricle of E9.5 *Dll4^{flox};Tie2-Cre* embryos *Hey2* transcription delineates a thin compact myocardium layer with a reduction in the endocardium, where this gene is a direct target of Notch activity (Fig. 8e-f). Mutant embryos also displayed reduced transcription of *EfnB2* (Fig. 8g-h) and *Nrg1* (Fig. 8i-j) in endocardial cells as well as reduction of myocardial *Bmp10* (Fig. 3k-l), previously shown to depend on Notch activity (Grego-Bessa et al., 2007). All these data clearly identified Dll4 as the ligand indispensable for triggering Notch1 activity during trabeculation.

Comparative transcriptome analysis of E9.5 WT and mutant hearts indicates Dll4-Notch1 signaling as crucial for cardiomyocyte proliferation

To identify the molecular targets downstream of Notch activation, we performed comparative transcriptome profiling by RNA sequencing (RNA-seq) analysis of gene expression in WT, *Dll4^{flox};Tie2-Cre, Dll4^{flox};Nfatc1-Cre* and *Notch1^{flox};Nfatc1-Cre* hearts at E9.5. RNA-seq identified 2101 affected genes in *Dll4^{flox};Tie2-Cre* mutants (1179 up-regulated and 922 down-regulated), 1321 in *Dll4^{flox};Nfatc1-Cre* mutants (916 up-regulated and 405 down-regulated) and 631 (472 up-regulated and 159 down-regulated) in *Notch1^{flox};Nfatc1-Cre* mutants ($P \leq 0.05$; Fig. 9a and supplementary table1).

Comparison of expression profiles showed that the three mutants shared 142 differentially expressed genes, while *Dll4^{flox};Tie2-Cre* and *Dll4^{flox};Nfatc1-Cre* mutants shared 702 altered genes, *Dll4^{flox};Tie2-Cre* and *Notch1^{flox};Nfatc1-Cre* mutants shared 238 and *Notch1^{flox};Nfatc1-Cre* and *Dll4^{flox};Nfatc1-Cre* mutants shared 202 (Fig. 9b and supplementary table1).

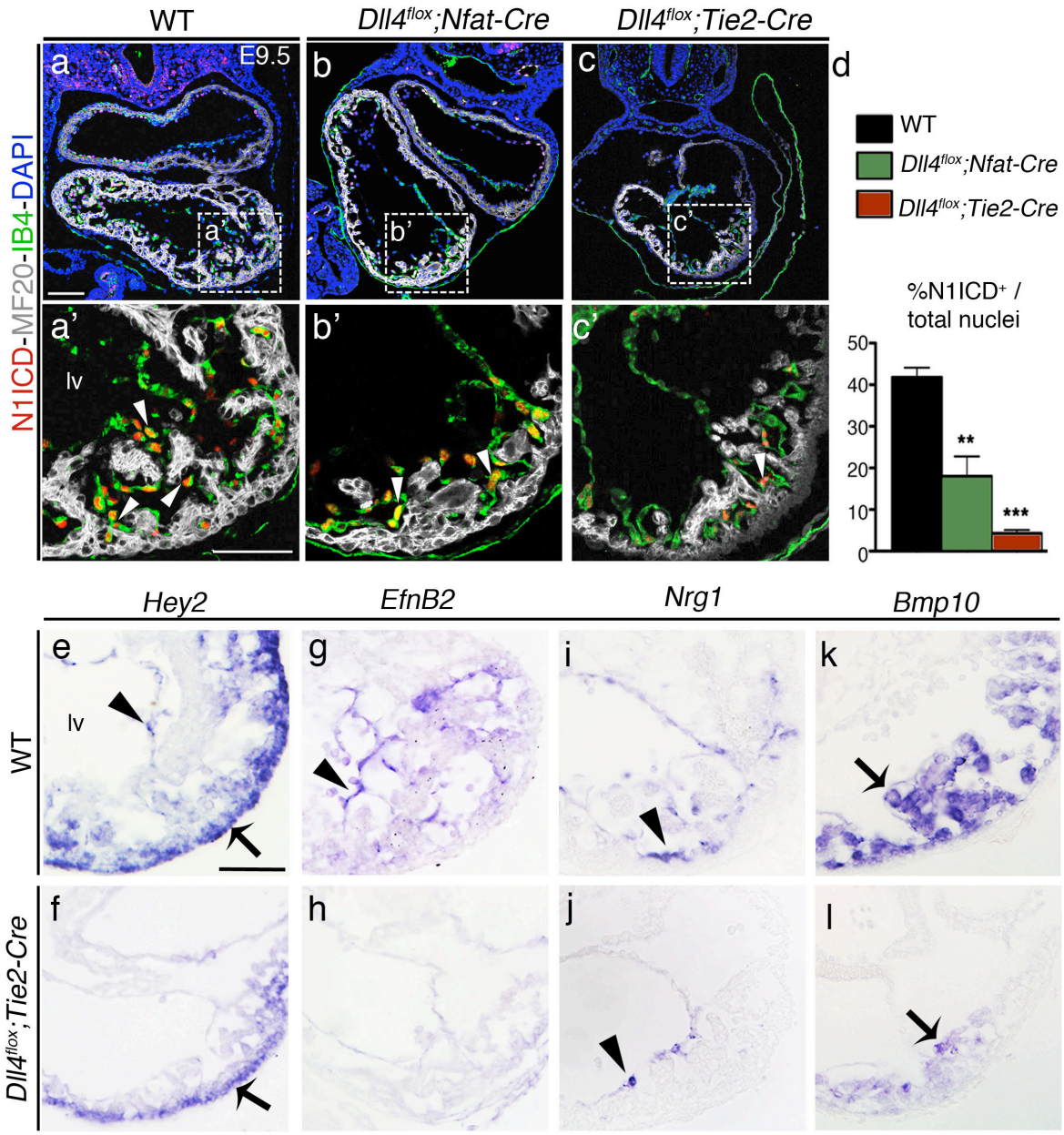

Figure 8. Dll4 activates Notch1 in the ventricular endocardium during trabeculation.
(**a-c'**) IHC of N1ICD (red nuclei) in E9.5 WT (**a,a'**), *Dll4^{flox};Nfat-Cre* (**b,b'**) and *Dll4^{flox};Tie2-Cre* (**c,c'**). The myocardium was counterstained with MF20 (gray) and the endocardium with isolectinB4 (IB4, green). Arrowheads indicate the nuclear expression of N1ICD in the endocardium expressing IB4. Note the reduced number of N1ICD positive cells in the ventricle of *Dll4^{flox};Tie2-Cre* (**c,c'**). (**d**) Ratios of N1ICD-positive to total endocardial nuclei. Data are represented as mean ± S.D. (3 WT ;3 *Dll4^{flox};Nfat-Cre* and 3 *Dll4^{flox};Tie2-Cre* mutant embryos, **P<0.01, ***P<0.001 by Student's *t* test) . (**e-l**) WISH analysis of E9.5 WT and *Dll4^{flox};Tie2-Cre* embryos. Expression levels of *Hey2* (**e-f**), *EphrinB2* (**g-h**) and *Nrg1* (**i-j**) are lower in the endocardium of mutant embryos Arrowheads indicate endocardial expression of the gene whereas arrows its myocardial expression. lv= left ventricle. Scale bar =50µm.

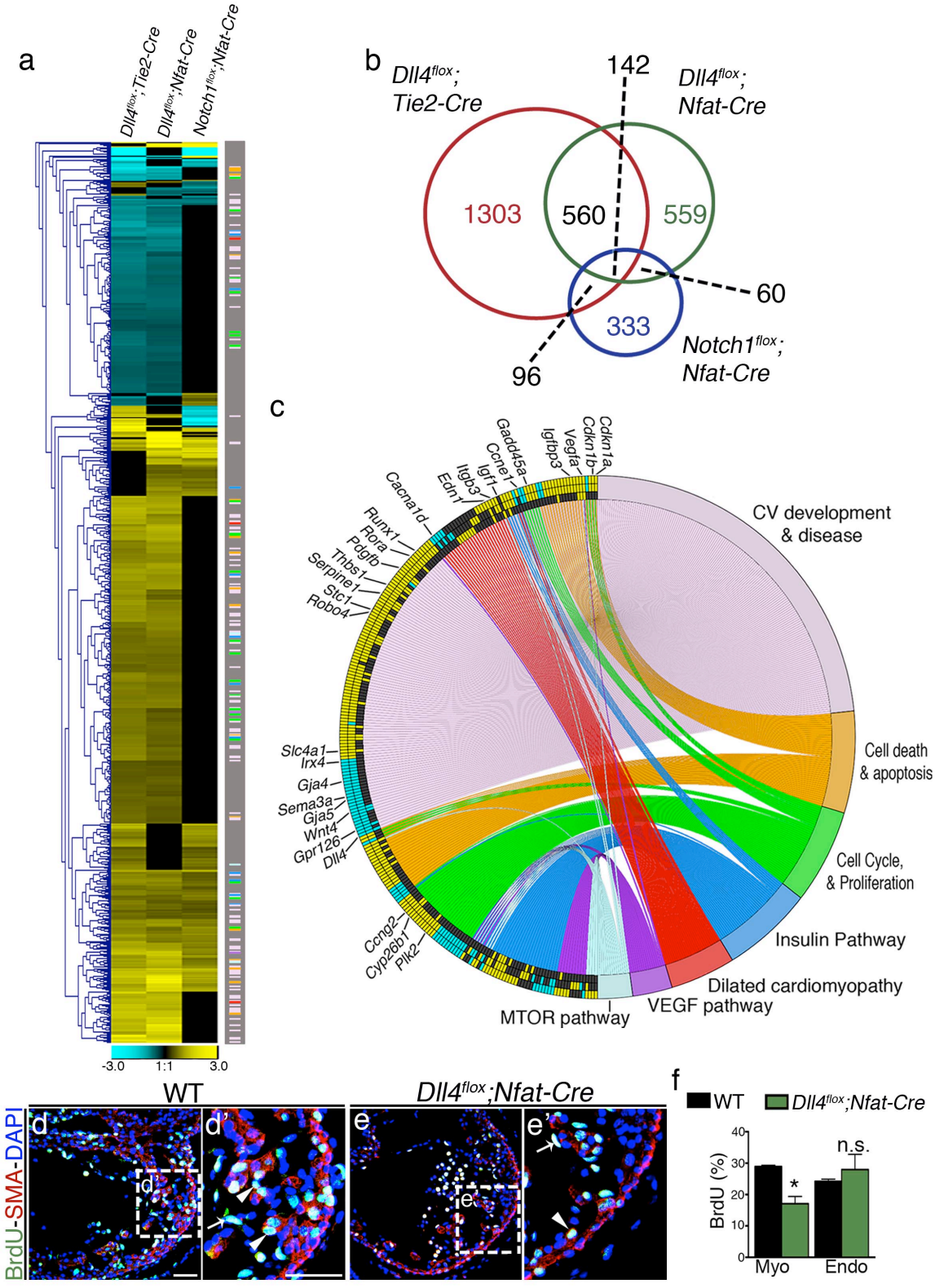
a
Dll4flox;Tie2-Cre
Dll4flox;Nfat-Cre
Notch1flox;Nfat-Cre
-3.0
1:1
3.0
b
Dll4flox; Tie2-Cre
Dll4flox; Nfat-Cre
Notch1flox; Nfat-Cre
1303
560
559
333
142
60
96
c
CV development & disease
Cell death & apoptosis
Cell Cycle, & Proliferation
Insulin Pathway
Dilated cardiomyopathy
VEGF pathway
MTOR pathway
Cdkn1a
Cdkn1b
Vegfa
Igfbp3
Gadd45a
Ccne1
Igf1
Itgb3
Edn1
Cacna1d
Runx1
Rora
Pdgfb
Thbs1
Serpine1
Slc1
Robo4
Slc4a1
Irx4
Gja4
Sema3a
Gja5
Wnt4
Gpr126
Dll4
Ccng2
Cyp26b1
Plk2
WT
Dll4flox;Nfat-Cre
BrdU-SMA-DAPI
d
d'
e
e'
f
WT
Dll4flox;Nfat-Cre
BrdU (%)
40
30
20
10
0
*
n.s.
Myo
Endo

Figure 9. Comparative gene expression profiling of E9.5 WT, *Dll4* and *Notch1* mutant hearts. Notch signaling mediates trabecular proliferation.
(**a**) Heat map from hierarchical clustering of differentially expressed genes ($P<0.05$) identified by RNA-seq in the indicated genotypes. For each genotype up-regulated genes are indicate in yellow; down-regulated genes are represented in blue. Note that the vast majority of dysregulated genes in the three mutants change in the same direction. (**b**) Venn diagram representation of the comparative analysis of the dysregulated genes in the three genotypes. Numbers in black indicate the total number of genes common to all pair-wise genotype combinations. (**c**) Circular plot of 257 differentially expressed genes belonging to various functional categories relevant to this study, simultaneously presenting a detailed view of the relationships between expression changes (left semicircle perimeter) and processes (right semicircle perimeter). In the left semicircle perimeter, the inner ring represents *Notch1^{flox};Nfat-Cre* data, the middle ring *Dll4^{flox};Nfat-Cre* data, and the outer ring *Dll4^{flox};Tie2-Cre* data. Twenty-eight of the 257 genes are named. (**d-e'**) BrdU proliferation analysis of E9.5 WT (d,d') and *Dll4^{flox};Nfat-Cre* mutants (e,e') performed in paraffin sections. The myocardium is counterstained with SMA (red). Arrowheads indicate the proliferative cells (BrdU-positive nuclei) in the myocardium; arrows indicate BrdU-positive nuclei in the endocardium. (**o**) Quantification of BrdU-positive nuclei as a percentage of total nuclei in myocardium (Myo) and endocardium (Endo). Data are represented as mean ± S.D. (3 WT and 3 *Dll4^{flox};Nfat-Cre*, *P<0.05, n.s. not significant, by Student's *t* test). Scale bar=50μm.

Gene ontology (GO) classification revealed deregulation of several genes involved in cardiovascular development and disease (*Wnt4, Gja5, Irx4*), cell cycle, growth and proliferation, cell death (*Ccne1*/*cyclin E1*, *Cited1*), dilated cardiomyopathy (*Myh6, Tnnc1, Tnnt2*) and several intercellular signaling pathways (Insulin, Vegf and mTOR pathways, Fig.9c and supplementary table1). *Dll4^{flox};Tie2-Cre* and *Dll4^{flox};Nfatc1pan-Cre* mutants showed up-regulation of the negative regulators of cellular proliferation *Cdkn1a/p21*, *Cdkn1b*, *Gadd45a*, *Foxo3*, *Cbx7*, *Ccng2*, *Ndrg1*, *Myct1* and *Runx1* (Fig. 9c and supplementary table1).

In agreement with these findings, cardiomyocyte proliferation in *Dll4^{flox};Nfatc1pan-Cre* mutants as measured by 5-bromodeoxyuridine (BrdU) incorporation was 42% below normal (Fig. 9d-f). In contrast, in the mutant hearts the proliferation of endocardial cells was similar to WT (Fig. 9d-f). These results show that abrogation of the Dll4-Notch1 interaction impairs cardiomyocyte proliferation in a non-cell-autonomous manner, suggesting that endocardial Dll4-Notch1 activity mediates expression of genes encoding signals that link ventricular endocardium and myocardium and are essential for trabeculation.

Dll4-Notch1 signaling triggers the expression of *Gpr126* in the endocardium

One of the most downregulated gene in all three genotypes was that encoding the signaling molecule Gpr126 (DREG) (Fig. 9c and supplementary table1), a member of the orphan adhesion G protein-coupled receptor family whose expression in the developing heart is restricted to the endocardium. In a recent work, it has been shown that targeted inactivation of Gpr126 in mice causes hypotrabeculation and a thinner ventricular wall (Patra et al., 2013, Waller-Evans, Promel et al., 2010). In this report, Patra and co-workers, hypothesized that the N-terminal fragment (NTF, 1-783 aa) of *Gpr126* functions independently of its C-terminal fragment (CTF) during heart development presumably in a paracrine fashion as an important signal linking endocardium and myocardium.

At E9.5 *Gpr126* was transcribed in the endocardium with a remarked expression at the base of the trabeculae where Notch1 activity is predominant (Fig. 10a-a'). *Gpr126* expression was severely down-regulated in the endocardium of *Dll4^{flox};Nfatc1-Cre* mutants (Fig. 10b-b'). Interestingly, zebrafish cardiac expression of the *Gpr126* homolog was abrogated in *Mib1^{ta52b}* mutant larvae, which are deficient for the Notch pathway (Fig. 10c-d'), and after treatment of WT larvae with the Notch inhibitor RO4929097 (Munch, Gonzalez-Rajal et al., 2013) (Fig. 10e-e'). Endocardial expression of *Gpr126*, the trabecular phenotype of the targeted mutant mice (Patra et al., 2013, Waller-Evans et al., 2010) and its down-regulation in mouse and zebrafish Notch mutants suggested it as a Notch target during trabeculation.

To substantiate the relationship between Notch and *Gpr126*, we conducted qRT-PCR analysis on human umbilical vein endothelial cells (HUVEC) stimulated with immobilized Dll4 ligand. Dll4 stimulation increased *Gpr126* expression in HUVEC, while simultaneous incubation with RO4929097 blocked this increase (Fig. 10f). As a control we determined the effect of Dll4 stimulation on the transcription of Notch targets *Hey1*, *Hey2*, *HeyL*, *Dll4* and *Nrarp*. Upon Dll4 stimulation the expression of all targets examined was significantly increased comparing with unstimulated cells (Fig. 10g).

In silico comparative genomic analysis of *Gpr126* revealed two conserved putative RBPJ-binding sites in the intronic region between exons 4 and 5 (Fig. 10h). The predicted RBPJ-binding sites were located 445 base pairs apart and were highly conserved among distantly related mammals (*mouse, rat, monkey, pig and human*) (Fig. 10i). We cloned the human genomic region containing these sites upstream of the firefly luciferase gene and performed luciferase assays in bovine aortic endothelial cells (BAEC). BAEC co-transfected with the reporter plasmid and empty vector showed basal luciferase activity, whereas increasing amounts of N1ICD were able to transiently activate the *Gpr126* reporter construct up to 5-fold in a dose-dependent manner (Fig. 10j). All these data indicate *Gpr126* as a possible new target of Notch1 activity in the endocardium during trabeculation.

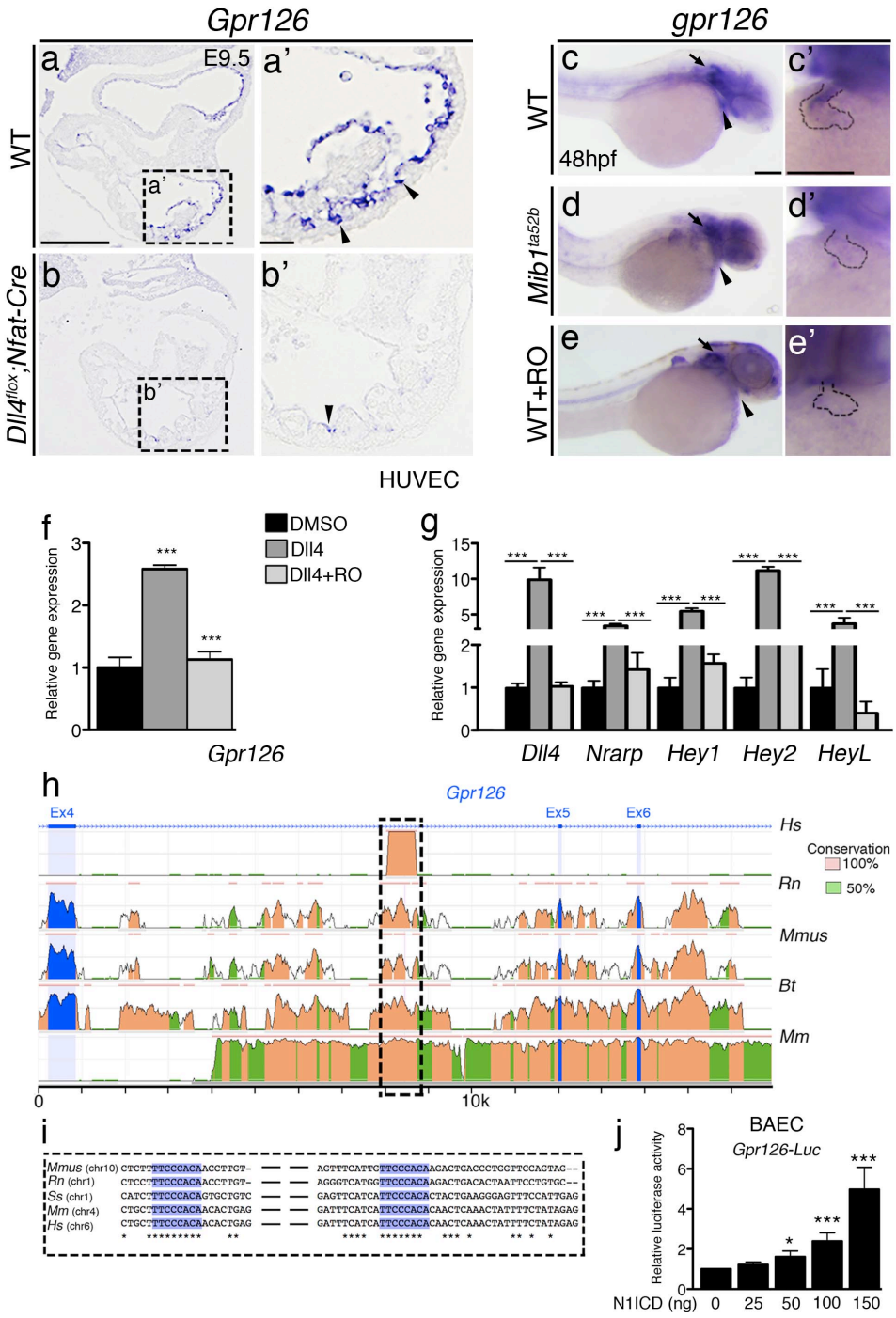

Dll4 is required for coronary vessel development during compaction

During late midgestation Dll4 expression in the heart is progressively reduced in the endocardium. In E12.5 WT heart sections we detected expression of Dll4 in the endothelium of the AVC region and in the endocardium of the right and left ventricle (Fig. 11a-a'). Interestingly, as coronary vessel development proceeds, its mRNA expression was dramatically reduced in the endocardium of both ventricles but in the forming coronary artery *Dll4* transcription was abundant (Fig. 11b-b').

Figure 10. Dll4-Notch1 sigaling induces endocardilal expression of *Gpr126*.
(**a-b'**) WISH of *Gpr126* in E9.5 WT (**a,a'**) and *Dll4^{flox};Nfat-Cre* hearts (**b,b'**). *Gpr126* is down-regulated in the endocardium (arrowheads) of mutant embryos. Scale bar=100µm. (**c-e'**) Reduced *gpr126* expression in zebrafish larvae with impaired Notch signaling. Panels show lateral and ventral views. Lateral and ventral views of the ISH of *gpr126* in WT (**c**,**c'**, 27 out of 29; 93%), *Mib1^{ta52b}* mutant (**d,d'**, 35 out of 38; 92%) and RO-treated WT (**e,e'**, 19 out of 22; 86%), 48-h.p.f. zebrafish embryos showing *gpr126* transcripts in the heart tube (arrowhead) and ear region (arrow) in **c**, and reduced expression in **d,e**. Scale bar=50µm. (**f-g**) qRT-PCR analysis in HUVEC stimulated with immobilized Dll4 alone or in the presence of the γ-secretase inhibitor RO. Dll4 significantly increases expression of *Gpr126 (***f**), *Dll4, Nrarp*, *Hey1*, *Hey2* and *HeyL (***g**) in HUVEC and simultaneous incubation with RO abolishes this effect (**f-g**). Data are represented as mean ± S.D. (3 independent biological replicates for each condition ***P<0.001, by Student's *t* test.). (**h**) Screening for evolutionarily conserved sequences using rVista 2.0 of Gpr126 locus in Homo sapiens (*Hs*), Bos taurus (*Bt*), Macaca mulatta (*Mm*), Rattus norvegicus (*Rn*) and Mus musculus *(Mmus)*. The chart shows a 17 Kb of the genomic region of Gpr126 in the different species analyzed. Two potential RBPJk binding sites were identified in the region between exon 4 and exon 5 (dot line). (**i**) Genomic alignment of the intronic region containing the two potential Rbpjk binding (blue box). Note the RBPJk consensus is highly conserved in all sequences analysed. (**g**) *Gpr126* reporter activity measured by luciferase assay in BAEC. Transfection with an increasing gene dose of N1ICD significantly increases reporter activity. Data are representaed as mean ± S.D. (3 independent biological replicates for each condition *P<0.05, ***P<0.001, by Student's *t* test.). Scale bar=50µm.

We therefore wanted to determine if this ligand plays a role at later stages of chamber development, when compaction occurs. In order to do this we combined the conditional *Dll4^{flox}* allele with the tamoxifen-inducible *Cre* driver line *Cdh5-Cre^{ERT}* (Luna-Zurita et al., 2010, Wang et al., 2010), which is active in both the endocardium and the vascular endothelium. *Dll4$^{flox/+}$;Cdh5-Cre$^{ERT/+}$* males were crossed with *Dll4$^{flox/flox}$* females. Pregnant females were administered with 4-hydroxy-tamoxifen (4-OHT) once by oral gavage at E12.5 and embryos were dissected at E15.5. *Dll4^{flox}*;*Cdh5-Cre^{ERT}* embryos were notably smaller in size than control littermates and showed edema in the back region, suggesting circulatory problems due to impaired vascularization (Fig. 11c;g). Histological analysis revealed reduction in the thickness of the ventricular wall in both left and right ventricles as well as hypoplastic trabeculae (Fig. 11d;h). To validate the efficiency of tamoxifen-inducible-Cre activity we performed *Dll4 ISH* in heart sections at E15.5. At this stage, the transcript was markedly reduced in the intramyocardial coronary artery of the mutants (Fig. 11e;i). These data confirmed that a single tamoxifen administration at E12.5 was sufficient to achieve a robust *Dll4* deletion in endothelial cells. Immunostaining revealed that N1ICD was still expressed in *Dll4^{flox}*;*Cdh5-Cre^{ERT}* chamber endocardium but was very weak in coronary vessels (Fig. 11f ;j). The compact myocardium of *Dll4^{flox}*;*Cdh5-Cre^{ERT}* mutant hearts showed normal *Hey2* expression (Fig. 11k;o) as well as normal expression of *Gja5* in the trabeculae (Fig. 11i;p).

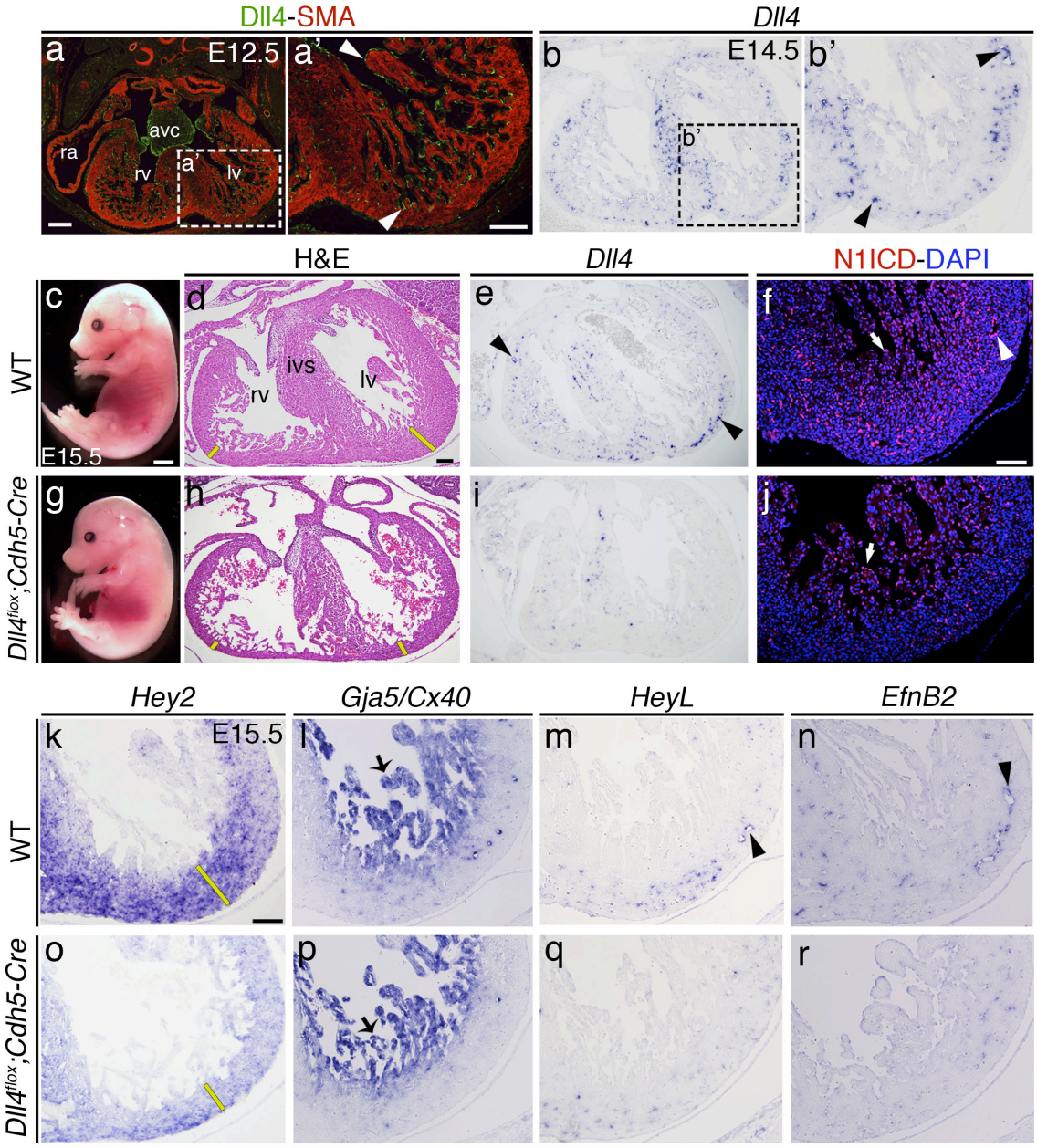

Figure 11. Dll4-Notch1 activity is required for coronary vessel formation.
(**a,a'**) IHC of Dll4 and SMA in an E12.5 WT heart section. Dll4 (green) is widely expressed in the endocardium lining the AVC (a) and to a lesser extent in endocardial cells in the ventricle (a', arrowheads). (**b-b'**) ISH of *Dll4* in an E14.5 heart section. *Dll4* is transcribed in the developing coronary endothelial cells (arrowhead) but not in the endocardium. (**c,g**) Images of whole-mount E15.5 WT (**c**) and *Dll4^{flox};Cdh5-Cre* mutant embryos (**c**). Note the dorsal edema (arrowhead) in the mutant embryos. Scale bar=2mm. (**d,h**) H&E stained sections of E15.5 WT (**d**) and *Dll4* mutant hearts (**h**). The heart in the mutant has thinner ventricular walls (**h**, yellow bars) than its WT littermate (**d**). (**e-i**) ISH of *Dll4* in E15.5 WT (**e**) and *Dll4* mutant hearts (**i**) shows reduced expression in the mutant (**i**). (**f-j**) N1ICD immunostaining. N1ICD marks the endocardium (arrowhead) and the coronary vessels (arrowhead) of WT ventricle (**f**) and is weak in coronary vessels of mutant embryos (**j**). (**k-r**) ISH analysis. (**k-o**) *Hey2* expression is similar in the compact myocardium of WT embryos (**k**) and mutants but it delineates a thinner compact myocardium in the mutant (yellow line, **k,o**). (**l,p**) *Cx40* is detected in the trabecular myocardium of WT (**l**) as well as in the trabeculae of *Dll4^{flox};Cdh5-Cre* (arrowheads, **p**), but not in the endothelium. The expression of coronary artery endothelial cell markers *HeyL* (**m-q**), *EphrinB2* (**n-r**) is markedly lower in mutant embryos. The arrowheads mark expression in coronary vessels in WT. Scale bar in (**a-b'and d-r**)=100μm.

In contrast in coronary vessels the expression of *Gja5* (Fig. 11 i;p), *HeyL* (Fig. 11m-q) and *EfnB2* (Fig. 11n-r) was abrogated. These results indicate that at the stages when trabecular compaction occurs, Dll4-Notch1 signaling is required for coronary vessel development, but Dll4 does not play a major role in the activation of Notch1 in chamber endocardium

Myocardial Jag1 is dispensable during trabeculation

We next examined the implication of the Jag1 ligand in chamber development. From early heart morphogenesis the expression pattern of Jag1 is restricted to the myocardium (Fig. 6h-h'' and Fig. 6k-k''). To specifically delete Jag1 in this tissue, we crossed mice bearing a conditional $Jag1^{flox}$ allele (Koch et al., 2008) with the early myocardial driver *cTnT-Cre* (Jiao et al., 2003).

Histological analysis of heart sections from E10.5 *Jag1* mutants revealed no obvious defects in the morphology of the heart (Fig. 12a-b). In *Jag1* mutants, the trabeculae were well formed and the thickness of the myocardial outer layer was similar to controls (Fig. 12a-b). To exclude that the lack of heart phenotype in the *Jag1flox;cTnT-Cre* mice was due to a weak Cre-recombinase activity, we stained mutant heart sections with a Jag1 antibody (Fig. 12c-d).

At E10.5 the expression of Jag1 in mutant hearts was detected only in the endocardium of the AVC confirming that *TnT-Cre* efficiently drives the deletion of $Jag1^{flox}$ in ventricular myocardium (Fig. 12c-d). Despite the complete absence of myocardial ligand, in E10.5 *Jag1* mutant embryos we did not detected significant differences in the expression of N1ICD compared to their WT counterparts (Fig. 12e-f and Fig. 12g). Additionally, the expression of *Hey2* (Fig. 12h-i), *EfnB2* (Fig. 12j-k), *Nrg1* (Fig. 12l-m) and *Bmp10* (Fig. 12n-o) appeared normal when compared with E10.5 control hearts. These results indicate that *Jag1* is not required for Notch1 activation during early ventricular chamber development.

Myocardial Jag1 signals to Notch1 and is required for adult heart function

Interestingly, the expression of Jag1 in ventricular myocardium persisted at later stages of heart development. At E12.5 Jag1 was strongly expressed in the trabeculae and at lower levels in the compact zone whereas the *CBF:H2B-Venus* reporter, detected by GFP, was expressed throughout the endocardium (Fig. 13a-a'') revealing Notch activity in this tissue. At E14.5 in the ventricles, the expression pattern of Jag1 was similar to those observed at E12.5. Moreover, at this stage Jag1 delineated the endothelium of the developing coronary vessels (Fig. 13b-b''). These data suggested that Jag1 from the myocardium could interact with Notch receptor in the adjacent endocardial cells during chamber compaction.

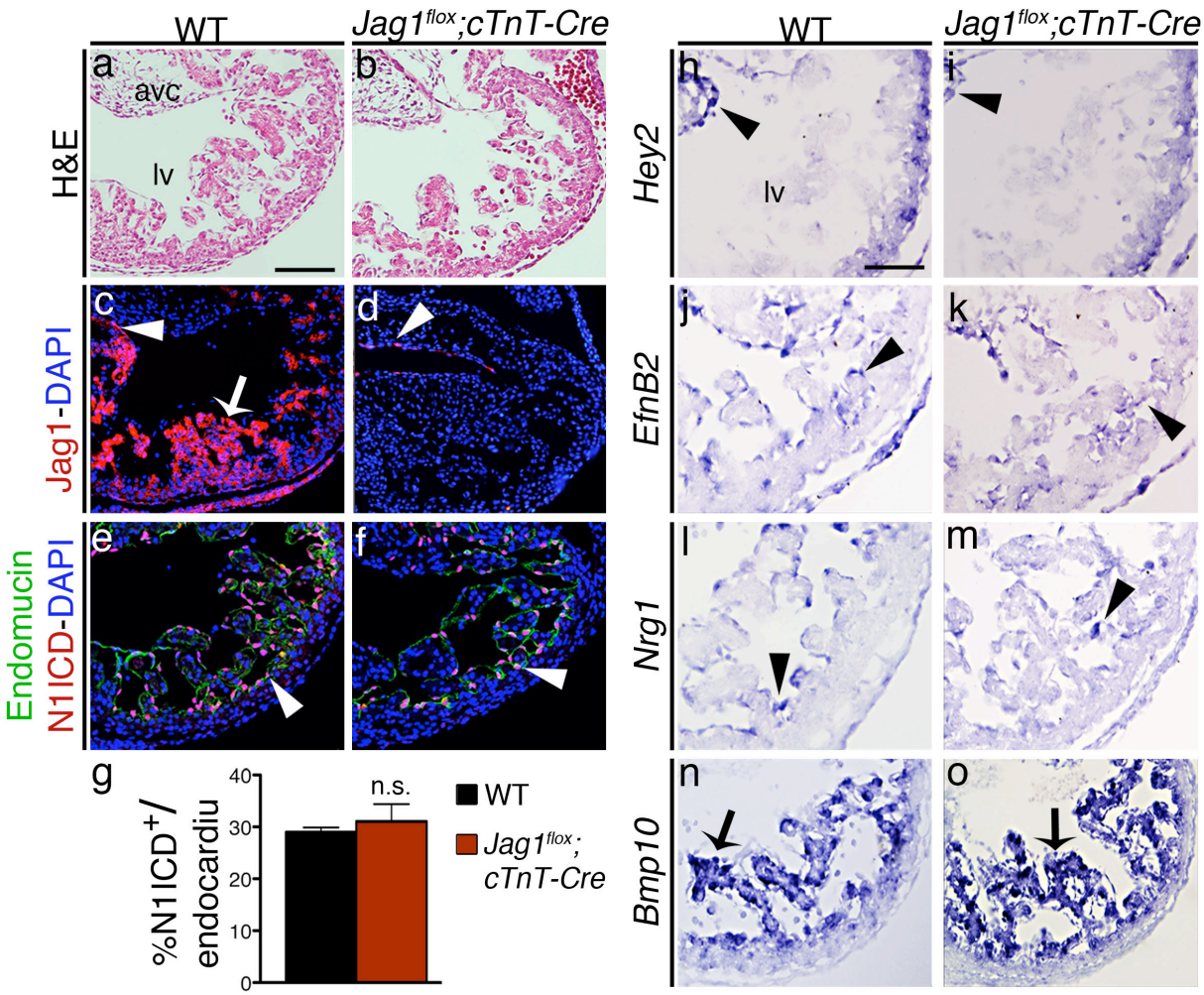

Figure 12. Myocardial Jag1 is dispensable for Notch signaling activation during trabeculation. (**a,b**) H&E staining of sections of E10.5 WT (**a**) and *Jag1*$^{flox/flox}$*;cTnT-Cre/+* (*Jag1*^{flox}*;cTnT-Cre*) mutant hearts (**b**). Trabeculae and compact myocardium thickness are similar in WT and mutant hearts. (**c,d**) Immunostaining of Jag1 in E10.5 WT and *Jag1*^{flox}*;cTnT-Cre* mutant embryos. Jag1 (red) is strongly expressed in the trabeculae of the WT ventricle (arrows, **c**) but is absent from the mutant ventricle (**d**). (**e,f**) N1ICD immunostaining (red, arrowheads) in the endomucin-delineated endocardium (green) of WT (**e**) and *Jag1*^{flox}*;cTnT-Cre* mutant embryos (**f**). (**g**) Quantification of N1ICD-positive nuclei as the mean percentage of total nuclei in WT and *Jag1*^{flox}*;cTnT-Cre* mutant embryos. Data are represented as mean ± S.D. (3 WT and 3 mutant embryos, determined by Student's *t* test, n.s. not significant). (**h-o**) ISH in E10.5 WT and mutant hearts. *Hey2* (**h,i**), *EphrinB2* (**j,k**), *Nrg1*(**l,m**), and *Bmp10* (**n,o**), are normally expressed in mutant hearts. Arrowheads indicate the endocardial expression of the genes; arrows myocardial expression of *Bmp10*. Scale bar=100μm.

Histological analysis of E16.5 WT mice showed well-developed compact myocardium and trabeculae (Fig. 13c-c'), whereas by comparison *Jag1^{flox};cTnT-Cre* embryos had thinner compact myocardium and disorganized trabeculae (Fig. 13d-d'). Newborn WT mice had a well-structured myocardium with muscular ventricular walls (Fig. 13e-e'), while *Jag1^{flox};cTnT-Cre* littermates had dilated ventricles and a thin compact myocardium (Fig. 13f-f'). These features were also apparent in the hearts of 6 month-old mutant mice (Fig. 13g-h'). We stained adult WT and mutant heart sections with Masson's trichome. Histological analysis evidenced that in mutants the wall of both ventricles was thinner and the heart appeared dilated compared with WT. In all sections analyzed we did not detect signs of fibrosis in the ventricles of the *Jag1^{flox};cTnT-Cre*.

We next asked if the morphological heart defects observed at different stages in *Jag1^{flox};cTnT-Cre* embryos may reflect impaired cardiac function in the mutant mice. Ultrasound analysis at 6 and 9 month old mice, revealed significantly impaired systolic function in the left ventricle of *Jag1^{flox};cTnT-Cre* mutants, with reduced ejection fraction, fractional shortening and diastolic interventricular septal wall thickness (Fig. 14a-b; g and video 2). As the majority of the morphological defects in *Jag1^{flox};cTnT-Cre* were observed in the right ventricle, to decipher possible cardiac dysfunction in the RV we submitted 6 month old *Jag1^{flox};cTnT-Cre* to high-resolution cardiac magnetic resonance imaging (CMRI). CMRI confirmed significant reduction in the thickness of the free wall of the right ventricle in *Jag1^{flox};cTnT-Cre* animals (Fig. 14c-f-b; h and video 3) that also showed segmental dyskinesia (video 4). Functional parameters as cardiac output, end-systolic (ES) mass, and end-diastolic (ED) volume in the LV and RV were below normal in mutant mice (Fig. 14h).

Notably, CMRI analysis confirmed significant reduction in *Jag1* mutant mice in left ventricular ejection fraction (EF, Fig. 14h), previously observed by ultrasound analysis (Fig. 14g). In the right ventricle we did not observe differences in EF between mutant and control animals. These results indicate that myocardial Jag1 signaling to Notch1 in the endocardium is not required for trabeculation but is later crucial for adult heart structure and function.

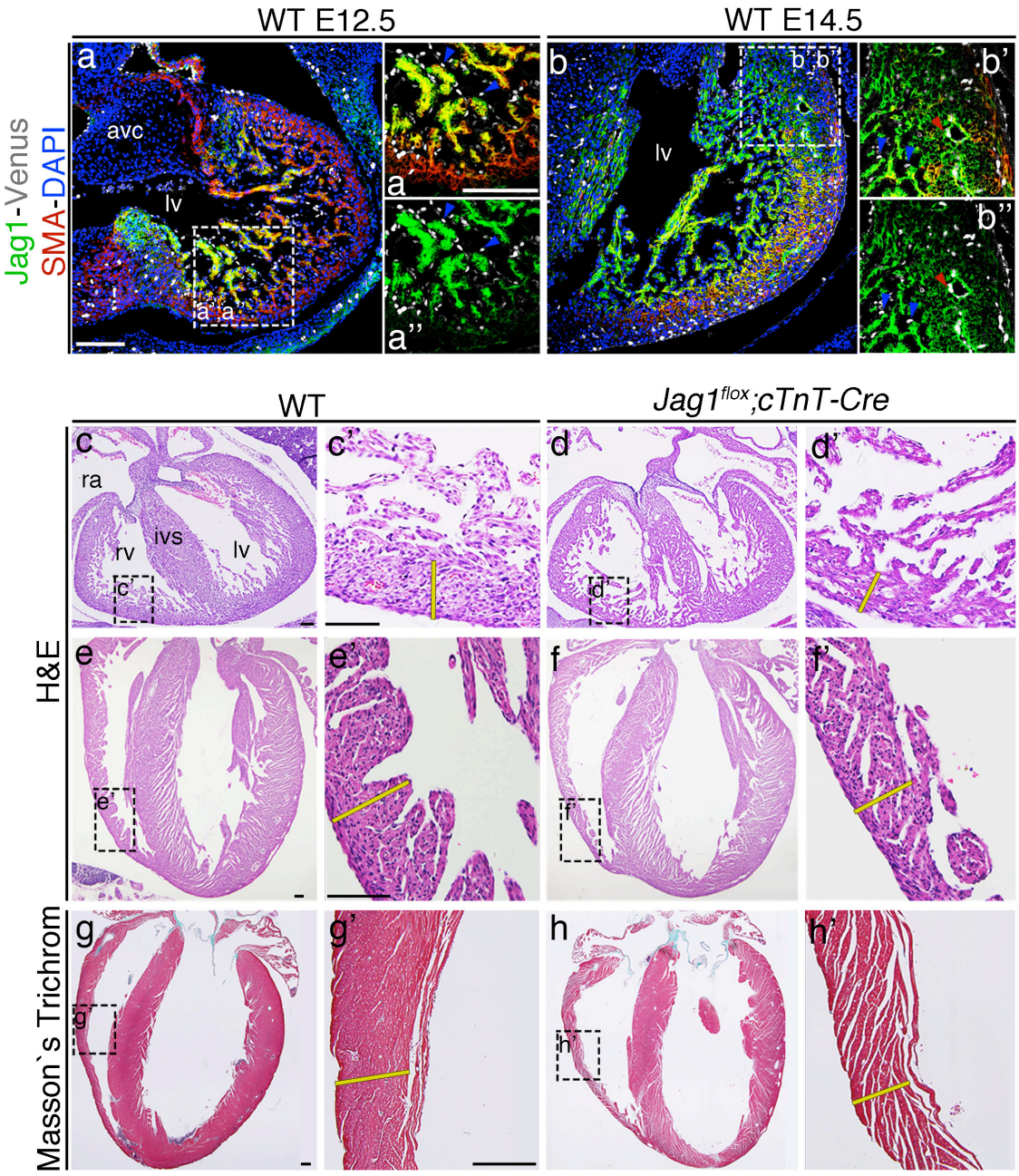

Figure 13. Myocardial inactivation of Jag1 impairs chamber compaction and maturation. (**a-b''**) Triple IHC of Jag1 (green), SMA (red), and GFP (grey) in E12.5 (**a-a''**) and E14.5 (**b-b''**) WT *CBF:H2B-Venus* ventricles. GFP^{+} cells (Notch activity) in the endocardium are adjacent to trabeculae expressing Jag1 (blue arrowheads). In E14,5 Jag1 is express also in the endothelium of the coronary vessels (red arrowhead, **b´,b''**). In (**a-b''**) nuclei are counterstained with DAPI. Scale bar =50µm. (**c-f'**) H&E staining of heart sections from WT and *Jag1^{flox};cTnT-Cre* E16.5 embryos (c-d') and postnatal day 3 (P3) neonates (**e-f'**). Mutant hearts show thinner and disorganized compact myocardium (**d',f'**). Masson's trichome staining of 6-month-old adult hearts. The myocardium is fully compacted in the WT heart (**g**, enlarged in **g'**) but appears thinner in the mutant (**h**, enlarged in **L**). The yellow bars indicate the thickness of the compact myocardium. lv=left ventricle; ra=right atrium; rv=right ventricle; ivs= interventricular septum. Scale bar=100µm.

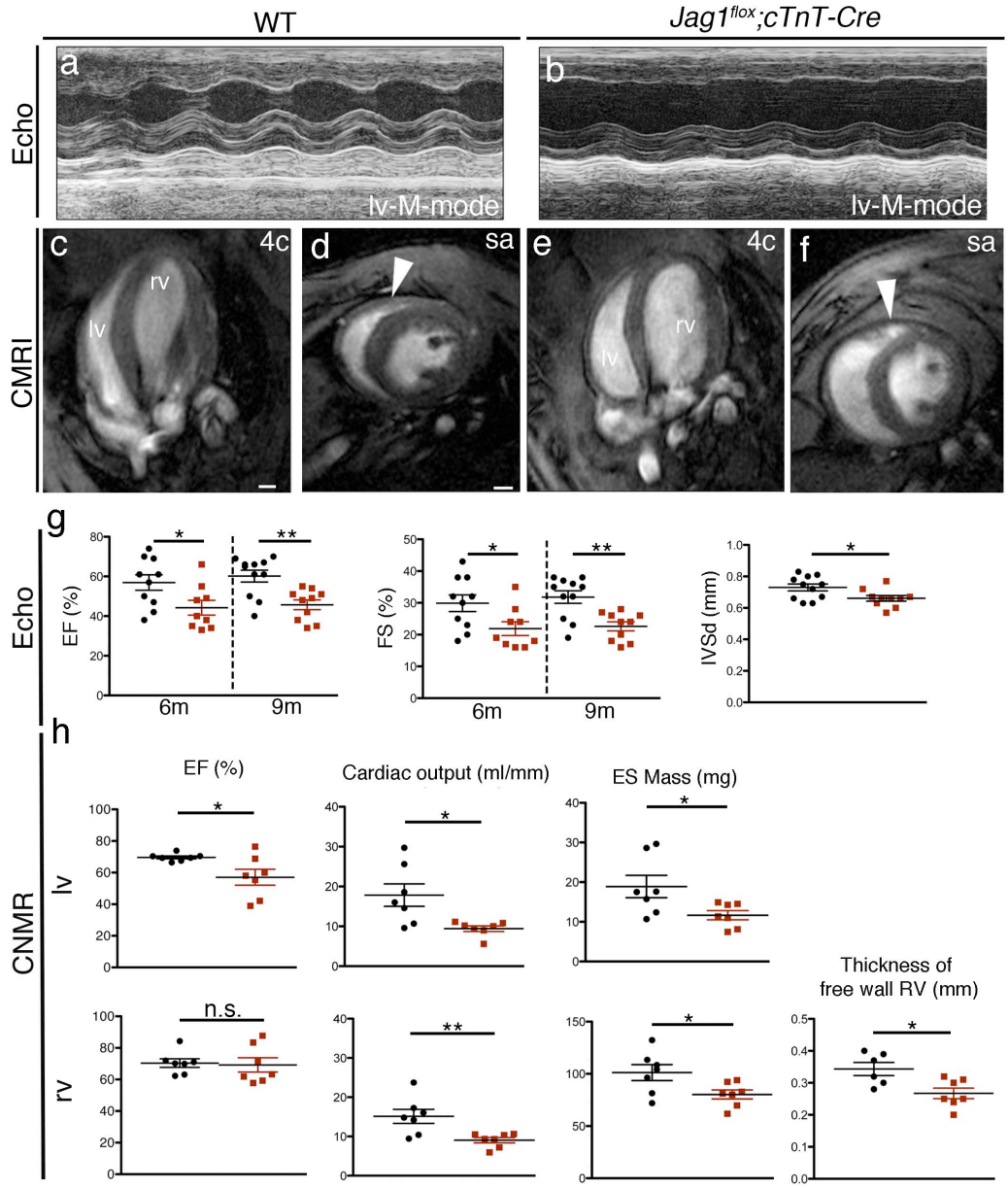

Figure 14. Myocardial *Jag1* leads to cardiomyopathy and systolic dysfunction.
(**a,b**) Echocardiography analysis in 6- and 9-month-old mice (6-9m), M mode views of the left ventricles (lv) of WT (**a**) and *Jag1*^{flox}*;cTnT-Cre* (**b**) 6m mice. CMRI analysis in a 6m WT mouse (c,d) and a *Jag1* mutant (e,f). Images show four-chamber (4c) and short axis (sa) views. Arrowheads mark the ventricular wall, which is thinner in the mutant heart. Scale bar=2mm. (**g**) Echocardiography analysis of left ventricular ejection fraction (EF) and fractional shortening (FS) measured at 6m and 9m and diastolic interventricular septal wall thickness (IVSd) in WT and mutant mice. Data are represented as mean ± S.D. (n=10WT and 9 mutants at 6m, n=11WT and 10 mutants at 9m * P<0.05 and ** P<0.01 by Student's t test). (**h**) CMRI analysis of physiological and morphometric parameters in the left (lv) and right ventricles (rv) of 6m WT and *Jag1*^{flox}*;cTnT-Cre* mice. ES Mass, mass in end-systole. Data are represented as mean ± s.e.m. (n=7 WT and 7 mutants, * P<0.05 and ** P<0.01 by Student's t test).

Jag1-Notch1 signaling sustains Ventricular Chamber Maturation and Cardiomyocyte Proliferation

Analysis of chamber markers in E16.5 *Jag1^{flox};cTnT-Cre* mice revealed expansion of the compact myocardium marker *Hey2* to the trabeculae (Fig. 15a-b') and low expression of the trabecular markers *Bmp10* (Fig. 15c-d'), *Anf* (Fig. 15e-f') and *Gja5/Cx40* (Fig. 15g-h'), especially in the right ventricle. The expression of *Hey2* within the trabecular myocardium concomitant with an impaired expression of trabecular markers suggests defects in the maintenance of trabecular maturation and patterning. BrdU incorporation analysis in E16.5 *Jag1^{flox};cTnT-Cre* embryos revealed a 25% lower than normal cardiomyocyte proliferation in the compact region of the ventricles (Fig. 15i-k). The altered gene expression and the reduced proliferation in the compact zone of E16.5 *Jag1* mutant embryos indicate Jag1-Notch interaction as crucial for chamber maturation.

To find molecular targets downstream of Jag1-Notch signaling during compaction, we carried out RNA-seq experiments with E15.5 WT and *Jag1^{flox};cTnT-Cre* ventricles. We identified 97 differentially expressed genes ($P < 0.05$), 74 of them up-regulated and 23 down-regulated relative to WT embryos (Fig. 16a and supplementary table1). GO classification revealed that most of these deregulated genes were involved in cell growth and proliferation (*Cdkn1a, Cdk6, E2f1*), differentiation (*Sort1, Acta1, Robo1*), fibrosis (*Mmp12, Casq1*), cardiovascular development and disease (*Cxcl12, Flnb, Cacna2d2*), focal adhesion (*Spp1, Thbs2*), ECM-receptor interaction (*Lama5, Col6a6*) and dilated cardiomyopathy (*Itga1, Socs2*) (Fig. 16b and supplementary table1). The gene encoding the chemokine ligand Cxcl12 was one of the most strongly down-regulated in *Jag1^{flox};cTnT-Cre* mutants (Fig. 16b). Interestingly, Cxcl12/Cxcr4 signaling has recently been shown to be crucial for coronary artery development (Ivins, Chappell et al., 2015), a process occurring simultaneously with and is essential for compaction (Tian, Pu et al., 2015). ISH of *Cxcl12* in E16.5 heart sections revealed strong expression in the trabecular myocardium of WT embryos. In agreement with the RNA-seq data, its expression was strongly down-regulated in *Jag1^{flox};cTnT-Cre* mutants (Fig. 17a-b'). The reduction of the transcript was also validated by qRT-PCR analysis (Fig. 17i). Indeed, by qRT-PCR on mutant ventricles we estimated a 70% reduction of *Jag1* levels compared with WT (Fig. 17i). ISH and qRT-PCR analyses also revealed markedly reduced *Gpr126* transcription in the endocardium of E16.5 *Jag1^{flox};cTnT-Cre* mutant endocardium (Fig. 17c-d'; i). Interestingly, the low expression of endocardial *Gpr126* was coincident with reduced myocardial proliferation observed in E16.5 *Jag1^{flox};cTnT-Cre* mutants (Fig. 15i-k) likewise the situation observed in *Dll4* mutants during trabeculation. This observation suggests that Gpr126 is an important component of Notch-mediated endocardium-myocardium interplay during ventricular chamber development.

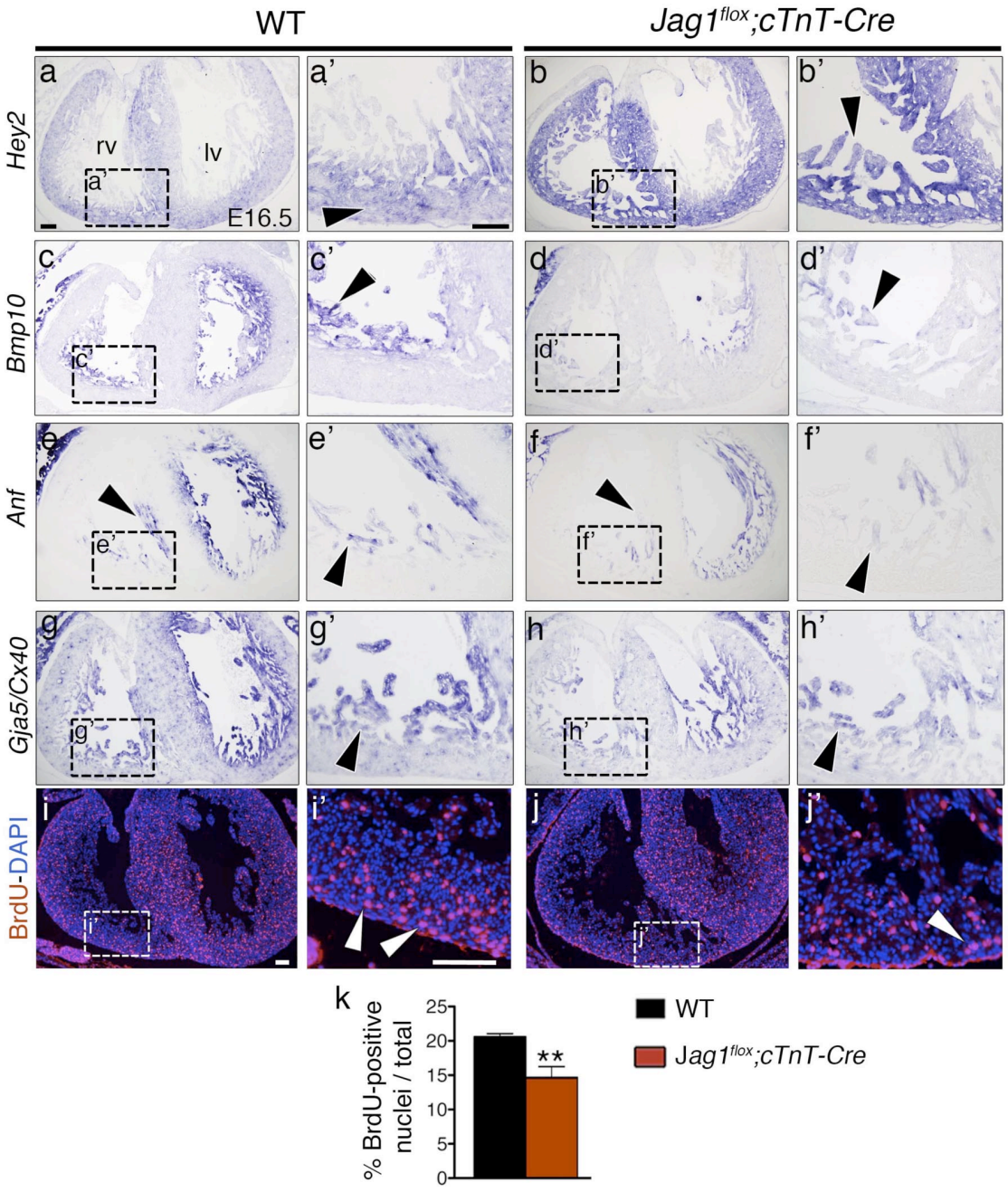

Figure 15. Defective ventricular maturation and myocardial proliferation in E16.5 *Jag1^{flox};cTnT-Cre* mutants.

(**a-h'**) ISH in E16.5 WT and *Jag1^{flox};cTnT-Cre* heart sections. rv (right ventricle), lv (left ventricle). (a-b') *Hey2* expression in compact myocardium (arrow in **a'**) is expanded to the trabeculae in mutant embryos (arrow in b') and the trabecular markers *Bmp10* (**c-d'**), *Anf* (**e-f'**) and *Cx40* (**g-h'**) are down-regulated. Arrowheads indicate where the genes are expressed. (**i-j'**) IHC of incorporated BrdU in E16.5 WT (**i.i'**) and *Jag1^{flox};cTnT-Cre* heart sections (**j,j'**). Arrowheads indicate BrdU-positive nuclei (red). Below normal proliferation is observed in the myocardium of the mutant heart (Z). Data are represented as mean ± S.D. (n=3 WT and 3 *Jag1^{flox};cTnT-Cre* mutants * $P < 0.05$ by Student's *t* test). Scale bar=100mm.

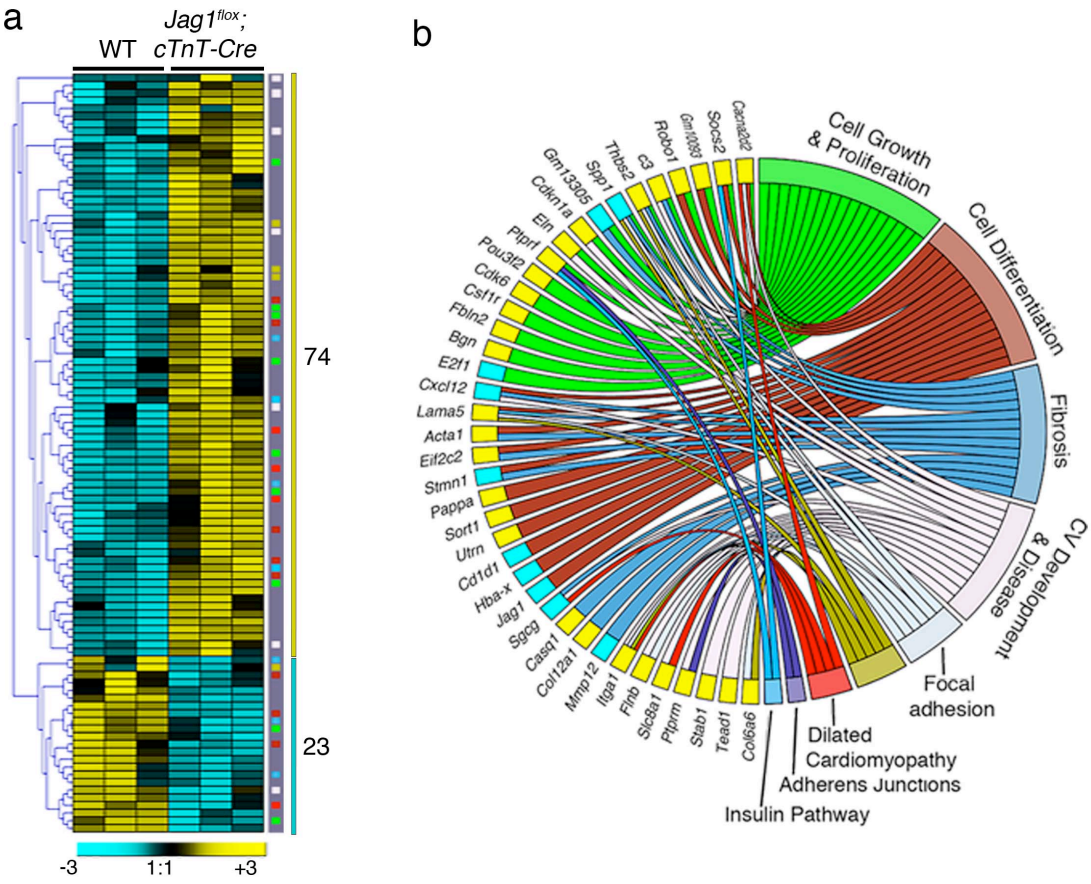

Figure 16. Gene expression analysis of E15.5 *Jag1^{flox};cTnT-Cre* mutant ventricles.
(**a**) Heat map from hierarchical clustering of differentially expressed genes (P<0.05) identified by RNA-seq in the three different pools of WT and *Jag1^{flox};cTnT-Cre* ventricles. The total number of down-regulated genes is indicated to the right side of the blue line; the total number of up-regulated genes is indicated to the right side of the yellow line. (**b**) Circular plot showing 39 representative differentially expressed genes in *Jag1^{flox};cTnT-Cre* hearts selected from a total of 97 genes belonging to various functional categories (yellow, up-regulated; blue, down-regulated). The most represented functional categories correspond to genes involved in cell growth and proliferation, cell differentiation and cardiovascular development and disease.

One of the most strongly up-regulated genes was the cell cycle inhibitor *Cdkn1a/p21* (Fig. 16b and supplementary table1). To determine if the reduced cardiomyocyte cell division was the cause of the thinner compact myocardium observed at E16.5 in mutant hearts, we performed the proliferation analysis earlier than the onset of the cardiac phenotype. Consistent with the RNA-seq data, p21 expression in E13.5 *Jag1^{flox};cTnT-Cre* mutant hearts was 30% above normal (Fig. 17e-f'; j). However, in the already formed trabeculae, the number of p21 positive cells was similar to the WT. This observation suggested that in controls, as well as in mutant embryos, proliferation of trabecular myocardium is arresting. In agreement with an increasing p21 expression in the compact myocardium, BrdU analysis from E13.5 WT and *Jag1^{flox};cTnT-Cre* hearts showed a remarkable reduction of cell division in the compact region of mutant embryos (Fig. 17g-h'; j).

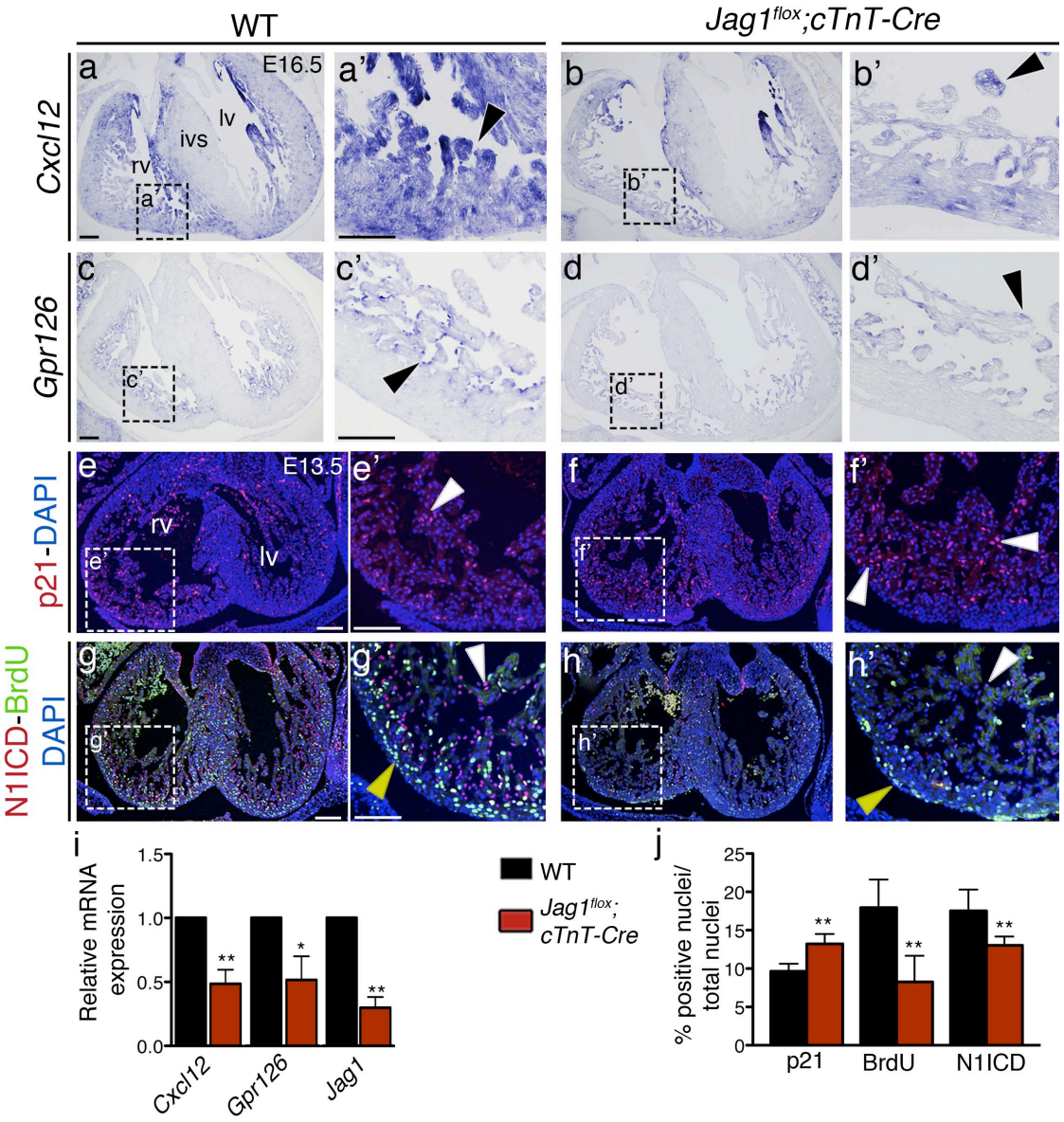

Figure 17. Jag1-Notch1 signaling is required for myocardial growth and differentiation. (**a-b'**) ISH of *Cxcl12* in E16.5 WT (**a,a'**) and *Jag1^{flox};cTnT-Cre* (**b-b'**) hearts. Myocardial expression (arrows) is impaired in mutant hearts. (**c-d'**) ISH of *Gpr126* in E16.5 WT (**c,c'**) and *Jag1^{flox};cTnT-Cre* (**d,d'**) hearts. *Gpr126* (arrowheads) is reduced in mutant hearts. (**e-h'**) IHC for p21 (red nuclei), N1ICD (red nuclei) and BrdU (green nuclei) in E13.5 WT and *Jag1^{flox};cTnT* hearts. In the WT heart (**e,e'**), p21 expression is observed in the trabeculae (**e'**, arrowhead) and in dispersed compact myocardium cardiomyocytes; in the mutant, expression is expanded throughout the ventricle (**f,f'**) and is significantly higher (**f'**). N1ICD is expressed throughout the endocardium in the WT ventricle (**g,g'**, arrowheads) and is markedly lower in the mutant heart (**h,h'**, arrowheads). In the WT, BrdU is predominantly incorporated in the compact myocardium (**g,g'**, yellow arrowheads) and is significantly lower in the *Jag1^{flox};cTnT* ventricle (**h,h'**, arrowhead). (**m**) qRT-PCR analysis of *Gpr126, Jag1* and *Cxcl12* in E15.5 WT and *Jag1^{flox};cTnT-Cre* ventricles. Data are represented as mean ± S.D. (n=3 pools of 3 WT ventricles each and 3 pools of 3 mutants ventricles each, * P<0.05, **P<0.01, determined by Student's *t* test). (**j**) Quantification of p21-, N1ICD- and BrdU-positive nuclei in E13.5 *Jag1^{flox};cTnT* ventricles. Data are represented as mean ± S.D. (3 WT and 3 mutant embryos, for p21 staining and 6 WT and 6 mutant embryos for BrdU and N1ICD staining; ** P<0.01, determined by Student's *t* test). lv=left ventricle; rv=right ventricle; ivs= interventricular septum. Scale bar=100mm.

Concomitant to a 56% reduction of BrdU, N1ICD expression in the endocardium was 28% lower than WT (Fig. 17g-h'; j). These results indicate that Jag1-mediated Notch1 activation in the endocardium is essential for compact myocardium proliferation and trabecular myocardium differentiation and patterning.

Morphological and functional differences between *Jag1* and *Mib1* mutants

We initially predicted that the cardiac phenotypes of *Mib1^{flox};cTnT-Cre* and *Jag1^{flox};cTnT-Cre* mutants would be similar, based on the assumption that Jag1 was the only ligand expressed in the myocardium and was therefore the only potential substrate for the ubiquitin ligase action of Mib1, responsible for Notch activation at later stages. We performed comparative morphological analysis of *Jag1^{flox};cTnT-Cre* and *Mib1^{flox};cTnT-Cre* mutants measuring the thickness of the compact myocardium and trabecular complexity in E16.5 heart sections. Myocardium was counterstained with cardiac Troponin T antiboby (cTnT). To delineate the chamber endocardium we used endomucin. *Mib^{flox};cTnT-Cre* mutant hearts showed thinner compact myocardium in the left and right ventricle (31% and 35% reduction respectively, Fig. 18c-c''), comparing with the well-developed structures in WT embryos (Fig. 18a-a''). In the Jag1 mutant hearts the reduction of compact zone was observed only in the right ventricle and it was less accentuated (20%, Fig. 18b-b''). In addition, *Mib^{flox};cTnT-Cre* mutant embryos showed an 80% and 68% increase in trabecular complexity in the left and right ventricles, respectively (Fig. 18c-c''). A significant increase was also observed in both left and right ventricle of Jag1 mutants (30% and 42% respectively, Fig. 18b-b''), although less accentuated than in *Mib^{flox};cTnT-Cre* mutant embryos. These results showed morphological differences between *Jag1* and *Mib1* mutant embryos. The chamber phenotype of *Jag1* mutant only in part resembled the features observed in *Mib1* mutant embryos. Notably, the morphological discrepancies between the two mutants reflected differences in the cardiac function. *Mib1^{flox};cTnT-Cre* mutants develop LVNC cardiomyopathy (Luxan et al., 2013); in contrast *Jag1^{flox};cTnT-Cre* mutants showed structural and functional signs of dilated cardiomyopathy and systolic dysfunction but no signs of LVNC.

These observations prompted us to examine whether a different Notch ligand expressed in the myocardium, non-redundant with Jag1, could account for the phenotypic differences between *Mib1* and *Jag1* mutants.

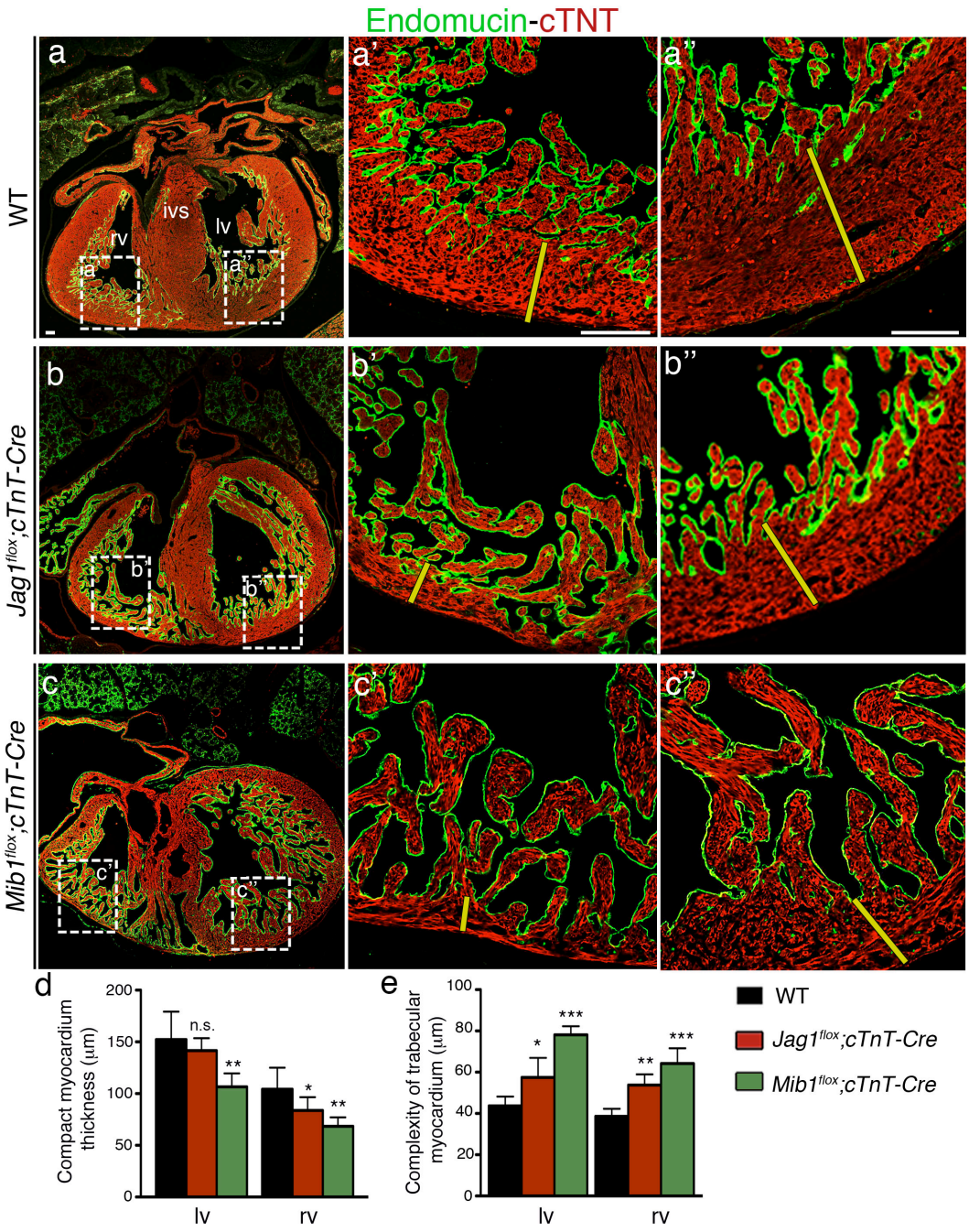

Figure 18. Morphological differences between *Jag1^{flox};cTnT-Cre* and *Mib1^{flox};cTnT-Cre* E16.5 mutant embryos. (**a-c''**) E16.5 heart sections stained with endomucin and cTnT. The WT heart (**a-a''**) shows a thick compact myocardium (red) in both ventricles, with compacting trabeculae (red) The *Jag1^{flox};cTnT-Cre* heart (**b-b''**), shows thin compact myocardium, especially in the right ventricle and uncompacted and dispersed trabeculae. In the *Mib1^{flox};cTnT-Cre* (**c-c''**) stronger chamber phenotype is observed comparing with *Jag1^{flox};cTnT-Cre.* Note the very large and uncompacted trabeculae invading the lumen of the ventricles (**c',c''**). The yellow bars indicate compact myocardium thickness. (**e,d**) Quantification of compact myocardium thickness (**e**) and complexity of trabecular myocardium (**d**) in *Jag1^{flox};cTnT-Cre* and *Mib1^{flox};cTnT-Cre* hearts comparing with corresponding WT. Data are mean ± S.D. (n=3 WT; 3 *Jag1^{flox};cTnT-Cre* and 3 *Mib1^{flox};cTnT*, *P<0.05, **P<0.01, ***P<0.001, n.s. not significant, determined by Student's *t* test). lv=left ventricle; rv=right ventricle; ivs= interventricular septum. Scale bar=100um.

Jag2 is required for chamber maturation and compaction

The full-length of human *Jag2*, a mammalian *Jag1* paralogue, was isolated by Biao Luo and co-workers in 1997. In this report, expression of the murine *Jag2* mRNA was also investigated. Northern blot analysis performed on RNA isolated from various tissues of 2-week-old mice revealed high expression of *Jag2* in the heart (Luo, Aster et al., 1997). More recently, myocardial expression of Jag2 was detected in embryonic heart sections by immunohistochemistry during post-mid-gestation (van den Akker, Molin et al., 2007). Considering these data, we evaluated the expression of *Jag2* during chamber development. ISH analysis of E10.5 WT heart sections showed basal *Jag2* expression in the E10.5 WT heart (Fig. 19a). Progressively, from E12.5 to E16.5 *Jag2* expression increased in the myocardium (Fig. 19b-d). Strong expression of the transcript was detected in the myocardium of the atria, especially in the region of the septum primum (SP) and in the trabecular myocardium of the ventricles (Fig. 19b-d). From E14.5 remarked *Jag2* expression was also detected in the endothelium of coronary vessels. qRT-PCR analysis showed that *Jag2* up-regulation paralleled the down-regulation of *Jag1* (Fig. 19f). Interestingly, during myocardial compaction, from E12.5 to E14.5, expression levels of both ligands were similar. Once myocardial compaction ends, *Jag2* levels were significantly higher (Fig. 19f). Expression analysis suggested Jag2 as an important ligand for Notch activity during chamber compaction and maturation.

To investigate its role we crossed $Jag2^{flox}$ mice with the *cTnT-Cre* driver line to generate homozygous $Jag2^{flox}$*;cTnT-Cre* mice. ISH showed strong down-regulation of *Jag2* expression in the myocardium of E16.5 $Jag2^{flox}$*;cTnT-Cre*. The Notch ligand was transcribed only in the endothelium of the coronary vessels where the *Cre* is not active (Fig. 19d-e). At this stage, the WT heart showed thick compact myocardium and the trabeculae were almost fused with each other (Fig. 19g-g'). In contrast, the mutant embryo had a thinner compact myocardium especially in the right ventricle, which appeared dilated and full of disorganized trabeculae (Fig. 19h-h'). Quantification of compact myocardium thickness revealed a 38% reduction in the right ventricle, paralleled by a 20% increase in trabecular complexity (Fig. 19i-f). To confirm that myocardial Jag2 is a potential activator of endocardial Notch1, we assayed N1ICD expression in E16.5 WT and $Jag2^{flox}$*;cTnT-Cre* mutant embryos. Notch activity was 35% below normal in the right ventricle of mutants (Fig. 20 a-c). This data indicated that Jag2 is the second ligand interacting with Notch1 during chamber compaction. $Jag1^{flox}$*;cTnT-Cre* mutants had reduced endocardial Notch activity concomitant with impaired cardiomyocyte proliferation. To strengthen the hypothesis that, during compaction, endocardial Notch signaling is necessary to sustain proliferation of cardiomyocytes in the compact layer, we performed BrdU incorporation analysis in E13.5 $Jag2^{flox}$*;cTnT-Cre* heart sections.

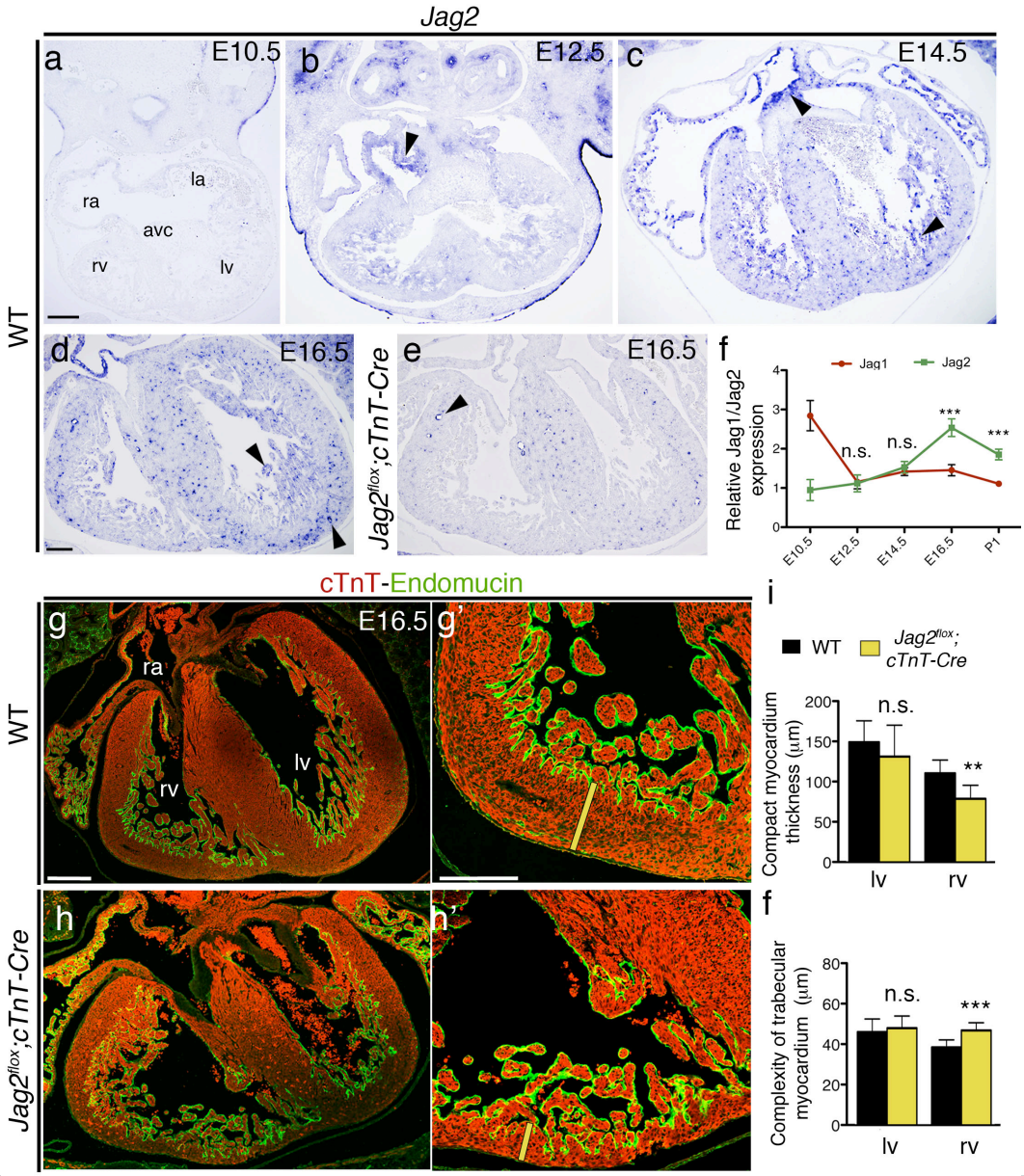

Figure 19. Myocardial Jag2 is required for ventricular maturation and compaction.
(**a-e**) ISH of *Jag2* in E10.5 (**a**), E12.5 (**b**), E14.5 (**c**), E16.5 (**d**) WT and *Jag2^{flox};cTnT-Cre* mutant (**e**) heart sections. *Jag2* is expressed in trabecular myocardium (arrows), atria and septum primum (arrowheads) from E12.5 onwards. At E16.5 *Jag2* is also observed in coronary vessels (**e**, arrowheads). (**d**) cTnT-Cre-mediated deletion completely abrogates *Jag2* expression in the myocardium but does not affect expression in coronary vessels (**d**, arrowheads). No expression is detected in E10.5 WT embryos (**a**). (**f**) Relative ratios of *Jag1* and *Jag2* gene expression in WT ventricles from E10.5 to P1 measured by qRT-PCR. Expression levels of *Jag1* and *Jag2* are similar at E12.5 and E14.5. Afterwards the levels of Jag2 are higher compared to *Jag1*. Data are represented as mean ± S.D. (n=3 pools of 3 WT ventricles per pool for each stage analyzed, ***P<0.01, n.s. not significant, determined by Student's *t* test). (**g-h'**) IHC in E16.5 WT (**g,g'**) and *Jag2^{flox};cTnT-Cre* (**h,h'**) stained with endomucin and cTnT. WT ventricles show a very thick compact myocardium (**g**, yellow line in **g'**) and compacting trabeculae. In contrast, the mutant heart shows a thinner compact myocardium (**h**, yellow line in **h'**), especially in the right ventricle. (**i-f**) Chart showing quantification of compact myocardium thickness (**i**) and complexity of trabecular myocardium (**f**) in *Jag2^{flox};cTnT-Cre* hearts comparing with corresponding WT. Data are mean ± S.D. (n=3 WT; 3 *Jag2^{flox};cTnT-Cre* *P<0.05, **P<0.01, n.s. not significant, determined by Student's *t* test). ra=right atria; la=left atria; rv=right ventricle; lv=left ventricle; avc=atrioventricular canal. Scale bar=100µm.

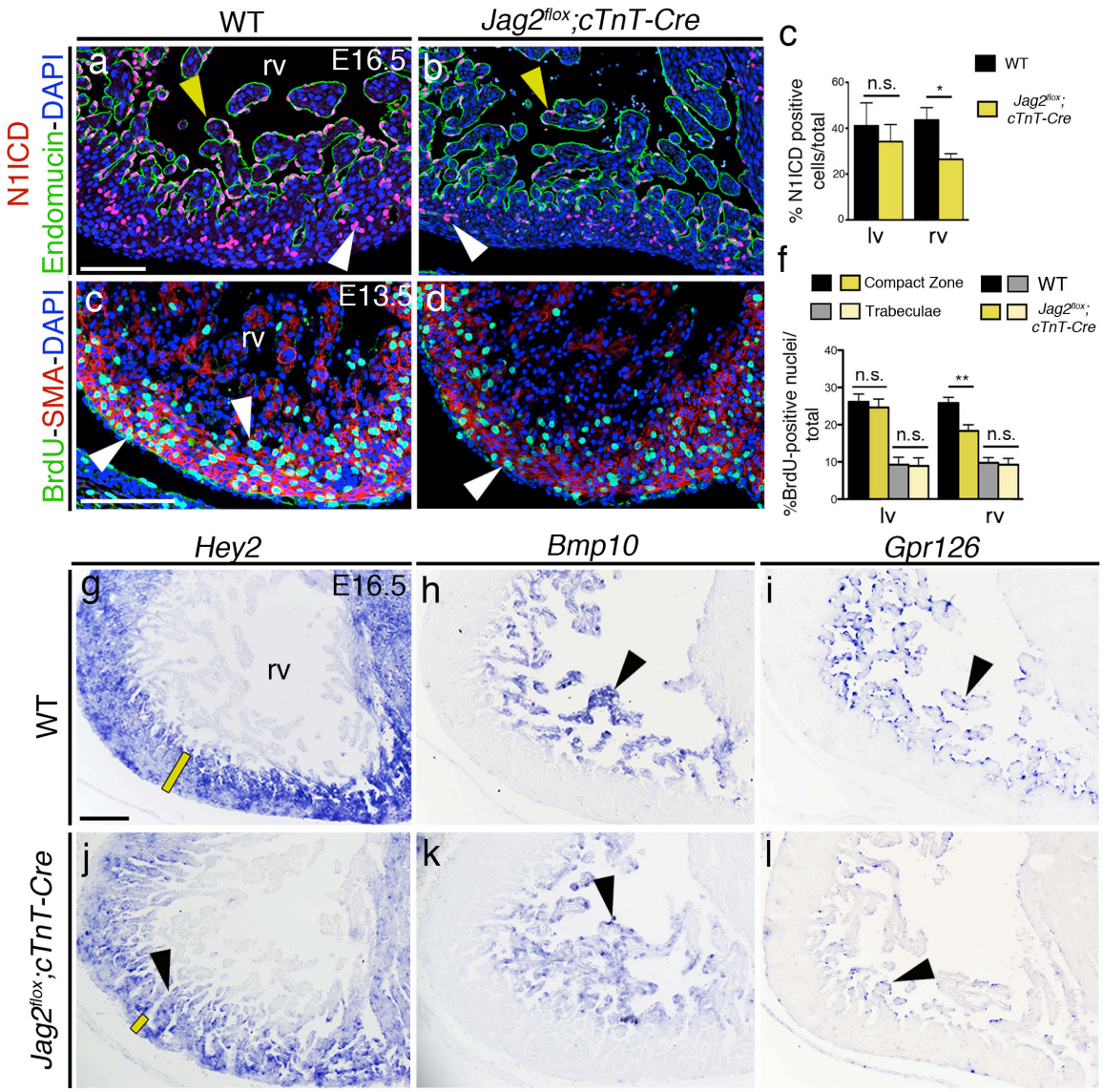

Figure 20. Jag2 interacts and activates Notch1 in the endocardium during ventricular compaction. (a,b) N1ICD immunostaining (red nuclei). In the E16.5 WT heart (**a**), N1ICD is expressed throughout the endocardium (yellow arrowheads), delineated by endomucin staining (green), and in coronary vessels (white arrowheads). (**b**) *Jag2^{flox};cTnT-Cre* heart shows below-normal N1ICD expression. The yellow and white arrowheads mark remnant endocardial- and coronary N1ICD-positive cells, respectively. (**c**) Quantification of N1ICD-positive cells in the left and right ventricle. Data are mean ± S.D. (n=3 WT and 3 *Jag2^{flox};cTnT-Cre* mutants, * P < 0.05, **P < 0.01, determined by Student's *t* test). (**d,e**) BrdU (green) and SMA (red) immunostaining in E13.5 WT (**d**) and *Jag2^{flox};cTnT-Cre* (**e**). BrdU is predominantly incorporated in WT compact myocardium (**c**); the mutant hearts show reduced BrdU incorporation in the compact layer. Within the trabeculae, cardiomyocyte proliferation is very low as indicated by the few BrdU positive cells in this region (**c-d**). Nuclei are counterstained with DAPI (blue). (**e**) BrdU quantification. The total number of BrdU positive nuclei was divided by the total number of cells (DAPI) for each region of interest; compact zone and trabecular myocardium of left and right ventricle. Data are represented as mean ± S.D. (n=3 WT and 3 *Jag2^{flox};cTnT-Cre* mutants, **P < 0.01, determined by Student's *t* test). (**g-l**) ISH analysis. *Hey2* is prominent in WT compact myocardium (**g**, yellow bar), which is thin in *Jag2^{flox};cTnT-Cre* (**j**, yellow bar). *Bmp10* labels trabecular myocardium in WT (**h**) and *Jag2^{flox};cTnT-Cre* (**k**). *Gpr126* delineates the endocardium in WT ventricles (**i**, arrowhead) and its expression is severely reduced in *Jag2^{flox};cTnT-Cre* mutants (**l**). lv=left ventricle; rv=right ventricle. Scale bar=100mm.

The total number of proliferative cardiomyocytes located in the compact myocardium of the *Jag2* mutants was 30% lower than WT, especially in the right ventricle (Fig. 20d-f). This result confirmed the strict relationship between endocardial Notch activity and cardiomyocyte proliferation. This result confirmed the strict relationship between endocardial Notch activity and cardiomyocyte proliferation.

Furthermore, the expression of *Hey2* and *Bmp10* evidenced clear defects of compaction in the right ventricle of E16.5 *Jag2^{flox};cTnT-Cre* embryos (Fig. 20g-k). In addition, *Gpr126* was down-regulated in the endocardium of Jag2 mutants (Fig. 20i-l). All these data indicate that Jag2 plays a non-redundant role to Jag1 in heart development during ventricular chamber maturation and compaction.

Molecular docking suggests binding of Jag1 and Jag2 to the same Notch1 homodimer

To explore the interaction of Notch1 with its ligands, we *in-silico* modeled the 3D structure of the complexes formed by the extracellular domains of two Notch1 receptors (Fig. 21a) interacting with its ligands (Fig. 21b-e and video 5). The models generated for the N1ECD monomer show a linear, rigid structure with a low degree of compaction, in line with published results (Blacklow, 2013, Chillakuri, Sheppard et al., 2012, Hambleton, Valeyev et al., 2004). Interaction of Notch1 with its ligands occurs in an antiparallel head-to-tail orientation of N1ECD EGF-like repeat 12 and DSL-EGF-like repeats 1-2 of the ligands expressed in neighboring cells (Andrawes, Xu et al., 2013, Chillakuri, Sheppard et al., 2013, Chillakuri et al., 2012). The biologically active Notch1 dimer binds Dll4 in a 1:1 stoichiometry (Narui & Salaita, 2013) and we assumed that this stoichiometry would be the same also for Jag1 and Jag2. In addition, we generated a 3D complex composed by a homodimer of N1ECD interacting with Jag1 and Jag2 (Fig. 21e).

According to data on the stability and free energy of the docking, the most favored ligand-receptor interaction in terms of strength and affinity/avidity is 2Dll4:2N1ECD (Fig. 21b;f and video 5). For Jag1 and Jag2 combinations, the Jag1/Jag2:2N1ECD complex had a slightly higher predicted stability (a smaller global energy, indicated by the lower total score) than the 2Jag1:2N1ECD complex, a consequence of the stronger Van der Waals attraction forces in the Jag1/Jag2:2N1ECD complex (smaller fa_atr term). In contrast, the repulsion (fa_rep) and solvation (fa_sol) forces were very similar for these complexes and smaller than for the 2Jag2:2N1ECD complex (Fig. 21f). This suggests that the affinity/avidity of the Jag1/Jag2:2N1ECD heterocomplex would be higher than that of the 2Jag1:2N1ECD complex, and that the presence of both ligands would favor formation of the Jag1/Jag2:2N1ECD heterocomplex (Fig. 21c-f and video 5). These results, together with the Jag1 and Jag2 expression observed *in vivo* support the idea that the Jag1 and Jag2 ligands activate the same Notch1 homodimer.

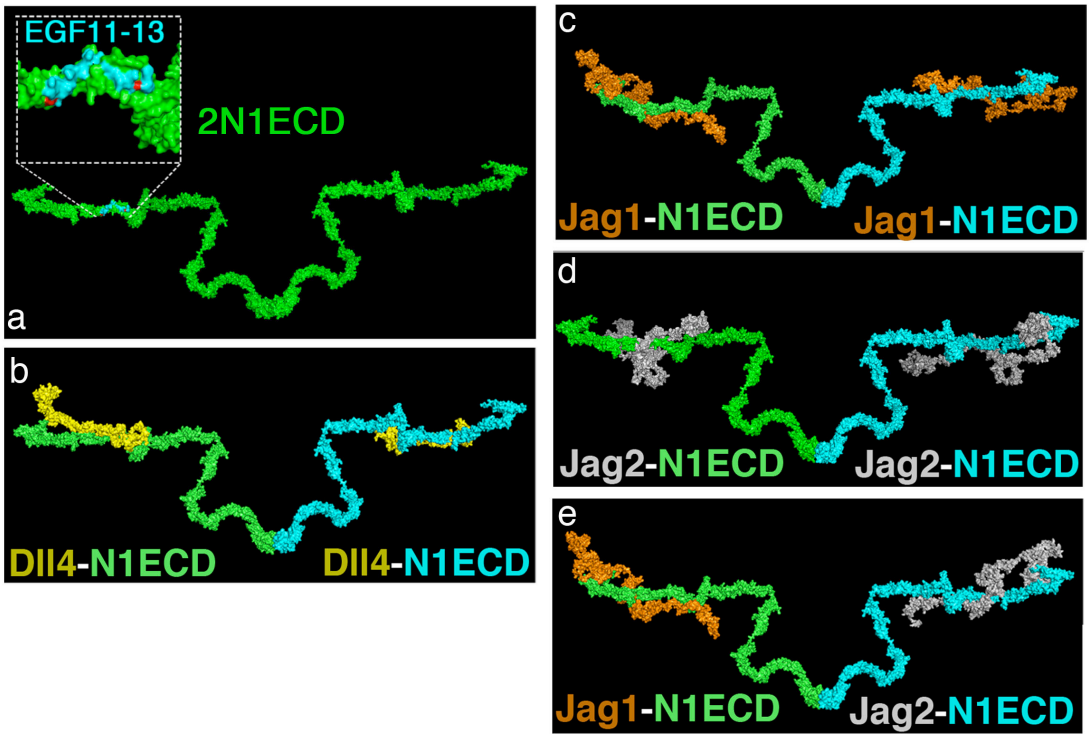

f

	total score	fa_atr	fa_rep	fa_sol
2NECD-2D4	12575.496	-5.257.335	14.370.857	2.692.552
2NECD-2J1	13518.949	-5.971.115	15.520.849	3.114.620
2NECD-2J2	13224.590	-6.617.143	15.724.893	3.356.488
2NECD-J2/J1	13307.341	-6.283.949	15.565.031	3.229.490

Figure 21. ***In silico*** **modeling of Notch ligand-receptor interaction.**
(**a**) 3D model of the extracellular domain of Notch1 forming a homodimer (2N1ECD, green). The inset highlights the EGF domains of one of the N1ECD involved in the ligand-receptor interaction (**a**). Docking between the Notch1 extracellular domain homodimer (NECD, green and cyan) and Dll4 (**a**, yellow), Jag1 (**b**, orange), Jag2 (**c**, gray), or Jag1 and Jag2 (**d**) dimers. (**e**) Summary of energy and force measurements. Total score indicates the total free energy, which is smallest for the most stable interaction (2Dll4-2NECD, **b;f**). Jag1/Jag2:2N1ECD (**e;f**) complex shows lower free energy compared to Jag1/Jag1:2N1ECD (**c;f**) or Jag2/Jag2:2N1ECD (**d;f**).

Both Jag1 and Jag2 are required for Notch1 activity during chamber compaction

The data collected from single myocardial *Jag1*- or *Jag2*- mutants indicated that both ligand interact and activate Notch1 in the endocardium during chamber compaction. However, in comparison with *Mib1^{flox};cTnT-Cre* embryos, the *Jag1^{flox}* or *Jag2^{flox};cTnT-Cre* embryos showed a milder cardiac phenotype. This observation suggested that in the myocardium Mib1 regulates the endocytosis and the recycling of both ligands, therefore the loss of myocardial *Mib1* would cause a stronger heart phenotype than single *Jag1*- or *Jag2*-deletions.

To test this hypothesis, we generated mice doubly deficient for *Jag1*- and *Jag2*- in the myocardium. We stained E16.5 WT and *Jag1^{flox};Jag2^{flox};cTnT-Cre* heart sections with antibodies against cTnT and endomucin to label the myocardium and endocardium, respectively, in order to perform morphological analysis (Fig. 22a-b''). This analysis revealed significant reduction in the thickness of right and left compact myocardium of double mutant embryos (Fig. 22c). Interestingly, in the single *Jag1* or *Jag2* myocardial mutants, we observed significant reduction only in the right ventricle. The trabecular complexity was 26% above normal in the right ventricle of *Jag1^{flox};Jag2^{flox};cTnT-Cre* mice (Fig. 22c), indicating defective trabecular compaction. The cardiac phenotype observed in E16.5 *Jag1^{flox};Jag2^{flox};cTnT-Cre* heart sections, was exacerbated in comparison to *Jag1^{flox}* or *Jag2^{flox};cTnT-Cre* mutants and it was reminiscent of *Mib1^{flox};cTnT-Cre* mice (Luxan et al., 2013).

Endocardial Notch1 activity was monitored by immunostaining of N1ICD in E16.5 WT and double mutant heart sections. (Fig. 22d-e'). The expression of N1ICD was significantly lower in the left and right ventricle of *Jag1^{flox};Jag2^{flox};cTnT-Cre* mutants, with an average of 32% reduction (Fig. 22f). In the single *Jag1* or *Jag2* mutant hearts, we observed a significant reduction of N1ICD positive cells, as well as, impaired cardiomyocyte proliferation only in the right ventricle. Proliferation analysis performed in E13.5 double *Jag1;Jag2* mutant embryos (Fig. 23a-b'') highlighted once again the strict relation between endocardial Notch activity and myocardial proliferation. Indeed, the number of BrdU positive cells in the compact myocardium of both ventricles was 40% below normal (Fig. 23c). ISH analysis in E16.5 WT and *Jag1^{flox};Jag2^{flox};cTnT-Cre* heart sections showed that *Hey2* delineated a very thin compact myocardium with deep recesses (Fig. 23d-g). In the mutant hearts *Bmp10* delineated very large and disorganized trabeculae (Fig. 23e-h). In addition, endocardial *Gpr126* expression was markedly attenuated (Fig. 23f-i). These results demonstrate that Jag1 and Jag2 are indispensable during ventricular myocardial compaction and both are necessary to trigger endocardial Notch1 activity in this process. The functional study performed on *Jag1^{flox};Jag2^{flox};cTnT-Cre* indicates that the two myocardial ligands are play a non-redundant role during chamber development and are substrate of the ubiquitin ligase Mib1.

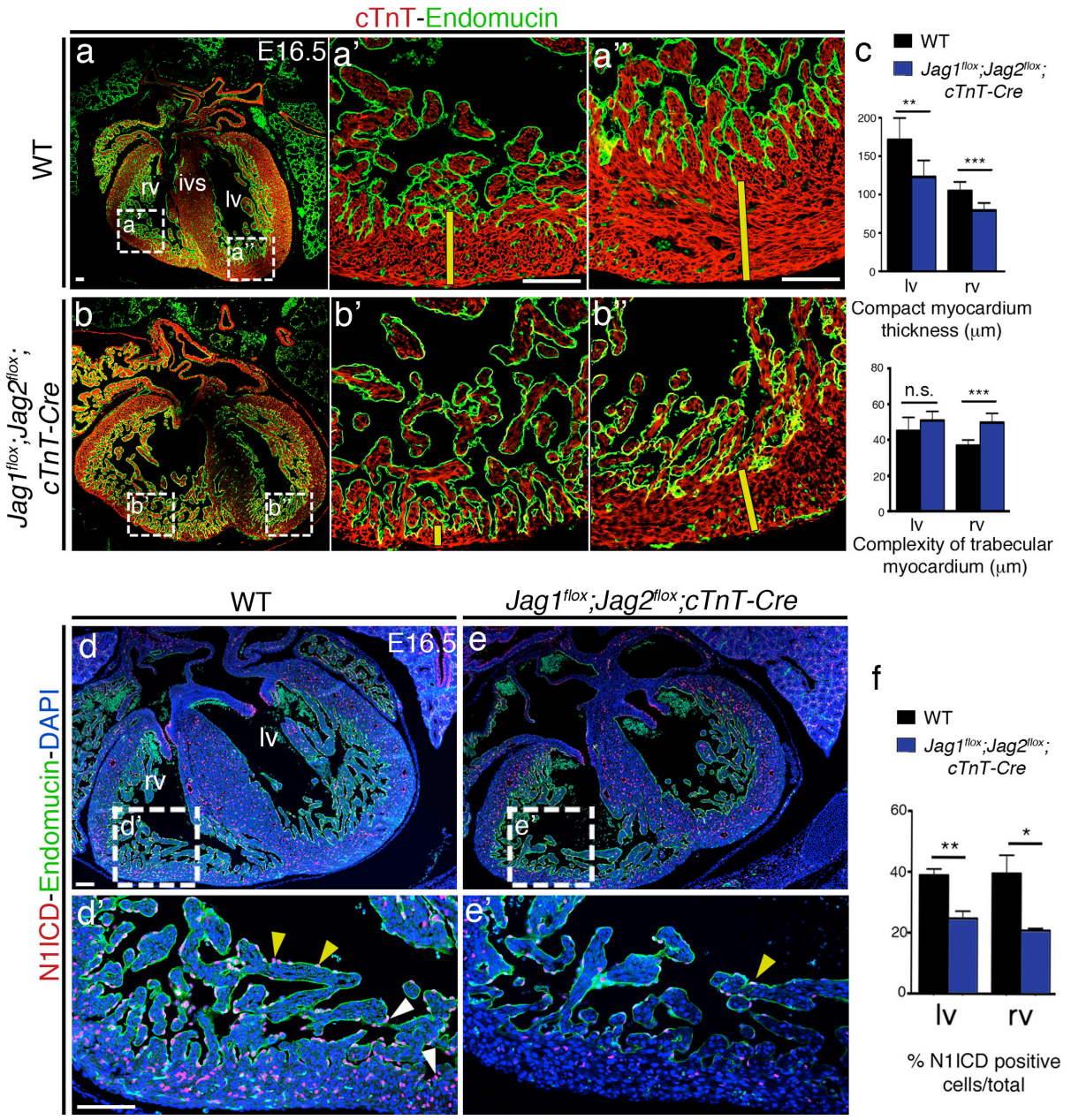

Figure 22. Myocardial deletion of *Jag1* and *Jag2* exacerbates the chamber phenotype observed in the single mutants. (**a-b''**) E16.5 heart sections from WT (**a,a''**) and *Jag1^{flox};Jag2^{flox};cTnT-Cre* (**b,b''**) embryos stained with endomucin (endocardium) and cTnT (myocardium). The WT ventricles show a thick compact myocardium in the left (yellow line in **a'**) and right ventricle (yellow line in **a''**) and compacting trabeculae. In contrast, the mutant heart shows very thin compact myocardium (yellow line in **b',b''**) with enlarge and disorganized trabeculae (**b',b''**). (**c**) Chart showing morphological parameters of compact myocardium thickness and complexity of trabecular myocardium in *Jag1^{flox};Jag2^{flox};cTnT-Cre* hearts comparing with corresponding WT. Data are mean ± S.D. (n=3 WT and 3 *Jag1^{flox};Jag2^{flox};cTnT-Cre* **P<0.01, ***P<0.001, n.s. not significant, determined by Student's *t* test). (**d-e'**) N1ICD immunostaining (red nuclei). In the E16.5 WT heart (**d,d'**), N1ICD is widely expressed in the endocardium (yellow arrowheads) marked by endomucin (green), and in coronary vessels (white arrowheads). (**d**) *Jag1^{flox};Jag2^{flox};cTnT-Cre* heart shows below-normal N1ICD expression. The yellow and white arrowheads mark remnant endocardial- and coronary N1ICD-positive cells, respectively. (**f**) Quantification N1ICD-positive cells in the left and right ventricle. Data are mean ± S.D. (n=3 WT and 3 *Jag1^{flox};Jag2^{flox};cTnT-Cre* * P < 0.05, **P < 0.01, determined by Student's *t* test). lv=left ventricle; rv=right ventricle; ivs= interventricular septum. Scale bar=100μm.

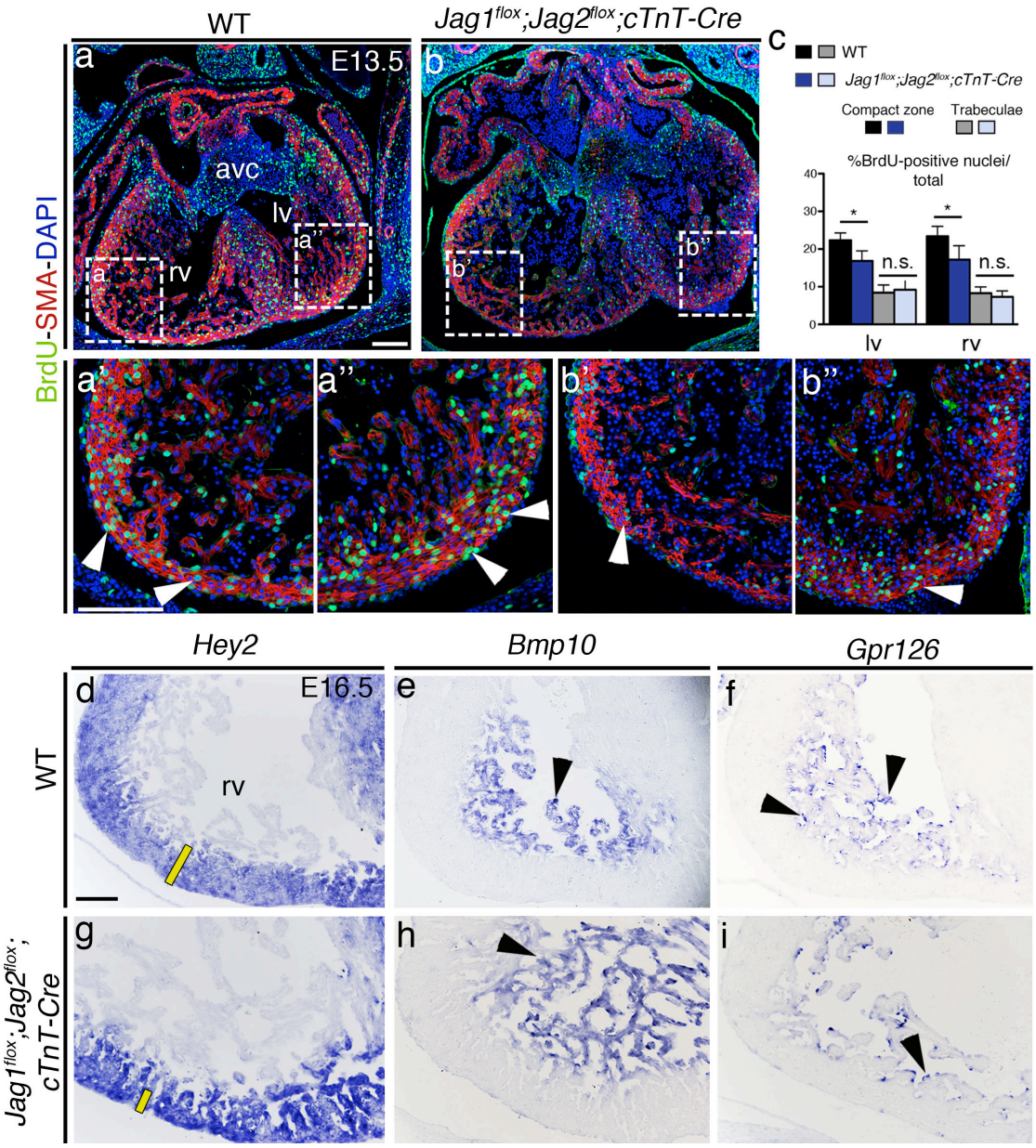

Figure 23. Reduced myocardial proliferation and impaired chamber gene expression in Jag1 and Jag2 double mutants. (**a-b'**) BrdU (green) and SMA (red) immunostaining in E13.5 WT (**a-a''**), and *Jag1^{flox};Jag2^{flox};cTnT-Cre* (**b-b''**) hearts. In the WT BrdU is predominantly incorporated in right (arrowheads in **a'**) and left ventricular (arrowheads in **a''**) compact myocardium; in both ventricles the trabecular cardiomyocytes proliferate less than in the compact layer (**a-a''**). In the mutant hearts the total number of BrdU positive cardiomyocytes in the compact layer of both ventricles (arrowheads in **b'** and **b''**) is reduced compared to the WT. (**a-b''**). Nuclei are counterstained with DAPI (blue). (**c**) BrdU quantification. The total number of BrdU positive nuclei was divided by the total number of cells (DAPI) for each region of interest; compact zone and trabecular myocardium of left and right ventricles. Data are represented as mean ± S.D. (n=3 WT and 3 *Jag1^{flox};Jag2^{flox};cTnT-Cre* *P < 0.01, determined by Student's *t* test). (**d-i**) ISH analysis. In E16.5 WT *Hey2* delineates very thick compact myocardium (**d**, yellow bar), which is thin in *Jag1^{flox};Jag2^{flox};cTnT-Cre* (**i**, yellow bar). *Bmp10* expression is found in the trabecular myocardium of WT (arrowhead in **h**) and in *Jag1^{flox};Jag2^{flox};cTnT-Cre* it shows how trabeculae are disorganized and uncompacted (arrowhead in **h**). *Gpr126* marks the endocardium in WT ventricles (**f**, arrowhead) and its expression is severely reduced in *Jag1^{flox};Jag2^{flox};cTnT-Cre* (**i**). rv=right ventricle; lv=left ventricle; avc=atrioventricular canal. Scale bar=100µm.

Manic Fringe modulates Notch selectivity towards its ligands in ventricular endocardial cells

We next investigated the mechanism underlying the spatio-temporal specificity of Dll4, Jag1 and Jag2 towards the Notch1 receptor during chamber development. The Fringe family of glycosyltransferases catalyses the elongation of O-linked fucose on the EGF-like repeats of Notch, contributing to receptor selectivity towards its ligands (Panin et al., 1997). Upon Notch glycosylation, Delta-Notch signaling is enhanced, and Jag/Ser-Notch signaling is diminished (Panin et al., 1997, Yang, Nichols et al., 2005). We evaluated the expression in the embryonic heart of the three mammalian Fringe paralogs by ISH and qRT-PCR. *Manic Fringe* (*MFng*) was strongly transcribed in chamber endocardium at E8.5 (Fig. 24a). Its expression declined progressively to a minimum at E11.5 and was detected only in the endocardium of the AVC (Fig. 24a-d). qRT-PCR analysis confirmed high levels of the transcript at E8.5 and significant down-regulation from E9.5 to E11.5 (Fig. 24m). In contrast, from E9.5 to E11.5, *Lunatic Fringe* (*LFng*) was only detected in the proepicardium and epicardium (Fig. 24f-h). *Radical Fringe (RFng)* was not expressed in the heart during these stages (Fig. 24j-l). qRT-PCR confirmed the basal levels of *RFng* mRNA in the ventricle and increasing expression of *LFng* from E8.5 to E11.5 (Fig. 24n).

We next performed *ISH* of *MFng* and *LFng* at later stages of heart development. At E14.5 *MFng* was expressed in the developing coronary vessels but not in the endocardium (Fig. 24e-e'). Its expression pattern resembled that of *Dll4* at this stage (Fig. 24b-b'). In E14.5 heart sections *LFng* was detected in the subepicardial endothelium and in the cells forming the mural leaflet of the left mitral valve (Fig. 24i-i'). Different studies based on linage tracing analysis described that EPDCs contribute to the development of these two regions, consistent with the epicardial expression of *LFng* during mid-gestation (E9.5-E11.5, Fig. 24f-h).

The endocardial expression of *MFng* during trabeculation (E8.5-10.5), in addition to the functional studies performed with *Dll4*, *Notch1, Jag1*, *Jag2* and double *Jag1*;*Jag2* mutant embryos, suggested that MFng activity would favor endocardial Dll4 signaling to the Fringe-modified Notch receptor. Furthermore, as development proceeds, the down-regulation of *MFng* expression after E11.5 would allow Jag1 and Jag2 signaling from the myocardium to activate Notch in the endocardium, but still favoring the Dll4-Notch signaling in the developing coronary vessels.

To understand how glycosylated Notch receptor interacts with its ligands, we performed an i*n-vitro* stimulation assay, as previously described (Benedito et al., 2009). For this experiment we isolated mouse embryonic ventricular endocardial cells (MEVEC) from E10.5 WT ventricles. To avoid the rapid senescence of the primary cell cultures, we immortalized MEVEC with SV40 T antigen expressing lentivirus (Fig. 5). Upon infection, the cells maintained their characteristic cobblestone-like morphology, proper of endothelial-like cells, and proliferated very fast. We next, transduced MEVEC with a lentiviral vector encoding the full-length of murine *MFng-IRES-eGFP*

(MFng-MEVEC) or with the lentiviral vector alone as control (GFP-MEVEC). The efficiency of transduction was evaluated measuring the levels of *MFng* by qPCR analysis (Fig. 24o). Transduced cells showed very high levels of *MFng* expression compared with GFP-MEVEC counterparts, whereas expression levels of *Notch1* and *Dll4,* as well as the chamber endocardium markers *Nfatc1*, *Nrg1* and *Gpr126* were normal. (Fig.24o).

We first compared the response of control-transduced MEVEC to stimulation with immobilized Dll4, Jag1 or Jag2, all of which can activate Notch in a cell-contact-independent manner (Benedito et al., 2009). As read-outs of Notch activation we measured by luciferase assay the activation of the Notch reporter CBF1-Luc (McKenzie, Stevenson et al., 2005) (Fig. 24p) and by qPCR the levels of *Hey1* expression (Fig. 24q), a well-known endocardial Notch target (Timmerman et al., 2004). Dll4 and Jag1 activated the Notch reporter to a similar extent in control-transduced MEVEC, whereas Jag2 elicited a weaker response (Fig. 24p); in contrast, all three ligands induced a similar increase in *Hey1* expression (Fig. 19q). Pairwise combinations of the ligands produced additive effects on Notch activation (Fig. 19p).

MFng overexpression in MEVEC strongly potentiated Notch reporter activity and *Hey1* expression in response to Dll4, whereas the response to Jag1 and Jag2 and subsequent *Hey1* expression remained weak (Fig. 24p-q). Combinations of Dll4+Jag1 and Dll4+Jag2 produced a similar response to stimulation with Dll4 alone (Fig. 24p-q), but the Jag1+Jag2 combination stimulated Notch signaling weakly (Fig. 24p-q). *In vitro* experiments indicated that upon MFng glycosylation, Notch activity was highly enhanced in response to Dll4, converting it in a "superactivator" of Notch signaling. In addition, combination of Jag1 or Jag2 with Dll4 did not reduce Notch activity. This result was in contrast with the inhibitory effect of Jag1 previously described (Benedito et al., 2009). In our system, overexpression of *MFng* mirrors the scenario during trabeculation in which Notch activity strongly depends on Dll4. In MEVEC, all ligands analyzed, similarly activated un-glycosylated Notch.

Interestingly, their combination enhanced Notch activity at least 2–fold more than single ligand stimulation, indicating an additive effect of Notch activity. These results suggested that the absence of MFng frees Jag1 and Jag2 to cooperate in the activation of Notch1 resembling the scenario during chamber compaction.

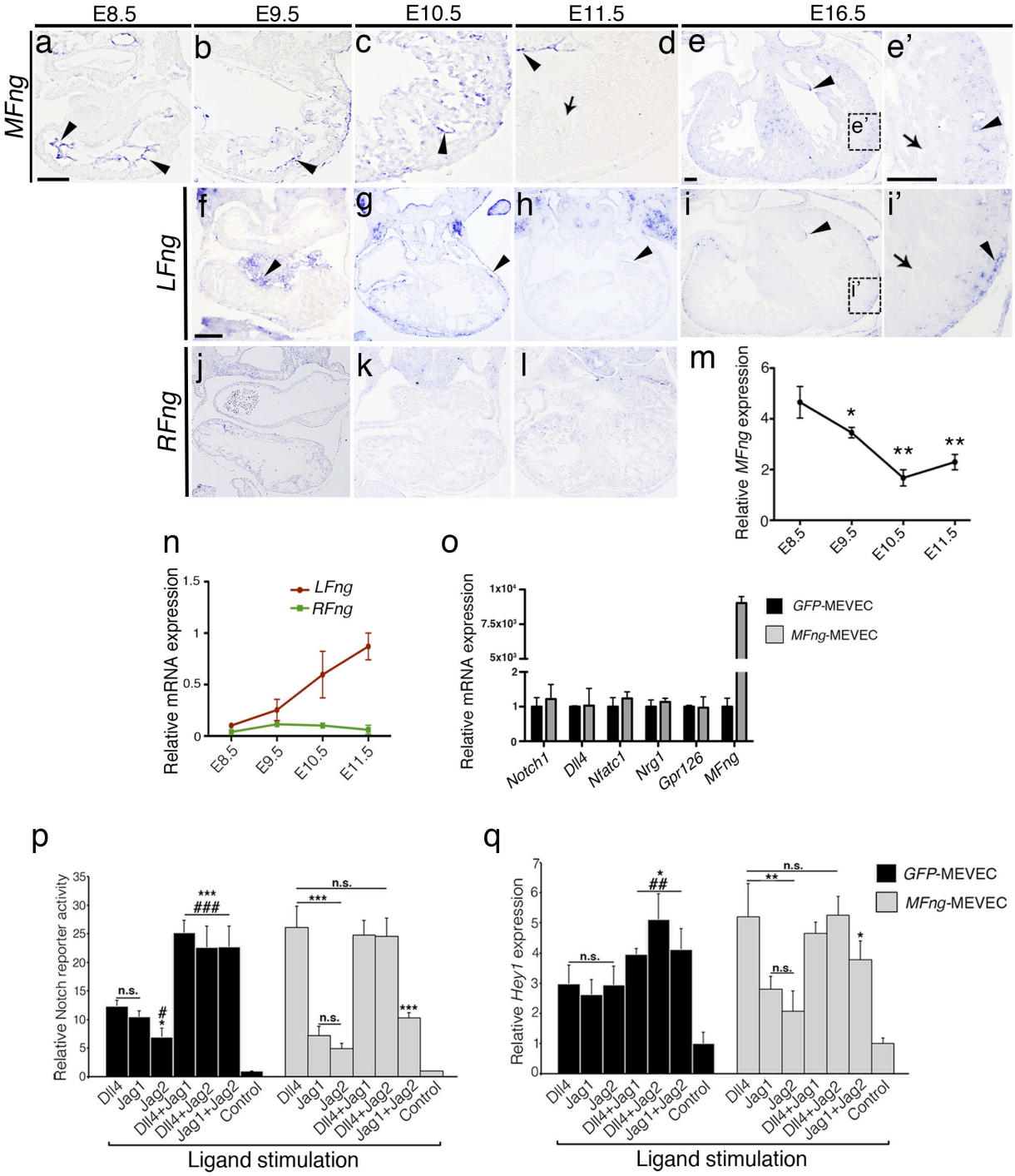

Systemic *Fng* inactivation affects coronary vessel development

The expression pattern of *MFng*, the phenotype of *Dll4* mutant embryos, the strong reduction of endocardial Notch activity in the double Jag1;Jag2 mutants and the ligand stimulation assay performed on MEVEC suggested that MFng may regulate the spatio-temporal specificity of Notch ligand-receptor interactions in the developing chamber. To elucidate the effect of Fringe-modified-Notch receptor *in vivo*, we used mice triply deficient for *MFng*, *LFng* and *RFng* ($M^{-/-};L^{-/-};R^{-/-}$).

Figure 24. Endocardial-endothelial *MFng* would favor Dll4-Notch1 signaling during trabeculation and coronary artery development. (**a-e'**) ISH analysis of *Manic Fringe* (*MFng*). At E8.5-10.5, *MFng* is transcribed in ventricular endocardium (**a-c**, arrowheads) and is downregulated at E11.5 (**d**). At E16 (**e-e'**), *MFng* is expressed in coronary vessel endothelium (arrowheads in **e'**) but not in endocardium (arrow in **e'**). ISH analysis of *Lunatic Fringe* (*LFng*) and *Radical Fringe* (*RFng*) in WT hearts at the indicated developmental stages. (**f-l**) *LFng* expression is detected in proepicardial cells of E9.5 WT embryos (**f**) and is restricted to the epicardium of E10.5 (**g**) and E11.5 (**h**) WT hearts. At E16.5 (**i,i'**), *LFng* is found in subepicardial veins (arrowheads in **i'**) but not in endocardium (arrow in **i'**). (**j-l**) ISH of *RFng* from E9.5 (**j**), E10.5 (**k**) and E11.5 (**l**) WT heart sections. *RFng* is not expressed in the heart at these stages. (**m**) Relative *MFng* expression measured by qRT-PCR from E8.5-11.5 indicates a progressive downregulation of the transcript from E10.5 onwards. Data are represented as mean ± S.D. (n=3 pools of 6 hearts at E8.5 and 3 pools of 3 ventricles each for other stages **P* <0.05, **P < 0.01, determined by Student's *t* test). (**n**) Relative mRNA expression of *LFng* and *RFng* in E.9.5, E10.5 and E11.5 ventricles. (**o**) MEVEC stimulation assay. qRT-PCR analysis of Notch pathway genes and endocardial markers, indicating similar expression levels of these genes in *GFP*-MEVEC and *MFng*-MEVEC. (**p**) Notch signaling activity measured by 10xCBF1-Luc reporter assay in MEVEC infected with control GFP lentivirus (*GFP*-MEVEC, solid black bars) or with a MFng-lentivirus (*MFng*-MEVEC, grey bars) and stimulated with immobilized Notch ligands. Stimulation of *GFP*-MEVEC with Dll4, Jag1 or Jag2 (or their combinations) triggers similar reporter activation. Stimulation of *MFng*-MEVEC with Dll4 strongly activates the Notch reporter, while Jag1 and Jag2 have a weak effect. Combinations of Dll4 with Jag1 or Jag2 trigger a response similar to that of Dll4 alone, while the Jag1+Jag2 combination has a weak effect. Control represents the activity of the Notch reporter in non-stimulated MEVEC. (**q**) qRT-PCR analysis of *Hey1* expression in *GFP*-MEVEC (black bars) or *MFng*-MEVEC (grey bars). Symbols: *, significant difference compared to Dll4; #, compared to Jag1. Data are represented as mean ± S.D. (n=4 biological replicates for each condition, *, # *P*<0.05, **, ## *P*<0.01, ***, ### *P*<0.001 by Student's *t* test, n.s. not significant). Scale bar=100µm

Systemic inactivation of *Fng* allowed us to avoid possible redundancy between the three different paralogs. Previous studies demonstrated that triple mutant mice develop to term and, although they are not found at the expected Mendelian frequency at weaning, no embryonic lethal phenotypes have been reported. $M^{-/-};L^{-/-};R^{-/-}$ deficient embryos were examined by histological analysis at E16.5, when chamber development is well advanced (Fig. 25a-b). $M^{-/-};L^{-/-};R^{-/-}$ mice showed a significant reduction in the thickness of the compact myocardium in both ventricles, indicating that Fng is required for chamber development at this stage (Fig. 25c). Interestingly, the mutant hearts did not display any difference in the complexity of the trabecular myocardium (Fig. 25c). ISH analysis of *Hey2*, a compact myocardial marker, was not expanded in the trabeculae, but clearly evidenced a reduced compact layer in $M^{-/-};L^{-/-};R^{-/-}$ deficient embryos (Fig 25d,g). In triple mutants, *Cx40/Gja5* was normally transcribed in trabeculae, but its expression was reduced in the coronary vessels (Fig 25e,f). The morphological defects observed in triple mutant mice and the low expression of *Cx40/Gja5* in the coronary artery indicated that Fng glycosyltransferases might be required for proper coronary vessel development during chamber compaction. We next assayed the expression of N1ICD in $M^{-/-};L^{-/-};R^{-/-}$ heart sections (Fig. 25f-i'). N1ICD appeared relatively normal

in the triple mutant ventricular endocardium but was attenuated in coronary vessels co-stained with isolectin B4 (Ib4). In addition, Ib4 immunostaining evidenced reduced calibre of the coronary endothelium. We then examined the expression of *Dll4* (Fig. 25j-n), *Hey1* (Fig. 25k-o), *HeyL* (Fig. 25l-p) and *EphrinB2* (Fig. 25m-q) in coronary arteries of Fng-deficient embryos. All of them showed reduced expression. We previously described reduced arterial marker expression in E15.5 $Dll4^{flox}$;$Cdh5\text{-}Cre^{ERT}$ mutant hearts (Fig. 11e-i; k-r). These data indicated that systemic *Fng* abrogation disrupts coronary vessel development, crucial for myocardium nourishment, thus indirectly affecting compaction. At later stages, *MFng* (Fig 24e-e'), as well as, the ligands Dll4 (Fig. 11e-i), Jag1 (Fig. 13b-b'') and Jag2 (Fig. 19c-d), are expressed in coronary vessels. The observation that the phenotype from *Fng* null embryos resembles those observed in $Dll4^{flox}$;$Cdh5\text{-}Cre^{ERT}$ mutants, strengthens the idea that Dll4 signals to Fng-modified-Notch in the developing coronaries.

Forced *MFng* expression disrupts Jag1/Jag2-Notch interaction

According to our *in-vitro* results, we speculated whether ectopic expression of *MFng* in the endocardium would prevent the activation of Notch1 by Jag1 and Jag2 at later stages of development, producing a chamber phenotype similar to that caused by inactivation of both ligands or *Mib1* inactivation. To test this hypothesis, we used a new transgenic line ($MFng^{tg}$) bearing a *Rosa26-CAG-floxNeoSTOPflox-MFng-EGFP* expression cassette (Fig. 26a). *Tie2-Cre*-mediated (Kisanuki et al., 2001) removal of the *NeoSTOP* sequences results in *MFng-EGFP* expression driven by the *Rosa26-CAG* promoter in vascular endothelium and endocardium. Two-photon imaging of fixed E9.5 $MFng^{tg}$;*Tie2-Cre* embryos showed expression of the transgene in the endothelial cells forming the dorsal aorta and all over the endocardium (Fig. 26b). Despite the strong expression of the *MFng-EGFP* in the endocardium we did not observed any obvious phenotype at this stage. Interestingly, at E16.5 ectopic expression of *MFng* produced a dilated heart, with severe cardiac defects (Fig. 26c-d'). Histological analysis evidenced very prominent ventricular septal defects (Fig. 26b). In addition, we observed a reduction of 50-60% in the thickness of the compact myocardium comparing with WT embryos (Fig. 26g). Concomitant with a thinner compact myocardium, transgenic mice showed a significant increase in trabecular complexity, indicating defective compaction (Fig. 26g).

The majority of transgenic mice did not survive beyond P5, and therefore we examined the phenotype in heart sections from newborn (P1) mice stained with endomucin to delineate the chamber endocardium and labeled with wheat-germ agglutinin to visualize cardiomyocytes (Fig. 26e-f'').

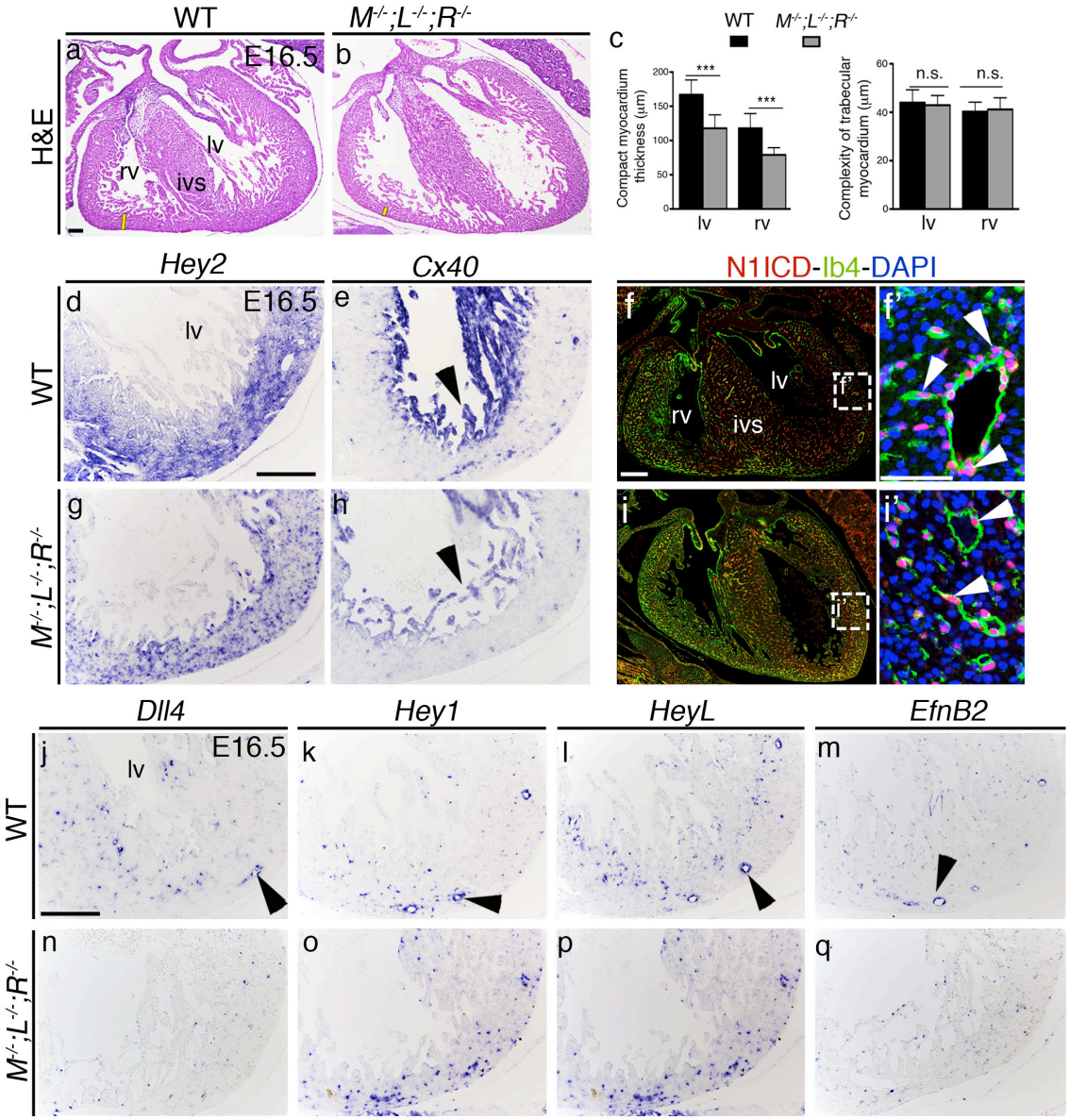

Figure 25. Systemic *Fng* abrogation impairs coronary vessel formation.
H&E staining of E16.5 WT (**a**) and *M;L;RFng*-deficient hearts (**b**). WT ventricles have compacting trabeculae and a thick compact myocardium. The $M^{-/-};L^{-/-};R^{-/-}$ heart has a thin compact myocardium and trabeculae. (**c**) Chart showing morphological parameters of compact myocardium thickness and complexity of trabecular myocardium in WT and $M^{-/-};L^{-/-};R^{-/-}$ mutants. Data are mean ± S.D. (n=3 WT and 3 $M^{-/-};L^{-/-};R^{-/-}$ ***P < 0.001, n.s. not significant, determined by Student's *t* test). ISH analysis of *Hey2* (**d,g**) and *Cx40* (**e,h**). *Hey2* expression delineates a reduced compact myocardium in the $M^{-/-};L^{-/-};R^{-/-}$ mutants, whereas *Cx40* shows few and very thin trabeculae invading the lumen of the mutant ventricle (**h**). Note the reduced expression of *Cx40* in the coronary endothelium of $M^{-/-};L^{-/-};R^{-/-}$ mutants (**h**). (f-i') N1ICD immunostaining in E16.5 WT and $M^{-/-};L^{-/-};R^{-/-}$ mutant heart sections. The endocardium and the endothelium are counterstained with isolectin B4 (IB4, green). Coronaries appear of irregular size and poorly N1ICD-stained in the $M^{-/-};L^{-/-};R^{-/-}$ heart (**i'**). (**f,i'**) Nuclei are counterstained with DAPI (blue). (**j,q**) ISH analysis of markers for coronary arteries. *Dll4* (**j,n**), *Hey1* (**k,o**), *HeyL* (**l,p**) and *EphrinB2* (**m,q**) expression is reduced in $M^{-/-};L^{-/-};R^{-/-}$ mice (arrowhead in **j,k,l,m** indicate the transcript localization in E16.5 WT). lv=left ventricle; rv=right ventricle; ivs= interventricular septum. Scale bar=100µm, except in (**f'; i'**) where bars =50µm.

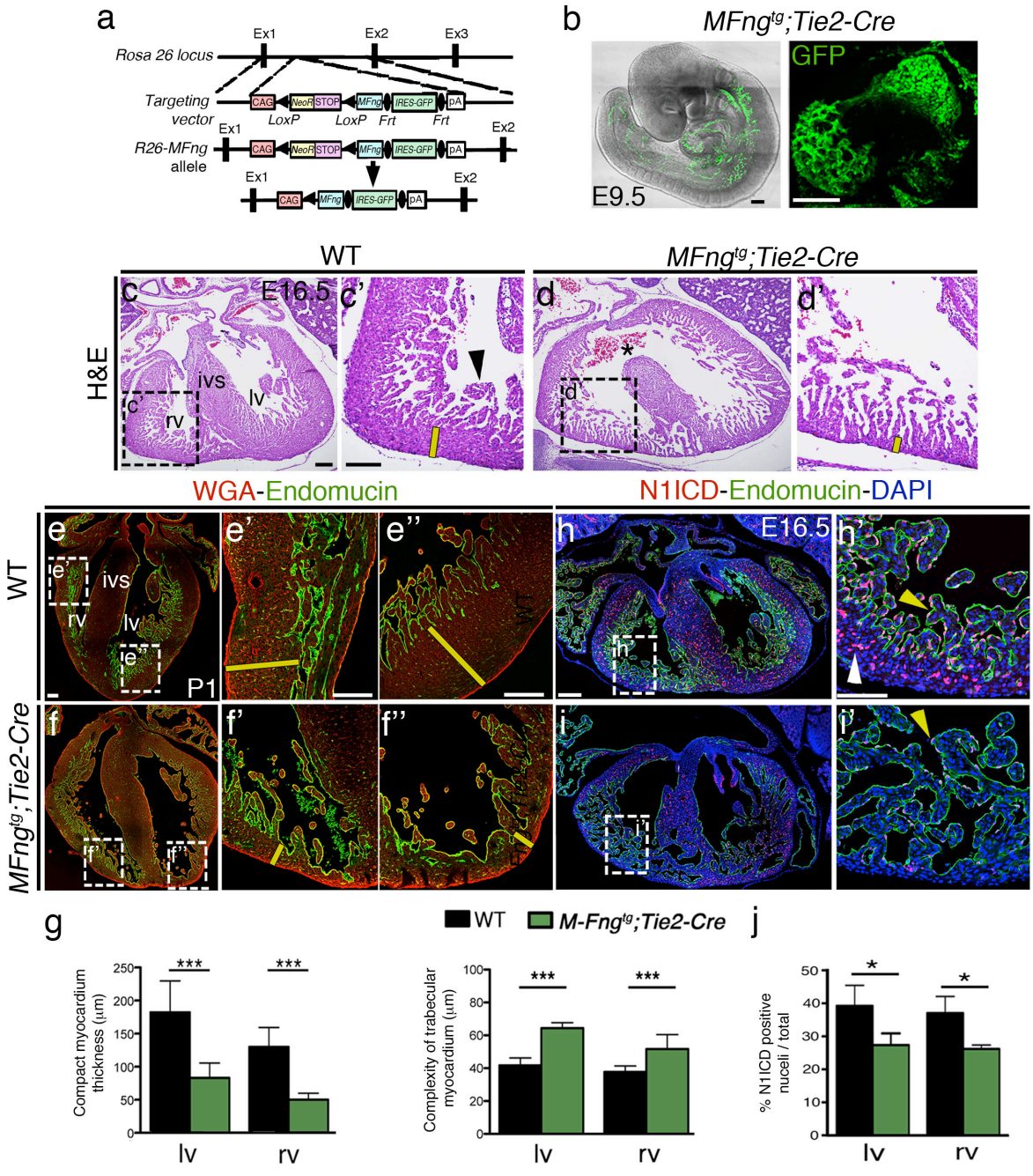

P1 WT mice had a thick compact myocardium with some compacting trabeculae (Fig. 26e-e''), whereas *MFng^{tg};Tie2-Cre* littermates had a thin compact myocardium and non-compacted trabeculae in both ventricles, with no effect on cardiomyocyte size (Fig. 26f-f').

The data from *MFng^{tg};Tie2-Cre* embryos and neonates were in agreement with the prediction that forced MFng expression in the endocardium would produce a chamber phenotype similar to those observed by inactivation of Jag1 and Jag2 or Mib1.

Figure 26. Forced endocardial *MFng* expression disrupts chamber compaction.
(**a**) Gene targeting strategy used to generate the conditional *M-Fng^{tg}* line. *Top*, The transgene is inserted between exons 1 and 2 of the *Rosa26* locus by homologous recombination. *Middle*, transgenic *MFng* and *IRES-GFP* expression is achieved under the control of the *CAG* promoter after Cre-mediated deletion of a *NeoR-STOP* cassette. (**b**) Whole-mount two-photon microscopy image of an E9.5 *MFng$^{tg/+}$;Tie2-Cre/+* embryo showing MFng-GFP expression in endocardium and vascular endothelium. Detail of the heart showing endocardial expression of the transgene. (**c-d**) H&E staining of E16.5 WT (**c,c'**) and *MFng$^{tg/tg}$;Tie2-Cre/+* (*MFng^{tg};Tie2-Cre*) ventricles (**d,d'**). WT hearts have a thick compact myocardium (**c**, yellow bar in **c'**) and compacting trabeculae (**c'**, arrow). In contrast, the *MFng^{tg};Tie2-Cre* heart has a very thin compact myocardium (**d**, yellow bar in **d'**), disorganized trabeculae (**d'**, arrows) and a defective ventricular septum (**d**, asterisk). (**e,f''**) Wheat-germ agglutinin (WGA) and endomucin staining at P1 reveal a thick myocardium with almost fully compacted trabeculae in WT hearts (**e-e''**, yellow bars) and a thin compact myocardium with relatively large trabeculae in *MFng^{tg};Tie2-Cre* hearts (**f-f''**, yellow bars). (**g**) Chart showing morphological parameters of compact myocardium thickness and complexity of trabecular myocardium in WT and *MFng^{tg};Tie2-Cre* mutants. Data are mean ± S.D. (n=3 WT and 3 *MFng^{tg};Tie2-Cre* ***P < 0.001, n.s. not significant, determined by Student's *t* test). (**h-i'**) N1ICD and endomucin staining. General view of the E16.5 WT heart (**h**) and detail of the right ventricle showing N1ICD expression throughout the endocardium delineated by endomucin expression (**h'**, yellow arrowheads) and in coronaries (**h'**, white arrowhead). General view of the E16.5 *MFng^{tg};Tie2-Cre* heart (**i**) and detail of the right ventricle (**i'**), with markedly reduced N1ICD expression (**i'**, yellow arrowheads). (**j**) Quantification of N1ICD-positive cells in the heart of E16.5 WT and transgenic embryos. Data are mean ± S.D. (3 WT and 3 *MFng^{tg};Tie2-Cre*, * P < 0.05, determined by Student's *t* test). Scale bar=100μm

To confirm that Notch1 activity was attenuated due to impairment of Jag1-Jag2 signaling to Notch receptor, we assayed N1ICD immunostaining in E16.5 WT and *MFng^{tg};Tie2-Cre* (Fig. 26h-i'). N1ICD expression was 40% below normal in the endocardium of both ventricles of transgenic animals (Fig. 26j). This data clearly indicate that ectopic expression of *MFng* impaired Notch activity in the endocardium presumably impeding Jag1;Jag2-Notch interactions.

Considering previous results showing that Notch activity mediates cardiomyocyte proliferation in a non-cell-autonomous manner, we performed BrdU incorporation analysis in *MFng^{tg};Tie2-Cre* embryos. In both ventricles of E13.5 *MFng^{tg};Tie2-Cre*, cardiomyocytes of the compact zone proliferated less than in the WT (Fig. 27a-b''; c). In trabecular myocardium, the number of dividing cardiomyocytes was similar to the WT (Fig. 27a-b''; c). Low proliferation in the compact myocardium could explain the reduction in the thickness of this layer observed at E16.5 in transgenic animals, but not the increasing trabecular complexity. To better characterize the chamber phenotype of transgenic animals at the molecular level, we assayed the expression of compact myocardial marker *Hey2* and trabecular markers *Bmp10* and Cx40. Intriguingly, *Hey2* expression delineated a thin compact myocardium and was expanded to but did not reach the tip of the trabeculae in E16.5 *MFng^{tg};Tie2-Cre* mice (Fig. 27d-g), while *Bmp10* (Fig. 27e-h) and *Cx40* (Fig. 27f-i) expression were restricted to the distal tip of the trabeculae. Indeed, *Hey2* and *Bmp10* or *Cx40* expression in the trabeculae were complementary.

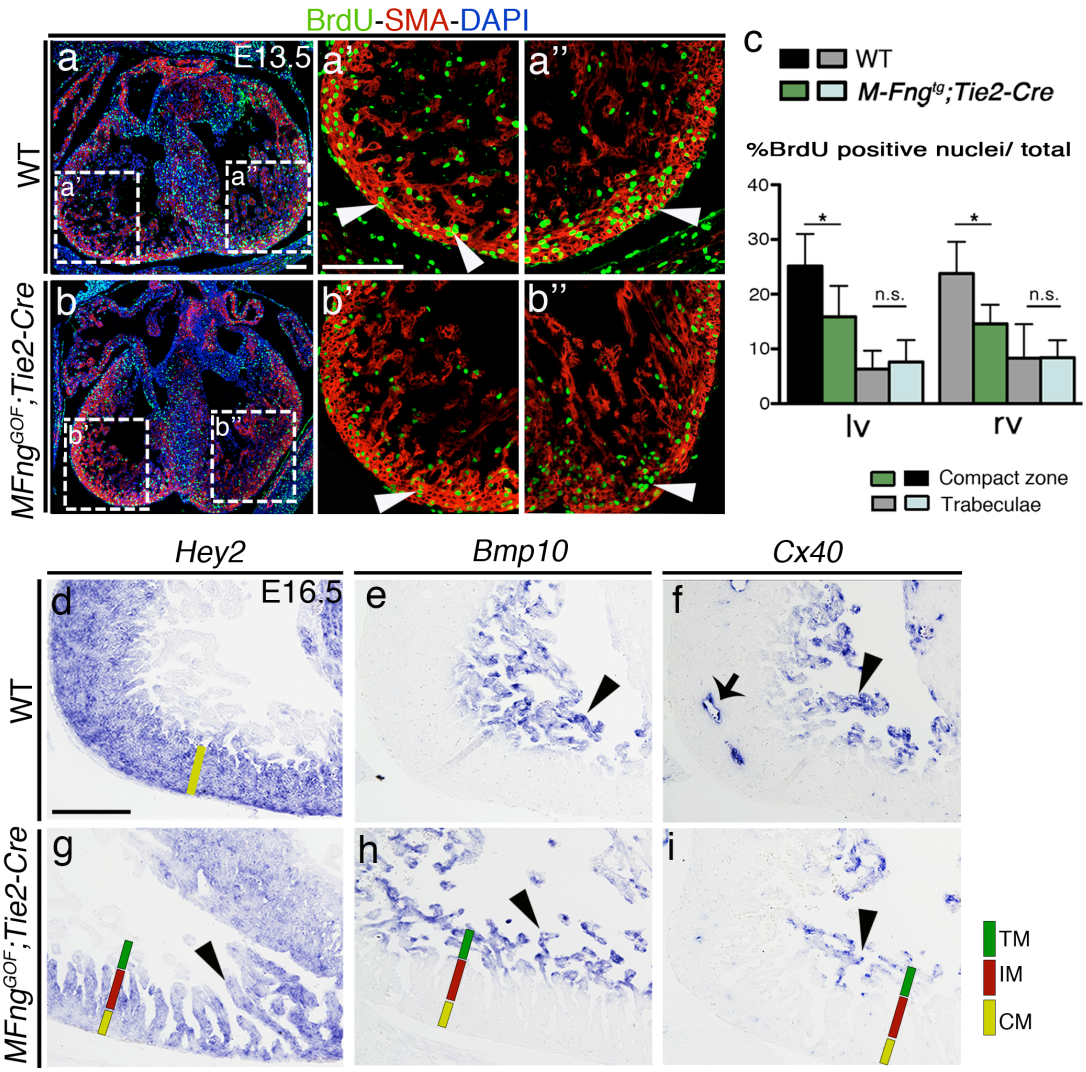

Figure 27. Ectopic endocardial *MFng* expression impairs cardiomyocyte proliferation and chamber maturation.

(**a-b'**) BrdU (green) and SMA (red) immunostaining in E13.5 WT (**a-a''**), and *MFng^{tg};Tie2-Cre* hearts (**b-b''**). In the WT hearts BrdU is predominantly incorporated in right (rv, arrowheads in **a'**) and left ventricular (lv, arrowheads in **a''**) compact myocardium; in the mutant hearts the total number of BrdU positive cardiomyocytes in the compact layer of both ventricles (arrowheads in **b' and b''**) is reduced compared to the WT. (**a-b''**). Nuclei are counterstained with DAPI (blue). (**c**) BrdU quantification. The total number of BrdU positive nuclei was divided by the total number of cells (DAPI) for each region of interest; compact zone and trabecular myocardium of left (lv) and right ventricle (rv). Data are mean ± S.D. (n=3 WT and 3 *MFng^{tg};Tie2-Cre* *P < 0.01, n.s. not significant, determined by Student's *t* test). (**d-i**) ISH analysis at E16.5. *Hey2* expression reveals a thick compact myocardium in the WT heart (**d**) and a very thin and disorganized counterpart in the *MFng^{tg};Tie2-Cre* heart (**g**). *Bmp10* and *Cx40* mark the trabeculae in WT (**e,f**) and *MFng^{tg};Tie2-Cre* ventricles (**h,i**). The yellow bar marks the compact myocardium (CM); the green bar marks the trabecular myocardium (TM) in (**g-i**) and the red bar in (**g,i**) marks the intermediate myocardium (IM). Scale bar=100µm

It appeared that in the ventricle of *MFng^{tg};Tie2-Cre* mice, compact myocardium cardiomyocytes (CM, *Hey2*+) entered into the trabeculae and formed an "intermediate myocardium" (IM, *Hey2*+, *Bmp10*$^{-}$ or *Cx40*$^{-}$) that defined a boundary between compact myocardium and trabecular myocardium (TM, *Hey2*$^{-}$, *Bmp10*$^{+}$ or *Cx40*$^{+}$). A similar albeit more subtle phenotype could be observed in *Jag2^{flox};cTnT-Cre* (Fig. 20g-k) and *Jag1^{flox};Jag2^{flox};cTnT-Cre* hearts (Fig. 23d-h).

All these results indicate that forced *MFng* expression in the endocardium prevents Notch1 activation, presumably by inhibiting Jag1 and Jag2 signaling leading to severely altered ventricular development and LVNC.

Comparative *Jag1, Jag2*, double *Jag1;Jag2* and *MFng^{tg}* cardiac gene profiling

The exacerbated cardiac phenotype and the lower Notch activity levels during chamber compaction observed in *Jag1;Jag2* double mutant embryos comparing with Jag1 or Jag2 single mutants suggested that both ligands had a mutual effect on endocardial Notch activity. To strengthen this hypothesis and to achieve a more global perspective of specific genes responsive to Jag1 and Jag2-Notch1 signaling, we carried out RNA-seq experiments with E15.5 WT, *Jag2^{flox};cTnT-Cre* and *Jag1^{flox};Jag2^{flox};cTnT-Cre* ventricles. In addition, taking into account the ventricular phenotype observed in the *MFng^{tg};Tie2-Cre* mice and to confirm the prediction that the ectopic expression of MFng would block Jag1 and Jag2 signaling to Notch, we included in the analysis this transgenic line. By RNA-seq analysis we identified 41 differentially expressed genes (31 up- and 10 down-regulated) in *Jag2^{flox};cTnT-Cre* mutants, 474 differentially expressed genes (320 up- and 154 down-regulated) in *Jag1^{flox};Jag2^{flox};cTnT-Cre* mutants and 1561 differentially expressed genes (979 up- and 582 down-regulated) in *MFng^{tg};Tie2-Cre* hearts (Fig. 28a supplementary table1). Comparison of expression profiles among single and double *Jag1*- and *Jag2*- mutants showed that *Jag1^{flox};cTnT-Cre* and *Jag2^{flox};cTnT-Cre* mutants shared only 7 differentially expressed genes, while *Jag1^{flox};cTnT-Cre* and *Jag1^{flox};Jag2^{flox};cTnT-Cre* mutants shared 73 altered genes and the *Jag2^{flox};cTnT-Cre* and *Jag1^{flox};Jag2^{flox};cTnT-Cre* mutants shared 20 (Fig. 28b supplementary table1). We then compared the expression profiles of *Jag1^{flox};Jag2^{flox};cTnT-Cre* and *MFng^{tg};Tie2-Cre* mice. We found 160 common genes between the two different genotypes (Fig. 28c supplementary table1). These data indicated that more than 30% of deregulated genes in the myocardial deficient *Jag1;Jag2* embryos were shared with transgenic embryos overexpressing *MFng* in endothelial-endocardial cells.

The heat map in Fig. 28d shows the 319 genes that were differentially expressed in at least two of the five mutant genotypes. Interestingly, while *Jag2* inactivation affected the expression of a small set of genes (41) compared to *Jag1* (97), in the double *Jag1^{flox};Jag2^{flox};cTnT-Cre* mutant the number of deregulated genes increased decisively (474) from single mutants, indicating that both

Notch ligands participate in a non-redundant manner in chamber development, and thus their simultaneous inactivation has a synergistic effect in gene deregulation (Fig. 28d). *MFng^{tg};Tie2-Cre* mice presented the largest number of deregulated genes, probably because of the early onset and strength of *Tie2-Cre* (Kisanuki et al., 2001) driving the expression of two extra copies of MFng cDNA in the endocardium, as well as, in the whole endothelium. The majority of the genes in common with the *Jag1^{flox};Jag2^{flox};cTnT-Cre* mutants changed in the same manner (up- or down-regulated; Fig. 28d supplementary table1), suggesting that *MFng* overexpression in the endocardium indeed blocks *Jag1* and *Jag2* signaling to the Notch1 receptor.

GO analysis identified several relevant functional categories among the deregulated genes (Fig. 28d supplementary table1). Genes involved in angiogenesis and vascular development (*Hey2*, *Angpt1*, *Cx40/Gja5*, *Ctgf*, *Tgfβ1*, *Shank3*, *Hif1a* and *Cxcl12*) were affected in at least two genotypes. *Hey2* is a Notch target in the endocardium (Luna-Zurita et al., 2010) and the vasculature (Fischer, Schumacher et al., 2004) and accordingly, its expression was down-regulated in *Jag1^{flox};Jag2^{flox};cTnT-Cre* and *MFng^{tg};Tie2-Cre* mice (Fig. 28d). Within this category, some of the deregulated genes were involved in coronary artery development (*Cxcl12* (Ivins et al., 2015), *Hey2* (Watanabe, Koibuchi et al., 2010)) and their down-regulated expression suggested that this process is impaired in *MFng^{tg};Tie2-Cre* and, to a lesser extend, in *Jag1^{flox};Jag2^{flox};cTnT-Cre* mice. Genes involved in cardiac fibrosis (*Ctgf* and *Tgfβ1*; (Leask, 2015)) were up-regulated in *Jag1^{flox};Jag2^{flox};cTnT-Cre* and *MFng^{tg};Tie2-Cre* mice (Fig. 28d). A gene specifically up-regulated in *Jag2^{flox};cTnT-Cre* mice (and also in *Jag1^{flox};Jag2^{flox};cTnT-Cre*) was *Shank3*, encoding a scaffolding protein present in the sarcolemma of cardiomyocytes (Grubb, Luo et al., 2015). A second GO category included cell cycle and proliferation genes, in which negative regulators of cell cycle (*Cdkn1a/p21*, *Plk2*, *Rps6ka2* and *Romo1*) were up-regulated in the majority of the genotypes (Fig. 28d supplementary table1). These results were consistent with the reduced cardiomyocyte proliferation observed in *Jag1-* and *Jag2-* mutants. *Romo1* transcription was specifically up-regulated in the heart of *Jag2^{flox};cTnT-Cre* mice, while *Cdkn1c/p57* up-regulation was detected only in *Jag1^{flox};Jag2^{flox};cTnT-Cre* mice. One exception was the positive cell cycle regulator *Ccnd2/CyclinD2* whose expression was up-regulated in *Jag1^{flox};Jag2^{flox};cTnT-Cre* and *MFng^{tg};Tie2-Cre* mice (Fig. 28d). A set of cell death-related genes was deregulated in *Jag2^{flox};cTnT-Cre*, *Jag1^{flox};Jag2^{flox};cTnT-Cre* and *MFng^{tg};Tie2-Cre* mice, including down-regulation of the apoptosis inhibitors *Spp1*, *Bcl6*, *Prnd*, and *Bcl2l11* and up-regulation of the pro-apoptotic gene *Cish* (Fig. 28d), suggesting that cardiac cell homeostasis was altered in these mice. GO also predicted that a large set of genes involved in cellular motion, axonal guidance and migration was specifically deregulated in *Jag1^{flox};Jag2^{flox};cTnT-Cre* and *MFng^{tg};Tie2-Cre* mice, including *Epha2*, *Sema3b*, *Sema5a*, *Efnb3*, *Lpar3*, *Ntn4*, *Epha3*, *Cxcl16* and *Slit2* (Fig. 28d). In the case of Semaphorins, recent research has identified their key functions in cardiac morphogenesis and vascular patterning (Epstein, Aghajanian et al., 2015).

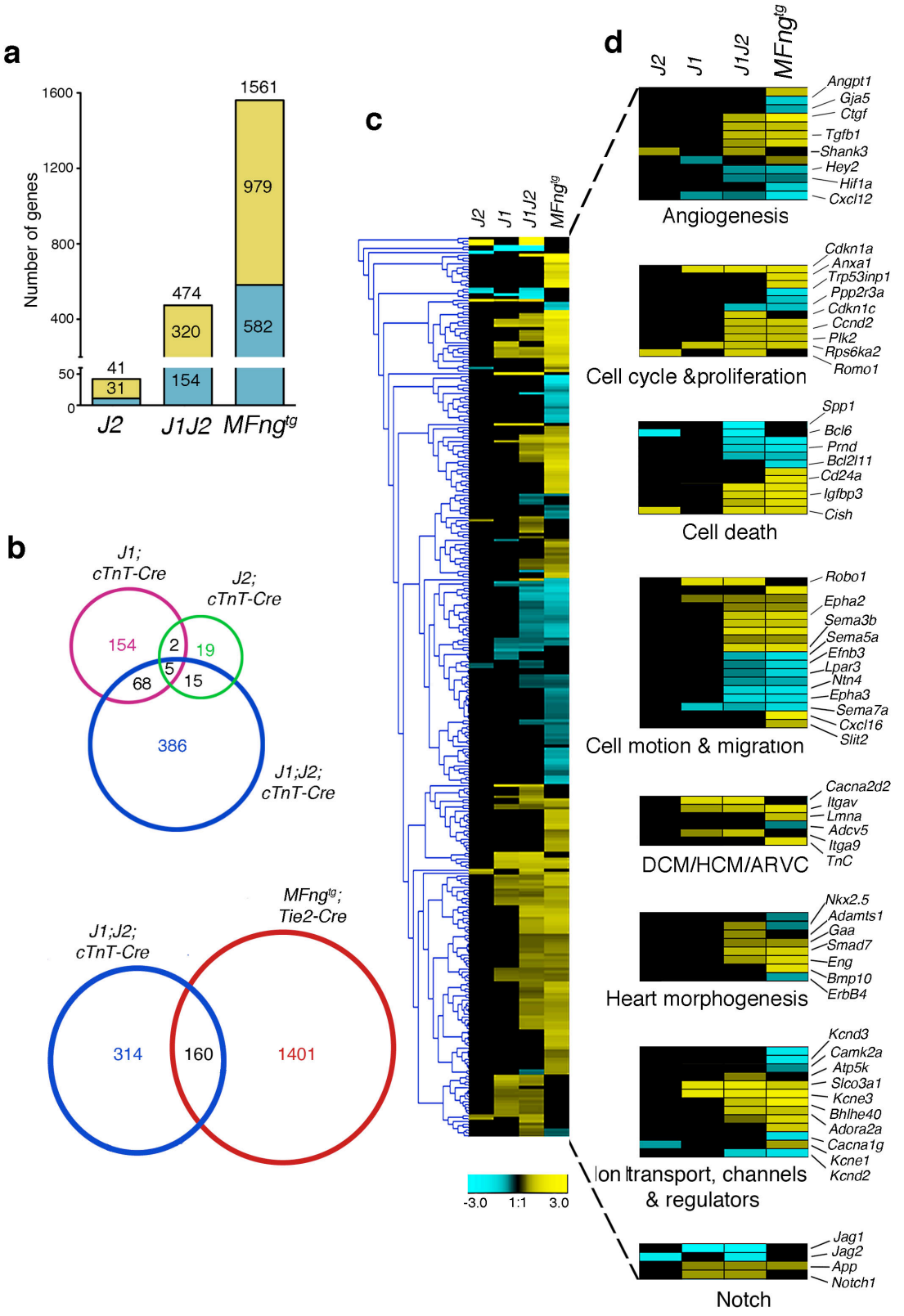
a
Number of genes
1600
1200
800
400
50
0
41
31
474
320
154
1561
979
582
J2
J1J2
MFngtg
b
J1;
cTnT-Cre
J2;
cTnT-Cre
154
2
19
5
68
15
386
J1;J2;
cTnT-Cre
MFngtg;
Tie2-Cre
J1;J2;
cTnT-Cre
314
160
1401
c
J2
J1
J1J2
MFngtg
-3.0
1:1
3.0
d
J2
J1
J1J2
MFngtg
Angpt1
Gja5
Ctgf
Tgfb1
Shank3
Hey2
Hif1a
Cxcl12
Angiogenesis
Cdkn1a
Anxa1
Trp53inp1
Ppp2r3a
Cdkn1c
Ccnd2
Plk2
Rps6ka2
Romo1
Cell cycle &proliferation
Spp1
Bcl6
Prnd
Bcl2l11
Cd24a
Igfbp3
Cish
Cell death
Robo1
Epha2
Sema3b
Sema5a
Efnb3
Lpar3
Ntn4
Epha3
Sema7a
Cxcl16
Slit2
Cell motion & migration
Cacna2d2
Itgav
Lmna
Adcv5
Itga9
TnC
DCM/HCM/ARVC
Nkx2.5
Adamts1
Gaa
Smad7
Eng
Bmp10
ErbB4
Heart morphogenesis
Kcnd3
Camk2a
Atp5k
Slco3a1
Kcne3
Bhlhe40
Adora2a
Cacna1g
Kcne1
Kcnd2
Ion transport, channels
& regulators
Jag1
Jag2
App
Notch1
Notch

Figure 28. Comparative expression profiling of *Jag2^{flox};cTnT-Cre*, *Jag1^{flox};cTnT-Cre*, *Jag1^{flox};Jag2^{flox};cTnT-Cre* and *MFng^{tg};Tie2-Cre* mutants. (**a**) Chart indicating the total number of genes significantly (P<0.05) up- or down-regulated in E15.5 *Jag2^{flox};cTnT-Cre* mutants (*J2*), *Jag1^{flox};Jag2^{flox};cTnT-Cre* mutants (*J1J2*) and *MFng^{tg};Tie2-Cre* transgenic embryos (*MFng^{tg})*. The total number of differentially expressed genes per genotype is indicated at the top of every column. Numbers in the yellow section indicate up-regulated genes; numbers in the blue section indicate down-regulated genes. (**b**) Venn diagram representation of the comparative analysis of the dysregulated genes in the four genotypes analyzed (*Jag1^{flox};cTnT-Cre*, *Jag2^{flox};cTnT-Cre*, *Jag1^{flox};Jag2^{flox};cTnT-Cre* and *MFng^{tg};Tie2-Cre*). Top, comparison of *J1*-, *J2*-single and *J1;J2;cTnT-Cre* double mutants. Bottom, comparison of *J1;J2;cTnT-Cre* and *MFng^{tg};Tie2-Cre* embryos. Numbers in black indicate the total number of genes common to all pair-wise genotype combinations. (**c**) Heat map representation of the 372 genes differentially expressed in at least two of the four mutant genotypes. Yellow colour, up-regulated; blue, down-regulated; black, not signficant change. (**d**) Subsets of genes clustered into functional classes (right panels).

In particular, Sema6d modulates compact layer expansion and trabeculation in the chicken (Toyofuku, Zhang et al., 2004). Of note, one down-regulated gene, *Efnb3*, has been associated with the cardiac hypertrophic response in the adult heart (Dirkx, Gladka et al., 2013).

Genes related with dilated-, hyperthrophic- and arrhythmogenic right ventricular cardiomyopathy (DCM, HCM and ARVC) such as *Cacna2d2*, *Itgav*, *Lmna*, *Adcv5*, *Itga9* and *TnC,* were also deregulated in *Jag1^{flox};cTnT-Cre, Jag1^{flox};Jag2^{flox};cTnT-Cre* and *MFng^{tg};Tie2-Cre* mice (Fig. 28d supplementary table1). Genes required for heart morphogenesis (*Nkx2.5*, *Adamts1*, *Smad7*, *Gaa* and *Eng*) were specifically up-regulated in *Jag1^{flox};Jag2^{flox};cTnT-Cre* mutants, while *Bmp10* and *ErbB4* expression changed in opposite directions in *MFng^{tg};Tie2-Cre* (Fig. 28d). Transcription of the Jag1 and Jag2 ligands was down-regulated and *MFng* expression was up-regulated in the corresponding mutant genotypes confirming the reliability of the global gene expression analysis (Fig. 28d). Lastly, a set of genes encoding voltage-dependent potassium and calcium channels (*Kcnd3*, *Kcne1*, *Kcnd2*, *Cacna1g*), ion transporters (*Slco3a1*) or ion-dependent regulatory proteins (*Camk2a*, *Atp5k*, Adora2a, *Bhlhe40*) were deregulated in *Jag1^{flox};Jag2^{flox};cTnT-Cre* and *MFng^{tg};Tie2-Cre* (Fig. 28d).

The comparative gene expression profiling analysis highlights that the specificity of Notch signaling is determined by its ligands. *Jag1* and *Jag2* single mutants shared only few deregulated genes. These data indicate that depending on the interacting ligand, Notch signaling controls the expression of a subset of target genes. Moreover, during compaction, the combination of both ligands is required to triggers higher levels of Notch activity, thereby activating more target genes required for the progression of chamber maturation and compaction.

DISCUSSION

The role of the Notch signaling pathway in human development and disease has been recognized since 1991, when mutations in *NOTCH1* were associated with a form of T-cell acute lymphoblastic leukemia (T-ALL) (Ellisen et al., 1991). Mutations in *NOTCH1* lead to an active protein isoform lacking the C-terminal domain, and have been identified in over 50% of T-ALL cases (Braggio, Egan et al., 2013). In the majority of leukemias, as well as in other solid tumors, the intracellular domain of Notch1 (N1ICD) is constitutively activated and functions as an oncogene.

In the same decade, *JAG1* mutations were identified in the Alagille syndrome (ALGS) (Li, Krantz et al., 1997). It is a dominant, multisystem disorder caused by mutations in the Jagged1 ligand in 94% of patients and in the NOTCH2 receptor in <1% of cases. A high percentage of patients with *JAG1* or *NOTCH2* mutations have cardiac disease, which includes (in order of frequency) branch pulmonary artery stenosis, peripheral pulmonary stenosis, TOF, pulmonary artery stenosis, VSD, ASD, coarctation of the aorta and several less common right and left sided lesions (Penton, Leonard et al., 2012). Double heterozygous mice for Notch signaling (*Jag1*$^{/+}$;*Notch2*$^{/+}$) have multisystem defects that strongly resemble those seen in patients with ALGS, including pulmonary artery stenosis and ventricular septal defects (McCright, Lozier et al., 2002). More recently, *NOTCH1* mutations were described in patients with calcific aortic valve disease, usually in the context of a bicuspid aortic valve (BAV) (Garg et al., 2005). Specific mutations of *NOTCH1* that reduce ligand (JAG1)-induced NOTCH1 signaling were also found across the spectrum of left ventricular outflow tract (LVOT) malformations (McBride, Riley et al., 2008). In contrast to solid or hematological tumors, where *Notch1* mutations usually lead to an over-activation of the pathway (Puente, Pinyol et al., 2011), in the case of other human syndromes as well as in congenital heart defects, mutations in Notch elements induce a downregulation of the pathway. In agreement with this, more recently, missense mutations of *MIB1* that promote endocytosis of Notch ligands were linked to LVNC, a cardiomyopathy characterized by prominent ventricular trabeculations and reduced cardiac systolic function (Luxan et al., 2013). In mice, conditional deletion of myocardial *Mib1* induces LVNC as a consequence of reduced endocardial Notch1 activity during chamber compaction and maturation (Luxan et al., 2013). In contrast, in *RBJk* or *Notch1* null embryos, abrogation of Notch1 signaling in the endocardium impairs EMT in the AVC (Timmerman et al., 2004) and trabeculation in the forming chambers (Grego-Bessa et al., 2007), causing early embryonic lethality. The differences between the phenotypes observed in mutant ventricles during mid-gestation and during compaction highlight the pivotal role of Notch signaling during early and late stages of chamber development.

Here we show that endocardial Notch1 is sequentially activated by its ligands Dll4, Jag1 and Jag2. The spatial and temporal distribution of Notch ligands defines the specificity of the ligand-receptor interaction whereas the response of Notch1 to its ligands is modulated by the glycosyl transferase Manic Fringe.

Dll4 and *MFng* show overlapping expression patterns during chamber development

Immunostaining of Notch ligands, Dll4 and Jag1, in E9.5 heart sections of the *CBF1:H2B-Venus* reporter line (Nowotschin et al., 2013) allowed us to detect the ligand expression in relation to the activity of Notch. Endocardial cells expressing Dll4 were in contact with neighboring Notch activated cells, detected by GFP. The ligand and activated receptor were expressed at the base of the forming trabeculae. Contrary to the endocardial expression of Dll4, Jag1 was strongly expressed in the trabecular myocardium in the proximity of Notch activated cells. Since the two ligands coexist in the developing chambers, they could either both trigger Notch activity during trabeculation or they could compete each other, as has been shown in retinal angiogenesis (Benedito et al., 2009). Specifically, Benedito and co-workers, using *in vivo* and *in vitro* approach, demonstrated that Dll4 and Jag1 ligands have an opposite effect on Notch activity during angiogenesis. In particular, Dll4 was shown to be a potent Notch activator, whereas Jag1 acts as an antagonist of Dll4-Notch signaling. Distinct biological roles for the Delta-like/Delta and Jagged/Serrate ligands have been demonstrated in a variety of tissues and processes, such as during inner ear development (Brooker, Hozumi et al., 2006, Petrovic et al., 2014) and hematopoiesis (Van de Walle et al., 2011). A possible mechanism that could explain how a ligand can prevent Notch signaling is considering that ligand–receptor interactions can also take place within the same cell. These *cis*-interactions reduce the ability of the cell to receive signals from neighboring cells by a process called '*cis*-inhibition' of the receptor by the ligand (del Alamo et al., 2011). During trabeculation, immunostaining of Notch ligands in the *CBF1:H2B-Venus* reporter line show that ligands and Notch1 receptors are not co-expressed suggesting that *cis*-inhibitory effect on Notch signaling could be excluded. Another mechanism that controls the strength of ligand-receptor interaction is the so-called "fringe effect". The Fringe proteins are glycosyltransferases that modulate Notch signaling by direct modification of O-linked fucose residues within the EGF repeats of the Notch extracellular domain (Moloney, Panin et al., 2000). Specifically, fringe modification of Notch potentiates signaling by Delta-like ligands and this could function to stimulate Notch activity when the ligand is limiting. In contrast, Serrate-like ligands are unable to activate fringe-modified Notch. The molecular basis of these differences appears to be at the level of ligand binding, such that fringe modification increases binding of Delta-like to Notch, whereas Serrate/Jagged binding is perturbed (D'Souza, Miyamoto et al., 2008).

During cardiac looping, the only glycosyltransferase transcribed in the endocardium is *MFng*. Its expression persists during trabeculation but, as development proceeds, *MFng* expression declines in endocardial cells. At later stage of cardiac development, it is transcribed in the endothelium of coronary vessels but not in endocardial cells. The expression pattern of *Mfng* is reminiscent of that of *Dll4*, whose expression is down-regulated after E12.5 in the endocardium and is restricted to the endothelium of coronary arteries during compaction. These results show a

relationship between Dll4 and MFng, suggesting that Dll4 could engage a Fringe-modified Notch receptor to trigger proper Notch activity in the endocardium during trabeculation and in the coronary arteries during chamber compaction.

Dll4 is a "superactivator" of Fringe-modified Notch receptor

The *in vitro* stimulation experiments performed on MEVEC allowed us to evaluate the differential ligand-dependent Notch signaling response. These cells were biologically relevant because of their embryonic endocardial origin, the tissue where Notch is active in the mouse heart. In addition, MEVEC proved to be an excellent tool to perform experiments like the ligand stimulation assay. In the absence of any stimuli they show basal Notch activity, measured by qRT-PCR of Notch target genes, even when cells are in contact with each other. The basal Notch activity in un-stimulated MEVEC is consistent with low expression of Notch ligands. In this context, upon exogenous ligand stimulation, we can turn on Notch signaling with a mechanism of transactivation.

In our system, recombinant Dll4 and Jag1 activate Notch to a similar level while Jag2 has a weaker effect. Interestingly, pairwise combinations of these ligands show an additive effect on Notch activation. Overexpression of MFng, mediated by lentiviral infection, decisively enhances Dll4-Notch signaling. This result is in agreement with those shown in HUVEC (Benedito et al., 2009). In the presence of MFng, Jag1 and Jag2 activate Notch quite poorly. In addition, they do not affect the response to Dll4 in pairwise combinations, suggesting that the Jag ligands do not have inhibitory effects on Notch activity, contrary to the effect of Jag1 observed in HUVEC (Benedito et al., 2009). In our setting, the transactivation of Notch mediated by recombinant ligands suggests that Dll4 behaves as a "superactivator" of the Fringe-modified Notch receptor. In presence of the same concentration of ligands glycosylated Notch is very strongly activated by Dll4 but not Jag1 or Jag2 and pairwise ligand combinations (Dll4+Jag1 or Dll4+Jag2) do not show an inhibitory effect of the Jag ligands on Notch signaling. This could perhaps be achieved if Jag1 or Jag2 were in excess in relation to Dll4.

These *in vitro* experiments, along with the observed endocardial-endothelial expression of *Mfng* and *Dll4*, indicate that the ligand-dependent Notch signaling response can be modulated by the glycosyltransferase MFng. Therefore, glycosylated Notch1 receptor would interact preferentially with Dll4 at the expense of Jag1, in the endocardium and in coronary endothelium during chamber development.

Manic Fringe favors Dll4-Notch interaction during trabeculation

Conditional deletion of *Dll4* with *Tie2-cre or Nfat-Cre* impaired heart development. EMT was abrogated and trabeculation was dramatically affected in both mutants. The cardiac defects observed in *Dll4* mutants were reminiscent of those observed in the *Notch1^{flox};Nfat-Cre*, indicating that Dll4 interacts with Notch1 in the endocardium and consequently triggers its nuclear translocation. Indeed, in the *Dll4^{flox};Tie2-Cre* as well as in the *Dll4^{flox};Nfatc-Cre* the expression of N1ICD was strongly down-regulated. In agreement with reduced Notch activity during trabeculation, the expression of endocardial Notch target genes, *Hey2* and *EphrinB2*, was markedly decreased in *Dll4* mutants. All these data indicate that Dll4-Notch1 signaling is crucial for trabeculation in the developing chambers. In contrast, myocardial deletion of Jag1 did not affect this process. The heart of E10.5 *Jag1^{flox};cTnT-Cre* mutant embryos appeared normal. The thickness of the compact myocardium was similar to controls as well as the expression of *Hey2* in this region. The trabeculae were well developed as indicated by the expression of the trabecular marker *Bmp10*. Despite the complete deletion of Jag1, we did not observe differences of N1ICD expression in *Jag1^{flox};cTnT-Cre* mutant embryos. These results indicate that myocardial Jag1 is dispensable for endocardial Notch activity and does not have an inhibitory effect on Notch signaling during trabeculation, contrary to what has been shown during angiogenesis (Benedito et al., 2009).

The reduction of Notch activity observed in *Dll4*-deficient embryos, the endocardial expression of *MFng* and the *in vitro* experiments in MEVEC confirmed that the response of Notch1 to its ligands during trabeculation is modulated by the glycosyl transferase MFng. In this context, early *MFng* expression favors endocardial Dll4-Notch1 signaling at the base of the developing ventricle and prevents Notch1 activation by myocardial Jag1.

Endocardial Dll4-Notch1 signaling orchestrates growth and differentiation of trabecular myocardium.

The obligatory role of the endocardium in orchestrating proliferation and differentiation of the trabecular myocardium has been extensively demonstrated by using systemic or conditional deletion of endocardial genes, such as *Nrg1* (Lee et al., 1995, Meyer & Birchmeier, 1995). To decipher the signals connecting endocardium to myocardium during trabeculation depending on Dll4-induced Notch activity, we performed comparative global gene expression analysis in hearts of endocardial-specific *Dll4* or *Notch1* mutants.

In the RNA-seq data obtained from these mutants we identified a common set of genes involved in cardiovascular system development and function, intercellular signaling, cellular proliferation and cardiovascular disease. Among them, *Gpr126* was of particular interest for us. Recently, Patra

and co-workers demonstrated that inactivation of the G protein-coupled receptor Gpr126 in mice was crucial for chamber development (Patra et al., 2013). *Gpr126 null* embryos show hypotrabeculation and a marked thinning of the ventricular wall, a phenotype reminiscent of those observed in endocardial *Dll4* or *Notch1* mutant embryos. We showed that *Gpr126* expression is dependent on Notch signaling in mouse, zebrafish and mammalian endothelial cells. In addition, computational analysis identified RBPJ/CBF1 binding sites within an intronic region of *Gpr126*. A *Gpr126* luciferase reporter with this intronic region was transiently activated upon transfection of the vector expressing N1ICD in a dose-dependent manner. All these data indicate that Notch1 activity enhances the expression of *Gpr126*. To demonstrate physical binding of the N1ICD/RBPJ complex on the *Grp126* intronic locus, chromatin immunoprecipitation would have to be performed. In the report from Patra and co-workers it was shown that a functional N-terminal fragment of Gpr126 (Gpr126-NTF) is able to rescue the trabeculation phenotype in *gpr126* zebrafish morphants, suggesting that the NTF can function as a secreted protein able to signal in a paracrine manner to nearby trabecular cardiomyocytes (Patra et al., 2013). We propose that in response to Notch activity, Gpr126 might influence the proliferation and differentiation of neighboring cardiomyocytes within the developing chamber in a similar manner. Concomitantly, cardiomyocyte proliferation is also affected in endocardial *Dll4* and *Notch1* mutants. The mechanism of how Gpr126 functions as a secreted ligand and which myocardial receptors could be involved in Gpr126-NTF binding remain to be elucidated. However, it seems clear that Gpr126 from the endocardium plays an essential role for the initiation of trabeculation. For further deciphering its role during heart development a $Gpr126^{flox}$ line would have to be generated in order to delete the gene only the endocardium. In addition, it would be very interesting to rescue, at least in part, the trabecular phenotype of *Dll4* or *Notch1* mutant embryos by overexpressing *Gpr126* specifically in endocardial cells of these mutants.

Furthermore, our RNA-seq data showed increased expression of various negative regulators of the cell cycle, suggesting that Notch signaling plays a more general role in the regulation of cardiomyocyte proliferation. Proliferation and differentiation of embryonic cardiomyocytes are intimately connected (Hertig, Kubalak et al., 1999) and our data strongly suggest that Fringe-modified Notch1 activated by Dll4 in the endocardium regulates both processes in the developing chamber (Fig 29a).

Dll4 engages and activates Fringe-modified Notch receptor during coronary vessel development

In the ventricles of mouse embryos between E9.5 and E13.5, trabeculae and compact myocardium increase in size. Exuberant cell proliferation can be observed in both layers of the

developing chamber. Later, cardiomyocytes from the compact zone undergo extensive cell division, whereas trabecular myocardium proliferates less (de Boer et al., 2012). The differences in cell proliferation between these two layers could explain how the trabecular myocardium undergoes "compaction" and coalesces with the compact myocardium (Tian et al., 2013).

The rapid expansion in cardiac size (E11.5-E13.5) coincides with the formation of the coronary vascular system (Ivins et al., 2015). Despite the fact that the origin of coronary vessels is still a matter of debate, its function in the heart is very well understood. Myocardial growth requires enhanced oxygen delivery and triggers an influx of endothelial cells that undergo vasculogenesis to form a capillary plexus (Mikawa & Fischman, 1992). After birth, proper coronary blood circulation is required to support heart homeostasis, and altered coronary function frequently leads to myocardial ischemia, infarction and heart failure (Ruiz-Villalba & Perez-Pomares, 2012). Previous works have demonstrated that Notch signaling from the epicardium, a tissue that contributes highly to coronary vessel morphogenesis is indispensable for coronary artery development (Del Monte et al., 2011, Grieskamp, Rudat et al., 2011). Epicardium-specific ablation of *Notch1* or *Rbpj* using *Wt1-Cre* or *Tbx18-Cre* driver lines impaired coronary artery formation (Del Monte et al., 2011) and smooth muscle cell differentiation of epicardial-derived cells (EPDCs) (Grieskamp et al., 2011). Defects in this process directly affect myocardial wall thickness and myocyte proliferation (Del Monte et al., 2011). However, in these reports the role of ligand-specific induction of Notch activity during coronary vessel formation was not addressed. In agreement with previous reports (Del Monte et al., 2011, Grieskamp et al., 2011) we found widespread expression of ligands (*Dll4*, *Jag1* and *Jag2*) as well as N1ICD in the developing coronary arteries. In addition, we detected expression of *MFng* in this tissue. Interestingly, *MFng* mirrors the expression of *Dll4*. Since the formation of the linear heart tube both *Dll4* and *MFng* are expressed in the endocardium. Once trabeculation ends, the two transcripts are down-regulated in the endocardium and start to be expressed in coronary endothelial cells. These data indicate that after trabeculation, Dll4 is not the ligand-inducing Notch signaling in the endocardium. Similarly to our observations on trabeculation, it seems likely that during coronary vessel formation MFng enhances the interaction between Dll4 and Notch1. To examine this hypothesis and avoid the early embryonic lethality of conditional *Dll4* mutant embryos we used the tamoxifen-inducible *Cdh5-Cre*^{ERT} driver line, which is active in the endocardium, vascular endothelium and coronary vessels (Luna-Zurita et al., 2010, Wang et al., 2010). E15.5 *Dll4*^{flox};*Cdh5-Cre*^{ERT} mutant embryos show downregulated expression of Notch target genes, such as *Hey1*, *HeyL* and *EphrinB2,* in the coronary vessels as a consequence of reduced Notch activity in this tissue. Consistent with the endocardial down-regulation of *Dll4* and *Mfng* expression at this stage, we did not observe differences in Notch1 activity in the endocardium, confirming that Dll4 is not activating Notch1 during chamber compaction. In addition, in the *Dll4* mutants, *Hey2* expression was not expanded to the trabeculae but delineated a thin compact layer of myocardium, a phenotype reminiscent of those observed in the epicardial deficient *Notch1* mutants.

These data identify Dll4 as the ligand required to trigger Notch activity in the endothelium of coronary vessels. Consistent with the expression of *MFng* during late mid-gestation, systemic *Fng* abrogation disrupts coronary vessel development. The down-regulated expression of coronary endothelial markers as well as the reduced N1ICD expression cause a phenotype very similar to those observed in $Dll4^{flox}$;$Cdh5\text{-}Cre^{ERT}$ mutant embryos. All these data indicate that Dll4 signals to glycosylated Notch1 receptor in the endothelium of coronary arteries (Fig. 29b). Therefore, it becomes clear that the MFng-Dll4 relationship not only exists in the endocardium during trabeculation, but also in the endothelium of the forming coronary arteries. This scenario resembles the situation described in retinal angiogenesis (Benedito et al., 2009) in which Delta-like/Delta and Jagged/Serrate ligands are co-expressed. To clarify the role of Jag1 and Jag2 during coronary vessel formation, we need to specifically delete the two ligands in endothelial cells. This would allow us to decipher whether Jag1 and Jag2 compete with Dll4 to activate the Notch1 receptor or whether Jagged ligands are dispensable for triggering Notch1 activity during coronary vessel formation.

Myocardial Jag1 activates Notch1 during chamber compaction and maturation

Recently, we showed that myocardial inactivation of the ubiquitin ligase *Mib1* causes LVNC in mice and that heterozygous germ-line mutations of the human counterpart cause the human disease (Luxan et al., 2013). Myocardium-specific *Mib1* mutants showed reduced Notch1 activity in the endocardium during chamber compaction. In addition, compact zone markers (*Hey2; Tbx20*) expanded to the trabeculae, suggesting that trabecular maturation and patterning were arrested. These data indicate that abrogation of endocardial Notch activity via deletion of myocardial Mib1 caused LVNC, furthermore demonstrating LVNC as a cardiomyopathy with developmental basis (Luxan et al., 2013). The role of Mib1 for generating functional ligands to activate Notch signaling has been well established (Koo, Lim et al., 2005). Null *Mib1* mice die prior to E11.5, with pan-Notch defects in somitogenesis, neurogenesis, vasculogenesis and cardiac development (Koo et al., 2005). In addition, conditional inactivation of *Mib1* in various tissues revealed representative Notch phenotypes: defects of arterial specification as *Dll4* mutants, abnormal cerebellum and skin development as *Jag1* conditional mutants, and syndactylism as *Jag2* mutants (Koo et al., 2007). At later stages of cardiac development, Jag1 is strongly expressed in the already formed trabeculae and *MFng* is down-regulated in the endocardium. In this scenario, unglycosylated Notch1 in endocardial cells surrounding the myocardium would be activated by myocardial Jag1. Considering all these data in addition to the known role of *Mib1*, we speculated that the myocardial deletion of *Jag1* should resemble the inactivation of *Mib1* in the myocardium, producing a LVNC phenotype.

Inactivation of *Jag1* in the embryonic myocardium results in mice with a dilated heart and a thin compact myocardium (Fig. 29c). The echocardiographic and CMRI data confirm this phenotype

showing below-normal ejection fraction, reduced myocardial mass and thinner free wall of the right ventricle compared to WT counterparts. The RNA-seq analysis of *Jag1^{flox};cTnT-Cre* mutants reveals dysregulated expression of genes involved in cardiovascular system development and function, cardiovascular disease, cell-to-cell signaling and cellular growth and proliferation. From this analysis we observed that a set of genes changes in the same direction (up or down) as in endocardial-*Dll4 or Notch1* mutants. This was the case for the negative regulator of cell cycle *cdkn1b/p21*. In agreement with this result, *Jag1* mutants show reduced myocardial proliferation with concomitant increased p21 expression in compact zone cardiomyocytes. In addition, expression of *Gpr126* is impaired in *Jag1* mutant embryos similarly to *Dll4* mutants. This result could suggest that Gpr126, from the endocardium, mediates the initial trabecular growth and at later stages sustains cardiomyocyte proliferation in the compact layer. The RNA-seq analysis reveals that Dll4- and Jag1-Notch signaling in the developing ventricles is required for the normal expression of a set of genes involved in the communication between endocardium and myocardium. These signals are crucial for the regulation of cardiomyocyte differentiation and proliferation during trabeculation (Fringe-modified Notch1 interacting with endocardial Dll4, Fig. 29a) and for later trabecular maturation and compaction (Fringe-unmodified Notch1 interacting with myocardial Jag1, Fig 29b;c).

Jag2 is the second ligand responsible for Notch1 activity during chamber compaction and maturation

The initial prediction that the cardiac phenotypes of *Mib1^{flox};cTnT-Cre* and *Jag1^{flox};cTnT-Cre* mutants would be similar, based on the assumption that Jag1 was the only ligand expressed in the myocardium, was assessed. In fact, the heart phenotype of *Jag1* mutant embryos was less severe and only partially phenocopied *Mib1* mutants. For instance, *Mib1^{flox};cTnT-Cre* mutant mice develop LVNC cardiomyopathy (Luxan et al., 2013), while *Jag1^{flox};cTnT-Cre* mutants show structural and functional signs of dilated cardiomyopathy with systolic dysfunction (Fig. 29c).

The finding that myocardial expression of *Jag2* increases from E12.5 to E14.5, mirroring the expression of *Jag1*, suggested that Jag2 could be an important Notch1 activator in the myocardium and a second substrate for Mib1. Indeed, myocardial inactivation of *Jag2* gave rise to defects in chamber maturation as a consequence of reduced endocardial Notch1 activity, similarly to those observed in *Jag1^{flox};cTnT-Cre* mutants. The resulting cardiac phenotype observed in *Jag2^{flox};cTnT-Cre* mutants suggests that both Jag1 and Jag2 activate Notch1 in a non-redundant manner. These findings raise further questions, for instance why the expression of *Jag2* appears relatively late in chamber myocardium development or why a second ligand is required for proper Notch activation during compaction.

The ligands Jag1-Jag2 trigger endocardial Notch activity during chamber compaction and maturation and are both substrates of Mib1

An intriguing possibility is to consider the Notch receptor as a homodimer. In this context two extracellular domains (2NECD) could directly interact with two ligands. The binding regions of the ligands and the receptor have been characterized by X-ray crystallography and nuclear magnetic resonance (NMR) (Chillakuri et al., 2013, Cordle et al., 2008a). These data have allowed us to clearly define the molecular mechanisms that govern the ligand-receptor interaction. Unfortunately, due to technical limitations, it is impossible to define the whole ligand-receptor interacting complex. Recently, using scanning transmission electron microscopy (STEM), it has been shown that the extracellular domain of human and *Drosophila* Notch1 forms a dimer and adopts distinct conformations (Kelly, Lake et al., 2010).

In agreement with published results (Blacklow, 2013, Chillakuri et al., 2012, Hambleton et al., 2004), we generated *in silico* models of the interaction between the ligands Dll4, Jag1 and Jag2 and the extracellular domain of the Notch1 homodimer. The biologically active Notch1 dimer binds Dll4 in a 1:1 stoichiometry (Narui & Salaita, 2013) and we assumed that this stoichiometry would be the same for all Notch ligands. The 2Dll4:2N1ECD complex is the most stable. Remarkably, the Jag1/Jag2:2N1ECD complex is more stable than the 2Jag1:2N1ECD complex. Our molecular docking suggests that when both ligands are expressed in the ventricle at similar levels (E12.5-E14.5) formation of the Jag1/Jag2:2N1ECD complex would be favored. In agreement to this hypothesis, the cardiac defects as well as the reduction of N1ICD in the double *Jag1;Jag2* myocardial mutants are exacerbated compared to single *Jag1* or *Jag2* mutants and the resulting phenotype resembles the one observed in *Mib1^{flox};cTnT-Cre* mutant embryos. These data indicate that Jag1 and Jag2 are both required for proper chamber compaction and maturation and both are substrates of Mib1 in the myocardium. Comparative global gene expression analysis performed in E15.5 WT, *Jag1^{flox};cTnT-Cre, Jag2^{flox};cTnT-Cre and Jag1^{flox}; Jag2^{flox};cTnT-Cre* ventricles revealed that the number of deregulated genes increased decisively when both ligands were deleted in the myocardium. Interestingly, we noted that Jag1 or Jag2-induced Notch activity differentially control the expression of a subset of genes. The specificity in terms of gene expression could reside in the differential ligand-dependent Notch signaling strength. The differentially expressed genes in each single mutant change in the same direction as in the double *Jag1;Jag2* mutants. These results reinforce the conclusion that Jag1 and Jag2 have non-redundant functions and both are necessary for properly triggering Notch activity, thereby activating more target genes required for the progression of chamber maturation and compaction. During T-cell maturation and leukemic transformation, it has been shown that a dimeric form of NICD exists and is required for the expression of Notch target genes, such as *c-Myc* and *pre-T-cell antigen receptor α* (*Ptcra*), whereas in the case of targets like *Hey1* or *CD25* such a dimeric Notch transcriptional complex is not formed

(Liu, Chi et al., 2010). These findings identify functionally important differences in the responsiveness among Notch target genes attributable to the formation of higher-order complexes (Liu et al., 2010). In our case, we could speculate that in endocardial cells Notch1 receptors can coexist and adopt a monomeric or a dimeric form. In this scenario, myocardial Jag1 and Jag2 engage the different forms of the receptor. The final amount of transcriptionally activated Notch receptor (N1ICD) will be defined by the different ligand-receptor interacting complexes that may be formed, assuming Notch will be present either as a monomer or as a dimer. It would be very interesting to provide *in vivo* evidence on the mechanism of ligand-receptor forming complex. This would be possible by taking advantage of the Bimolecular Fluorescent Complementation (BIFC) technology. This is a powerful tool to validate protein-protein interactions. Two separated fragments, *C* and *N-terminus*, of a fluorescent protein (i.e. half-GFP) can form a fluorescent complex (GFP) when they are fused to two proteins that interact with each other (Kerppola, 2006). Ideally, we could generate a Notch1 receptor carrying half-N-GFP and a Notch1 receptor carrying half-C-GFP. This experiment would allow us to understand whether two receptors interact with each other and form a homodimer. In addition, measuring GFP signal intensity, we can confirm whether the Jag1/Jag2:2N1ECD complex would be favored, reinforcing the hypothesis that Jag1 and Jag2 during compaction (E12.5-E14.5) interact with a homodimer of Notch1.

The expression of *Manic Fringe* defines the specificity of ligand-receptor interaction during chamber development

The down-regulation of *Mfng* in the endocardium would allow Jag1 and Jag2 to trigger Notch1 activity in the endocardium during chamber compaction (Fig. 29b); a proposal consistent with results obtained overexpressing *Mfng* throughout the endocardium. Similar to the myocardial inactivation of *Jag1;Jag2* or *Mib1*, the ectopic expression of *MFng* causes a very severe chamber phenotype, reminiscent of LVNC (Fig. 29c). The phenotype observed in the Mfg^{tg}*;Tie2-Cre* is caused by a down-regulation of Notch1 activity in the endocardium. As we have previously shown, during compaction N1ICD expression is crucial to sustain cardiomyocyte proliferation in the compact myocardium. In the Mfg^{tg}*;Tie2-Cre*, *Hey2* expression delineates a very thin compact layer and marks an intermediate region in between the compact myocardium and the trabecuale indicating defects in chamber maturation and compaction. Moreover, gene profiling identified a large set of differentially expressed genes implicated in cell cycle and proliferation that partially overlaps with those affected in $Jag1^{flox}$;$Jag2^{flox}$*;cTnT-Cre* mutants. The stronger phenotype and the higher number of deregulated genes observed in Mfg^{tg}*;Tie2-Cre* compared with $Jag1^{flox}$;$Jag2^{flox}$*;cTnT-Cre* can be explained considering the pan endothelial-endocardial expression of the *Tie-2* driver line. In this setting, ectopic expression of *MFng* in the coronary endothelium would favor Dll4 signaling to Notch and would resemble a GOF of Notch1 in the vasculature and

coronary development. In according to this hypothesis, GO-terms analysis in *Mfg^{tg};Tie2-Cre* revels angiogenesis as the most enriched category. Thus, the morphological and molecular data indicate that *MFng* overexpression throughout the endocardium effectively blocks Jag1 and Jag2 myocardial signaling to Notch1 and presumably, its ectopic expression in the endothelium overactivates Notch signaling mediated by Dll4.

We propose that during chamber development, the endocardial expression of *MFng* determines the specificity of Notch1 towards its ligands, so that ligand-receptor interactions follow a temporal sequence. In this model, Dll4 acts in the early ventricle to promote cardiomyocyte proliferation and differentiation leading to trabeculation. Subsequent MFng (and Dll4) down-regulation in the endocardium allows signaling by Jag1 and Jag2 to sustain trabecular patterning, cardiomyocyte proliferation and chamber maturation (Fig29 a-c). Simultaneously, Dll4 signals to the MFng-modified Notch1 receptor in developing coronary vessels to stimulate coronary development and sustain compaction (Fig29 b). As aforementioned, inactivation of the ubiquitin ligase MIB1 causes LVNC in mice and humans (Luxan et al., 2013). Here we show that combined myocardial inactivation of *Jag1* and *Jag2* causes a chamber phenotype reminiscent of *Mib*1 mutants, suggesting that both ligands are substrates of Mib1 in the myocardium (Fig29 c). This is independently supported by the LVNC-like phenotype found after forced *MFng* expression in the endocardium (Fig29 c).

Taken altogether, we have shown that the Notch signaling pathway is crucial for ventricular chamber development, first for the formation of the trabecular network and later for chamber maturation, that includes the process of trabecular compaction and coronary vessel formation.

To further understand the clinical implications of the Notch pathway, Exome Sequencing of different Notch elements from patients with various types of cardiomyopathies, including LVNC, would be necessary in order to identify potential new diagnostic and therapeutic disease targets.

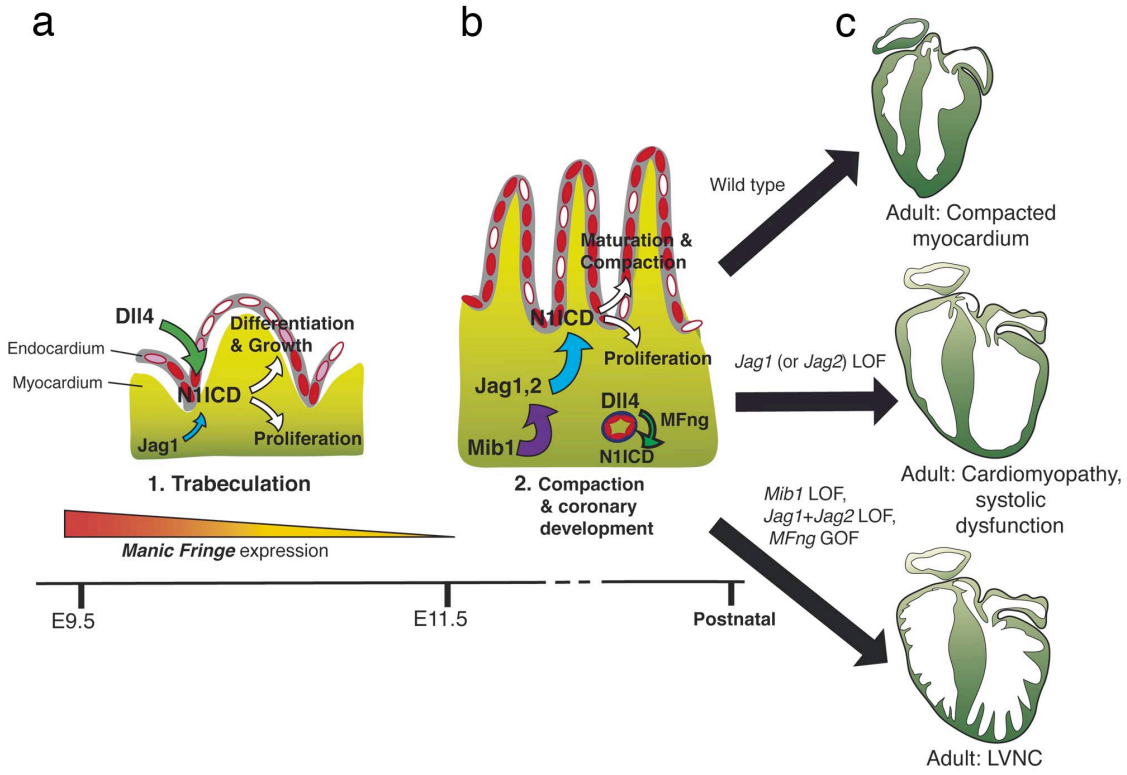

Figure 29. Sequential Notch Ligand-Receptor activation during ventricular chamber development. In the early ventricle (**a**) endocardial Dll4 and myocardial Jag1 can activate Notch1 in the endocardium. Expression of MFng in the endocardium favors Dll4 signaling to Notch1 (large green arrow) and Jag1 signaling is low (small blue arrow). Notch1 activation (red) promotes cardiomyocyte proliferation, trabecular growth and patterning. As chamber development proceeds, endocardial MFng expression reduces progressively (similarly to Dll4) allowing myocardial Jag1 to activate Notch1 in the myocardium (**b**). As Jag2 expression is progressively upregulated in chamber myocardium, it acts together with Jag1 to promote chamber proliferation; patterning and trabecular compaction to give rise to the functional ventricular wall (large blue arrow, **b**). At this time, MFng and Dll4 are required for Notch1 activation in coronary vessels (small green arrow, **b**). Inactivation of *Jag1* (or *Jag2*) in the myocardium disrupts chamber maturation and leads to cardiomyopathy (**c**). Mib1 acts upstream of Jag1 and Jag2 in this process: *Mib1* inactivation in the myocardium causes LVNC. A similar phenotype is produced when both *Jag1* and *Jag2* are deleted in the myocardium and when *MFng* is constitutively expressed in the endocardium (presumably causing persistent inhibition of Jag1 and Jag2 signaling, **c**).

CONCLUSION/ CONCLUSIONES

1. Dll4 is the ligand activating Notch1 during trabeculation. Dll4-Notch1 signaling mediates cardiomyocyte proliferation and differentiation in a non-cell autonomous manner.

2. Gpr126 is a potential Notch target gene in the endocardium during chamber development. Its expression is strongly dependent on Dll4-Notch1 during trabeculation and of Jag1/Jag2-Notch1 at during chamber maturation and compaction.

3. Dll4 signaling to MFng-modified Notch1 is crucial during coronary vessel development. Reduced Notch signaling activity in the coronary endothelium also indirectly affects compaction.

4. Myocardial Jag1 is dispensable for Notch activation during trabeculation, but is required during chamber compaction and maturation by activating Notch1 in the endocardium.

5. Myocardial expression of *Jag2* increases from E12.5 onwards. Myocardial deletion of *Jag2* also disrupts chamber maturation, and the combined deletion of *Jag1* and *Jag2* causes a very severe chamber phenotype, reminiscent of LVNC. Both Jag ligands are likely targets of Mib1-mediated regulation in the myocardium.

6. Gene profiling identified a specific set of Jag1- or Jag2-dependent genes that is widely expanded after combined *Jag1* and *Jag2* inactivation, indicating that the two ligands have non-redundant roles in chamber development.

7. The LVNC-like phenotype was also observed after forced *MFng* expression in the endocardium, suggesting that MFng overexpression effectively blocks Jag1- and Jag2-signaling and confirming the requirement of these ligands for compaction.

8. The expression pattern of the glycosyltransferase *Manic Fringe* defines the glycosylation status of the Notch1 receptor. By doing so it determines the spatio-temporal specificity of ligand-receptor interactions during chamber development, favoring Dll4-Notch1 and preventing Jag-Notch1 activation.

1. Durante el proceso de trabeculación, el ligando Dll4 activa desde el endocardio a Notch1. La activación de Notch1 mediada por Dll4 dirige efectos no celulares autónomos en el miocardio esenciales para la proliferación y la diferenciación de cardiomiocitos

2. Gpr126 es una diana potencial de Notch en el endocardio durante el desarrollo de las cámaras ventriculares. Su expresión depende de la activación de Notch1 mediada por Dll4 durante la trabeculación y de los ligandos Jag1/Jag2 durante el proceso de compactación.

3. En el endotelio coronario, Dll4 interactúa y activa Notch1 modificado por MFng. Dicha activación resulta indispensable para el desarrollo de este tejido. La reducción de la actividad de Notch en el endotelio coronario afecta indirectamente a la compactación.

4. Desde el miocardio, el ligando Jag1 no activa Notch1 durante la trabeculación, pero es indispensable para la activación de Notch1 en el endocardio durante el proceso de maduración y compactación de los ventrículos.

5. La expresión de Jag2 en el miocardio aumenta a partir de E12.5 y en adelante. La eliminación de Jag2 afecta la maduración de las cámaras. La inactivación combinada de Jag1 y Jag2 en el miocardio causa un fenotipo similar a la cardiomiopatía humana LVNC. La función de ambos ligandos es regulada por MIB1 en el miocardio.

6. El análisis comparativo del transcriptoma identificó un conjunto de genes específicos de la señalización mediata bien por Jag1 o por Jag2. Sin embargo la eliminación combinada de ambos ligandos afecta a un numero de genes mucho mas amplio que la inactivación de cada ligando por separado. Este dato indica que los dos ligandos tienen papeles no redundantes en el desarrollo de la cámara.

7. La expresión ectópica de MFng en el endocardio produce un fenotipo similar a la cardiomiopatía humana LVNC, lo que sugiere que la sobreexpresión de MFng bloquea de facto la señalización mediada por Jag1 y Jag2, confirmando el papel de estos ligandos como activadores secuenciales de Notch durante la compactación de los ventriculos.

8. El patrón de expresión de Manic Fringe define el estado de glicosilación del receptor Notch1. Esta glicosilación determina la especificidad espacio-temporal de Notch1 con sus distintos ligandos. Durante el desarrollo de los ventrículos favorece la activación Dll4-Notch1 lo que previene la activación por parte de los otros ligandos

BIBLIOGRAPHY

Acar M, Jafar-Nejad H, Takeuchi H, Rajan A, Ibrani D, Rana NA, Pan H, Haltiwanger RS, Bellen HJ (2008) Rumi is a CAP10 domain glycosyltransferase that modifies Notch and is required for Notch signaling. Cell 132: 247-58

Andrawes MB, Xu X, Liu H, Ficarro SB, Marto JA, Aster JC, Blacklow SC (2013) Intrinsic selectivity of Notch 1 for Delta-like 4 over Delta-like 1. The Journal of biological chemistry 288: 25477-89

Artavanis-Tsakonas S, Rand MD, Lake RJ (1999) Notch signaling: cell fate control and signal integration in development. Science (New York, NY) 284: 770-6.

Benedito R, Roca C, Sorensen I, Adams S, Gossler A, Fruttiger M, Adams RH (2009) The notch ligands Dll4 and Jagged1 have opposing effects on angiogenesis. Cell 137: 1124-35

Bettenhausen B, Hrabe de Angelis M, Simon D, Guenet JL, Gossler A (1995) Transient and restricted expression during mouse embryogenesis of Dll1, a murine gene closely related to Drosophila Delta. Development (Cambridge, England) 121: 2407-18

Blacklow SC (2013) Refining a Jagged edge. Structure (London, England : 1993) 21: 2100-1

Braggio E, Egan JB, Fonseca R, Stewart AK (2013) Lessons from next-generation sequencing analysis in hematological malignancies. Blood Cancer J 3: e127

Brooker R, Hozumi K, Lewis J (2006) Notch ligands with contrasting functions: Jagged1 and Delta1 in the mouse inner ear. Development 133: 1277-86

Brutsaert DL (2003) Cardiac endothelial-myocardial signaling: its role in cardiac growth, contractile performance, and rhythmicity. Physiol Rev 83: 59-115

Buckingham M, Meilhac S, Zaffran S (2005) Building the mammalian heart from two sources of myocardial cells. Nature reviews Genetics 6: 826-35

Camenisch TD, Schroeder JA, Bradley J, Klewer SE, McDonald JA (2002) Heart-valve mesenchyme formation is dependent on hyaluronan-augmented activation of ErbB2-ErbB3 receptors. Nature medicine 8: 850-5

Camenisch TD, Spicer AP, Brehm-Gibson T, Biesterfeldt J, Augustine ML, Calabro A, Jr., Kubalak S, Klewer SE, McDonald JA (2000) Disruption of hyaluronan synthase-2 abrogates normal cardiac morphogenesis and hyaluronan-mediated transformation of epithelium to mesenchyme. The Journal of clinical investigation 106: 349-60

Campos-Ortega JA (1996) Numb diverts notch pathway off the tramtrack. Neuron 17: 1-4

Captur G, Lopes LR, Patel V, Li C, Bassett P, Syrris P, Sado DM, Maestrini V, Mohun TJ, McKenna WJ, Muthurangu V, Elliott PM, Moon JC (2014) Abnormal cardiac formation in hypertrophic cardiomyopathy: fractal analysis of trabeculae and preclinical gene expression. Circ Cardiovasc Genet 7: 241-8

Captur G, Nihoyannopoulos P (2010) Left ventricular non-compaction: genetic heterogeneity, diagnosis and clinical course. Int J Cardiol 140: 145-53

Chen H, Zhang W, Li D, Cordes TM, Mark Payne R, Shou W (2009) Analysis of ventricular hypertrabeculation and noncompaction using genetically engineered mouse models. Pediatric cardiology 30: 626-34

Cheng HT, Kim M, Valerius MT, Surendran K, Schuster-Gossler K, Gossler A, McMahon AP, Kopan R (2007) Notch2, but not Notch1, is required for proximal fate acquisition in the mammalian nephron. Development (Cambridge, England) 134: 801-11

Chillakuri CR, Sheppard D, Ilagan MX, Holt LR, Abbott F, Liang S, Kopan R, Handford PA, Lea SM (2013) Structural analysis uncovers lipid-binding properties of Notch ligands. Cell reports 5: 861-7

Chillakuri CR, Sheppard D, Lea SM, Handford PA (2012) Notch receptor-ligand binding and activation: insights from molecular studies. Semin Cell Dev Biol 23: 421-8

Chitnis A, Henrique D, Lewis J, Ish-Horowicz D, Kintner C (1995) Primary neurogenesis in Xenopus embryos regulated by a homologue of the Drosophila neurogenic gene Delta [see comments]. Nature 375: 761-6

Christoffels VM, Hoogaars WM, Tessari A, Clout DE, Moorman AF, Campione M (2004) T-box transcription factor Tbx2 represses differentiation and formation of the cardiac chambers. Developmental dynamics : an official publication of the American Association of Anatomists 229: 763-70

Conlon RA, Reaume AG, Rossant J (1995) Notch1 is required for the coordinate segmentation of somites. Development (Cambridge, England) 121: 1533-45

Cordle J, Johnson S, Tay JZ, Roversi P, Wilkin MB, de Madrid BH, Shimizu H, Jensen S, Whiteman P, Jin B, Redfield C, Baron M, Lea SM, Handford PA (2008a) A conserved face of the Jagged/Serrate DSL domain is involved in Notch trans-activation and cis-inhibition. Nature structural & molecular biology 15: 849-57

Cordle J, Redfieldz C, Stacey M, van der Merwe PA, Willis AC, Champion BR, Hambleton S, Handford PA (2008b) Localization of the delta-like-1-binding site in human Notch-1 and its modulation by calcium affinity. The Journal of biological chemistry 283: 11785-93

Cruz-Adalia A, Jimenez-Borreguero LJ, Ramirez-Huesca M, Chico-Calero I, Barreiro O, Lopez-Conesa E, Fresno M, Sanchez-Madrid F, Martin P (2010) CD69 limits the severity of cardiomyopathy after autoimmune myocarditis. Circulation 122: 1396-404

D'Souza B, Miyamoto A, Weinmaster G (2008) The many facets of Notch ligands. Oncogene 27: 5148-67

Daudet N, Lewis J (2005) Two contrasting roles for Notch activity in chick inner ear development: specification of prosensory patches and lateral inhibition of hair-cell differentiation. Development (Cambridge, England) 132: 541-51

Davis RL, Turner DL (2001) Vertebrate hairy and Enhancer of split related proteins: transcriptional repressors regulating cellular differentiation and embryonic patterning. Oncogene 20: 8342-57

de Boer BA, Soufan AT, Hagoort J, Mohun TJ, van den Hoff MJ, Hasman A, Voorbraak FP, Moorman AF, Ruijter JM (2011) The interactive presentation of 3D information obtained from reconstructed datasets and 3D placement of single histological sections with the 3D portable document format. Development (Cambridge, England) 138: 159-67

de Boer BA, van den Berg G, de Boer PA, Moorman AF, Ruijter JM (2012) Growth of the developing mouse heart: an interactive qualitative and quantitative 3D atlas. Developmental biology 368: 203-13

de Celis JF, Bray SJ (2000) The Abruptex domain of Notch regulates negative interactions between Notch, its ligands and Fringe. Development (Cambridge, England) 127: 1291-302

de la Pompa JL, Epstein JA (2012) Coordinating tissue interactions: notch signaling in cardiac development and disease. Developmental cell 22: 244-54

de la Pompa JL, Wakeham A, Correia KM, Samper E, Brown S, Aguilera RJ, Nakano T, Honjo T, Mak TW, Rossant J, Conlon RA (1997) Conservation of the Notch signalling pathway in mammalian neurogenesis. Development (Cambridge, England) 124: 1139-48

de Lange FJ, Moorman AF, Anderson RH, Manner J, Soufan AT, de Gier-de Vries C, Schneider MD, Webb S, van den Hoff MJ, Christoffels VM (2004) Lineage and morphogenetic analysis of the cardiac valves. Circulation research 95: 645-54

De Strooper B, Annaert W, Cupers P, Saftig P, Craessaerts K, Mumm JS, Schroeter EH, Schrijvers V, Wolfe MS, Ray WJ, Goate A, Kopan R (1999) A presenilin-1-dependent gamma-secretase-like protease mediates release of Notch intracellular domain. Nature 398: 518-22

Deblandre GA, Lai EC, Kintner C (2001) Xenopus neuralized is a ubiquitin ligase that interacts with XDelta1 and regulates Notch signaling. Developmental cell 1: 795-806

del Alamo D, Rouault H, Schweisguth F (2011) Mechanism and significance of cis-inhibition in Notch signalling. Current biology : CB 21: R40-7

Del Monte G, Casanova JC, Guadix JA, Macgrogan D, Burch JB, Perez-Pomares JM, de la Pompa JL (2011) Differential Notch Signaling in the Epicardium Is Required for Cardiac Inflow Development and Coronary Vessel Morphogenesis. Circulation research 108: 824-36

Del Monte G, Grego-Bessa J, Gonzalez-Rajal A, Bolos V, De La Pompa JL (2007) Monitoring Notch1 activity in development: Evidence for a feedback regulatory loop. Developmental dynamics : an official publication of the American Association of Anatomists 236: 2594-614

Devgan V, Mammucari C, Millar SE, Brisken C, Dotto GP (2005) p21WAF1/Cip1 is a negative transcriptional regulator of Wnt4 expression downstream of Notch1 activation. Genes & development 19: 1485-95

Dirkx E, Gladka MM, Philippen LE, Armand AS, Kinet V, Leptidis S, El Azzouzi H, Salic K, Bourajjaj M, da Silva GJ, Olieslagers S, van der Nagel R, de Weger R, Bitsch N, Kisters N, Seyen S, Morikawa Y, Chanoine C, Heymans S, Volders PG et al. (2013) Nfat and miR-25 cooperate to reactivate the transcription factor Hand2 in heart failure. Nat Cell Biol 15: 1282-93

Dunwoodie SL, Henrique D, Harrison SM, Beddington RS (1997) Mouse Dll3: a novel divergent Delta gene which may complement the function of other Delta homologues during early pattern formation in the mouse embryo. Development (Cambridge, England) 124: 3065-76

Eddison M, Le Roux I, Lewis J (2000) Notch signaling in the development of the inner ear: lessons from Drosophila. Proceedings of the National Academy of Sciences of the United States of America 97: 11692-9

Eisenberg LM, Markwald RR (1995) Molecular regulation of atrioventricular valvuloseptal morphogenesis. Circulation research 77: 1-6

Ellisen LW, Bird J, West DC, Soreng AL, Reynolds TC, Smith SD, Sklar J (1991) TAN-1, the human homolog of the Drosophila notch gene, is broken by chromosomal translocations in T lymphoblastic neoplasms. Cell 66: 649-61

Engberding R, Bender F (1984) Identification of a rare congenital anomaly of the myocardium by two-dimensional echocardiography: persistence of isolated myocardial sinusoids. The American journal of cardiology 53: 1733-4

Epstein JA, Aghajanian H, Singh MK (2015) Semaphorin signaling in cardiovascular development. Cell Metab 21: 163-73

Esteban V, Mendez-Barbero N, Jimenez-Borreguero LJ, Roque M, Novensa L, Garcia-Redondo AB, Salaices M, Vila L, Arbones ML, Campanero MR, Redondo JM (2011) Regulator of calcineurin 1 mediates pathological vascular wall remodeling. J Exp Med 208: 2125-39

Fernandez-Valdivia R, Takeuchi H, Samarghandi A, Lopez M, Leonardi J, Haltiwanger RS, Jafar-Nejad H (2011) Regulation of mammalian Notch signaling and embryonic development by the protein O-glucosyltransferase Rumi. Development (Cambridge, England) 138: 1925-34

Fischer A, Schumacher N, Maier M, Sendtner M, Gessler M (2004) The Notch target genes Hey1 and Hey2 are required for embryonic vascular development. Genes & development 18: 901-11

Garg V, Muth AN, Ransom JF, Schluterman MK, Barnes R, King IN, Grossfeld PD, Srivastava D (2005) Mutations in NOTCH1 cause aortic valve disease. Nature 437: 270-4

Golson ML, Le Lay J, Gao N, Bramswig N, Loomes KM, Oakey R, May CL, White P, Kaestner KH (2009) Jagged1 is a competitive inhibitor of Notch signaling in the embryonic pancreas. Mechanisms of development 126: 687-99

Grego-Bessa J, Luna-Zurita L, del Monte G, Bolos V, Melgar P, Arandilla A, Garratt AN, Zang H, Mukouyama YS, Chen H, Shou W, Ballestar E, Esteller M, Rojas A, Perez-Pomares JM, de la Pompa JL (2007) Notch signaling is essential for ventricular chamber development. Developmental cell 12: 415-29

Grieskamp T, Rudat C, Ludtke TH, Norden J, Kispert A (2011) Notch signaling regulates smooth muscle differentiation of epicardium-derived cells. Circulation research 108: 813-23

Grubb DR, Luo J, Woodcock EA (2015) Phospholipase Cbeta1b directly binds the SH3 domain of Shank3 for targeting and activation in cardiomyocytes. Biochem Biophys Res Commun 461: 519-24

Haigh JJ, Gerber HP, Ferrara N, Wagner EF (2000) Conditional inactivation of VEGF-A in areas of collagen2a1 expression results in embryonic lethality in the heterozygous state. Development (Cambridge, England) 127: 1445-53

Hambleton S, Valeyev NV, Muranyi A, Knott V, Werner JM, McMichael AJ, Handford PA, Downing AK (2004) Structural and functional properties of the human notch-1 ligand binding region. Structure (London, England : 1993) 12: 2173-83

Hartmann D, de Strooper B, Serneels L, Craessaerts K, Herreman A, Annaert W, Umans L, Lubke T, Lena Illert A, von Figura K, Saftig P (2002) The disintegrin/metalloprotease ADAM 10 is essential for Notch signalling but not for alpha-secretase activity in fibroblasts. Hum Mol Genet 11: 2615-24

Heitzler P, Bourouis M, Ruel L, Carteret C, Simpson P (1996) Genes of the Enhancer of split and achaete-scute complexes are required for a regulatory loop between Notch and Delta during lateral signalling in Drosophila. Development (Cambridge, England) 122: 161-71

Hermida-Prieto M, Monserrat L, Castro-Beiras A, Laredo R, Soler R, Peteiro J, Rodriguez E, Bouzas B, Alvarez N, Muniz J, Crespo-Leiro M (2004) Familial dilated cardiomyopathy and isolated left ventricular noncompaction associated with lamin A/C gene mutations. The American journal of cardiology 94: 50-4

Hertig CM, Kubalak SW, Wang Y, Chien KR (1999) Synergistic roles of neuregulin-1 and insulin-like growth factor-I in activation of the phosphatidylinositol 3-kinase pathway and cardiac chamber morphogenesis. The Journal of biological chemistry 274: 37362-9.

High FA, Epstein JA (2008) The multifaceted role of Notch in cardiac development and disease. Nature reviews Genetics 9: 49-61

High FA, Zhang M, Proweller A, Tu L, Parmacek MS, Pear WS, Epstein JA (2007) An essential role for Notch in neural crest during cardiovascular development and smooth muscle differentiation. The Journal of clinical investigation 117: 353-63

Huang da W, Sherman BT, Lempicki RA (2009) Systematic and integrative analysis of large gene lists using DAVID bioinformatics resources. Nature protocols 4: 44-57

Ichida F, Tsubata S, Bowles KR, Haneda N, Uese K, Miyawaki T, Dreyer WJ, Messina J, Li H, Bowles NE, Towbin JA (2001) Novel gene mutations in patients with left ventricular noncompaction or Barth syndrome. Circulation 103: 1256-63

Irvine KD, Vogt TF (1997) Dorsal-ventral signaling in limb development. Curr Opin Cell Biol 9: 867-76

Iso T, Kedes L, Hamamori Y (2003) HES and HERP families: multiple effectors of the Notch signaling pathway. J Cell Physiol 194: 237-55

Itoh M, Kim CH, Palardy G, Oda T, Jiang YJ, Maust D, Yeo SY, Lorick K, Wright GJ, Ariza-McNaughton L, Weissman AM, Lewis J, Chandrasekharappa SC, Chitnis AB (2003) Mind bomb is a ubiquitin ligase that is essential for efficient activation of Notch signaling by Delta. Developmental cell 4: 67-82

Ivins S, Chappell J, Vernay B, Suntharalingham J, Martineau A, Mohun TJ, Scambler PJ (2015) The CXCL12/CXCR4 Axis Plays a Critical Role in Coronary Artery Development. Developmental cell 33: 455-68

Jafar-Nejad H, Norga K, Bellen H (2002) Numb: "Adapting" notch for endocytosis. Developmental cell 3: 155-6

Jenni R, Oechslin E, Schneider J, Attenhofer Jost C, Kaufmann PA (2001) Echocardiographic and pathoanatomical characteristics of isolated left ventricular non-compaction: a step towards classification as a distinct cardiomyopathy. Heart 86: 666-71

Jenni R, Oechslin EN, van der Loo B (2007) Isolated ventricular non-compaction of the myocardium in adults. Heart 93: 11-5

Jiao K, Kulessa H, Tompkins K, Zhou Y, Batts L, Baldwin HS, Hogan BL (2003) An essential role of Bmp4 in the atrioventricular septation of the mouse heart. Genes & development 17: 2362-7

Johnson WE, Li C, Rabinovic A (2007) Adjusting batch effects in microarray expression data using empirical Bayes methods. Biostatistics 8: 118-27

Johnston SH, Rauskolb C, Wilson R, Prabhakaran B, Irvine KD, Vogt TF (1997) A family of mammalian Fringe genes implicated in boundary determination and the Notch pathway. Development (Cambridge, England) 124: 2245-54

Joutel A, Corpechot C, Ducros A, Vahedi K, Chabriat H, Mouton P, Alamowitch S, Domenga V, Cecillion M, Marechal E, Maciazek J, Vayssiere C, Cruaud C, Cabanis EA, Ruchoux MM,

Weissenbach J, Bach JF, Bousser MG, Tournier-Lasserve E (1996) Notch3 mutations in CADASIL, a hereditary adult-onset condition causing stroke and dementia. Nature 383: 707-10

Kanzler B, Kuschert SJ, Liu YH, Mallo M (1998) Hoxa-2 restricts the chondrogenic domain and inhibits bone formation during development of the branchial area. Development (Cambridge, England) 125: 2587-97

Kelly DF, Lake RJ, Middelkoop TC, Fan HY, Artavanis-Tsakonas S, Walz T (2010) Molecular structure and dimeric organization of the Notch extracellular domain as revealed by electron microscopy. PLoS One 5: e10532

Kelly RG, Brown NA, Buckingham ME (2001) The arterial pole of the mouse heart forms from Fgf10-expressing cells in pharyngeal mesoderm. Developmental cell 1: 435-40

Kerppola TK (2006) Design and implementation of bimolecular fluorescence complementation (BiFC) assays for the visualization of protein interactions in living cells. Nature protocols 1: 1278-86

Kisanuki YY, Hammer RE, Miyazaki J, Williams SC, Richardson JA, Yanagisawa M (2001) Tie2-Cre transgenic mice: a new model for endothelial cell-lineage analysis in vivo. Developmental biology 230: 230-42.

Klaassen S, Probst S, Oechslin E, Gerull B, Krings G, Schuler P, Greutmann M, Hurlimann D, Yegitbasi M, Pons L, Gramlich M, Drenckhahn JD, Heuser A, Berger F, Jenni R, Thierfelder L (2008) Mutations in sarcomere protein genes in left ventricular noncompaction. Circulation 117: 2893-901

Koch U, Fiorini E, Benedito R, Besseyrias V, Schuster-Gossler K, Pierres M, Manley NR, Duarte A, Macdonald HR, Radtke F (2008) Delta-like 4 is the essential, nonredundant ligand for Notch1 during thymic T cell lineage commitment. J Exp Med 205: 2515-23

Koo BK, Lim HS, Song R, Yoon MJ, Yoon KJ, Moon JS, Kim YW, Kwon MC, Yoo KW, Kong MP, Lee J, Chitnis AB, Kim CH, Kong YY (2005) Mind bomb 1 is essential for generating functional Notch ligands to activate Notch. Development (Cambridge, England) 132: 3459-70

Koo BK, Yoon MJ, Yoon KJ, Im SK, Kim YY, Kim CH, Suh PG, Jan YN, Kong YY (2007) An obligatory role of mind bomb-1 in notch signaling of mammalian development. PLoS One 2: e1221

Kopan R, Ilagan MX (2009) The canonical Notch signaling pathway: unfolding the activation mechanism. Cell 137: 216-33

Kramer R, Bucay N, Kane DJ, Martin LE, Tarpley JE, Theill LE (1996) Neuregulins with an Ig-like domain are essential for mouse myocardial and neuronal development. Proceedings of the National Academy of Sciences of the United States of America 93: 4833-8

Krantz ID, Smith R, Colliton RP, Tinkel H, Zackai EH, Piccoli DA, Goldmuntz E, Spinner NB (1999) Jagged1 mutations in patients ascertained with isolated congenital heart defects. Am J Med Genet 84: 56-60

Krebs LT, Iwai N, Nonaka S, Welsh IC, Lan Y, Jiang R, Saijoh Y, O'Brien TP, Hamada H, Gridley T (2003) Notch signaling regulates left-right asymmetry determination by inducing Nodal expression. Genes & development 17: 1207-12

Krebs LT, Shutter JR, Tanigaki K, Honjo T, Stark KL, Gridley T (2004) Haploinsufficient lethality and formation of arteriovenous malformations in Notch pathway mutants. Genes & development 18: 2469-73

Krzywinski M, Schein J, Birol I, Connors J, Gascoyne R, Horsman D, Jones SJ, Marra MA (2009) Circos: an information aesthetic for comparative genomics. Genome Res 19: 1639-45

Kurooka H, Honjo T (2000) Functional interaction between the mouse notch1 intracellular region and histone acetyltransferases PCAF and GCN5. The Journal of biological chemistry 275: 17211-20

Lai EC, Deblandre GA, Kintner C, Rubin GM (2001) Drosophila neuralized is a ubiquitin ligase that promotes the internalization and degradation of delta. Developmental cell 1: 783-94

Le Garrec JF, Ragni CV, Pop S, Dufour A, Olivo-Marin JC, Buckingham ME, Meilhac SM (2013) Quantitative analysis of polarity in 3D reveals local cell coordination in the embryonic mouse heart. Development (Cambridge, England) 140: 395-404

Leask A (2015) Getting to the heart of the matter: new insights into cardiac fibrosis. Circulation research 116: 1269-76

Lee KF, Simon H, Chen H, Bates B, Hung MC, Hauser C (1995) Requirement for neuregulin receptor erbB2 in neural and cardiac development. Nature 378: 394-8

Lewis J (1998) Notch signalling and the control of cell fate choices in vertebrates. Semin Cell Dev Biol 9: 583-9.

Li B, Dewey CN (2011) RSEM: accurate transcript quantification from RNA-Seq data with or without a reference genome. BMC Bioinformatics 12: 323

Li L, Krantz ID, Deng Y, Genin A, Banta AB, Collins CC, Qi M, Trask BJ, Kuo WL, Cochran J, Costa T, Pierpont ME, Rand EB, Piccoli DA, Hood L, Spinner NB (1997) Alagille syndrome is caused by mutations in human Jagged1, which encodes a ligand for Notch1. Nature genetics 16: 243-51.

Liao W, Bisgrove BW, Sawyer H, Hug B, Bell B, Peters K, Grunwald DJ, Stainier DY (1997) The zebrafish gene cloche acts upstream of a flk-1 homologue to regulate endothelial cell differentiation. Development (Cambridge, England) 124: 381-9

Lindsell CE, Shawber CJ, Boulter J, Weinmaster G (1995) Jagged: a mammalian ligand that activates Notch1. Cell 80: 909-17

Liu H, Chi AW, Arnett KL, Chiang MY, Xu L, Shestova O, Wang H, Li YM, Bhandoola A, Aster JC, Blacklow SC, Pear WS (2010) Notch dimerization is required for leukemogenesis and T-cell development. Genes & development 24: 2395-407

Lu FM, Lux SE (1996) Constitutively active human Notch1 binds to the transcription factor CBF1 and stimulates transcription through a promoter containing a CBF1-responsive element. Proceedings of the National Academy of Sciences of the United States of America 93: 5663-7.

Luna-Zurita L, Prados B, Grego-Bessa J, Luxan G, del Monte G, Benguria A, Adams RH, Perez-Pomares JM, de la Pompa JL (2010) Integration of a Notch-dependent mesenchymal gene program and Bmp2-driven cell invasiveness regulates murine cardiac valve formation. The Journal of clinical investigation 120: 3493-507

Luo B, Aster JC, Hasserjian RP, Kuo F, Sklar J (1997) Isolation and functional analysis of a cDNA for human Jagged2, a gene encoding a ligand for the Notch1 receptor. Mol Cell Biol 17: 6057-67

Luxan G, Casanova JC, Martinez-Poveda B, Prados B, D'Amato G, MacGrogan D, Gonzalez-Rajal A, Dobarro D, Torroja C, Martinez F, Izquierdo-Garcia JL, Fernandez-Friera L, Sabater-Molina M, Kong YY, Pizarro G, Ibanez B, Medrano C, Garcia-Pavia P, Gimeno JR, Monserrat L et al. (2013)

Mutations in the NOTCH pathway regulator MIB1 cause left ventricular noncompaction cardiomyopathy. Nature medicine 19: 193-201

Ma L, Lu MF, Schwartz RJ, Martin JF (2005) Bmp2 is essential for cardiac cushion epithelial-mesenchymal transition and myocardial patterning. Development (Cambridge, England) 132: 5601-11

Mancini SJ, Mantei N, Dumortier A, Suter U, MacDonald HR, Radtke F (2005) Jagged1-dependent Notch signaling is dispensable for hematopoietic stem cell self-renewal and differentiation. Blood 105: 2340-2

Martin M (2011) Cutadapt removes adapter sequences from high-throughput sequencing reads. EMBnetjournal 17: 10-12

Matsuno K, Ito M, Hori K, Miyashita F, Suzuki S, Kishi N, Artavanis-Tsakonas S, Okano H (2002) Involvement of a proline-rich motif and RING-H2 finger of Deltex in the regulation of Notch signaling. Development (Cambridge, England) 129: 1049-59.

McBride KL, Riley MF, Zender GA, Fitzgerald-Butt SM, Towbin JA, Belmont JW, Cole SE (2008) NOTCH1 mutations in individuals with left ventricular outflow tract malformations reduce ligand-induced signaling. Hum Mol Genet 17: 2886-93

McCright B, Lozier J, Gridley T (2002) A mouse model of Alagille syndrome: Notch2 as a genetic modifier of Jag1 haploinsufficiency. Development (Cambridge, England) 129: 1075-82

McKenzie GJ, Stevenson P, Ward G, Papadia S, Bading H, Chawla S, Privalsky M, Hardingham GE (2005) Nuclear Ca2+ and CaM kinase IV specify hormonal- and Notch-responsiveness. J Neurochem 93: 171-85

Meyer D, Birchmeier C (1995) Multiple essential functions of neuregulin in development. Nature 378: 386-90.

Mikawa T, Fischman DA (1992) Retroviral analysis of cardiac morphogenesis: discontinuous formation of coronary vessels. Proceedings of the National Academy of Sciences of the United States of America 89: 9504-8

Mikawa T, Gourdie RG (1996) Pericardial mesoderm generates a population of coronary smooth muscle cells migrating into the heart along with ingrowth of the epicardial organ. Developmental biology 174: 221-32

Miquerol L, Gertsenstein M, Harpal K, Rossant J, Nagy A (1999) Multiple developmental roles of VEGF suggested by a LacZ-tagged allele. Developmental biology 212: 307-22

Mizuhara E, Nakatani T, Minaki Y, Sakamoto Y, Ono Y, Takai Y (2005) MAGI1 recruits Dll1 to cadherin-based adherens junctions and stabilizes it on the cell surface. The Journal of biological chemistry 280: 26499-507

Mjaatvedt CH, Yamamura H, Capehart AA, Turner D, Markwald RR (1998) The Cspg2 gene, disrupted in the hdf mutant, is required for right cardiac chamber and endocardial cushion formation. Developmental biology 202: 56-66

Moloney DJ, Panin VM, Johnston SH, Chen J, Shao L, Wilson R, Wang Y, Stanley P, Irvine KD, Haltiwanger RS, Vogt TF (2000) Fringe is a glycosyltransferase that modifies Notch. Nature 406: 369-75

Moloney DJ, Shair LH, Lu FM, Xia J, Locke R, Matta KL, Haltiwanger RS (2000) Mammalian Notch1 is modified with two unusual forms of O-linked glycosylation found on epidermal growth factor-like modules. The Journal of biological chemistry 275: 9604-11

Moorman AF, Christoffels VM (2003) Cardiac chamber formation: development, genes, and evolution. Physiological reviews 83: 1223-67

Moran JL, Shifley ET, Levorse JM, Mani S, Ostmann K, Perez-Balaguer A, Walker DM, Vogt TF, Cole SE (2009) Manic fringe is not required for embryonic development, and fringe family members do not exhibit redundant functions in the axial skeleton, limb, or hindbrain. Developmental dynamics : an official publication of the American Association of Anatomists 238: 1803-12

Munch J, Gonzalez-Rajal A, de la Pompa JL (2013) Notch regulates blastema proliferation and prevents differentiation during adult zebrafish fin regeneration. Development (Cambridge, England) 140: 1402-11

Narui Y, Salaita K (2013) Membrane tethered delta activates notch and reveals a role for spatio-mechanical regulation of the signaling pathway. Biophysical journal 105: 2655-65

Neeb Z, Lajiness JD, Bolanis E, Conway SJ (2013) Cardiac outflow tract anomalies. Wiley Interdiscip Rev Dev Biol 2: 499-530

Nowotschin S, Xenopoulos P, Schrode N, Hadjantonakis AK (2013) A bright single-cell resolution live imaging reporter of Notch signaling in the mouse. BMC developmental biology 13: 15

Oda T, Elkahloun AG, Pike BL, Okajima K, Krantz ID, Genin A, Piccoli DA, Meltzer PS, Spinner NB, Collins FS, Chandrasekharappa SC, Washburn T, Schweighoffer E, Gridley T, Chang D, Fowlkes BJ, Cado D, Robey E (1997) Mutations in the human Jagged1 gene are responsible for Alagille syndrome. Nature genetics 16: 235-42. lineage decision.

Oechslin EN, Attenhofer Jost CH, Rojas JR, Kaufmann PA, Jenni R (2000) Long-term follow-up of 34 adults with isolated left ventricular noncompaction: a distinct cardiomyopathy with poor prognosis. Journal of the American College of Cardiology 36: 493-500

Oka C, Nakano T, Wakeham A, de la Pompa JL, Mori C, Sakai T, Okazaki S, Kawaichi M, Shiota K, Mak TW, Honjo T (1995) Disruption of the mouse RBP-J kappa gene results in early embryonic death. Development (Cambridge, England) 121: 3291-301

Okajima T, Irvine KD (2002) Regulation of notch signaling by o-linked fucose. Cell 111: 893-904

Okochi M, Steiner H, Fukumori A, Tanii H, Tomita T, Tanaka T, Iwatsubo T, Kudo T, Takeda M, Haass C (2002) Presenilins mediate a dual intramembranous gamma-secretase cleavage of Notch-1. EMBO J 21: 5408-16

Palomero T, Lim WK, Odom DT, Sulis ML, Real PJ, Margolin A, Barnes KC, O'Neil J, Neuberg D, Weng AP, Aster JC, Sigaux F, Soulier J, Look AT, Young RA, Califano A, Ferrando AA (2006) NOTCH1 directly regulates c-MYC and activates a feed-forward-loop transcriptional network promoting leukemic cell growth. Proceedings of the National Academy of Sciences of the United States of America 103: 18261-6

Panin VM, Papayannopoulos V, Wilson R, Irvine KD (1997) Fringe modulates Notch-ligand interactions. Nature 387: 908-12

Parks AL, Klueg KM, Stout JR, Muskavitch MA (2000) Ligand endocytosis drives receptor dissociation and activation in the Notch pathway. Development (Cambridge, England) 127: 1373-85

Patra C, van Amerongen MJ, Ghosh S, Ricciardi F, Sajjad A, Novoyatleva T, Mogha A, Monk KR, Muhlfeld C, Engel FB (2013) Organ-specific function of adhesion G protein-coupled receptor GPR126 is domain-dependent. Proceedings of the National Academy of Sciences of the United States of America 110: 16898-903

Penton AL, Leonard LD, Spinner NB (2012) Notch signaling in human development and disease. Semin Cell Dev Biol 23: 450-7

Perez-Pomares JM, Carmona R, Gonzalez-Iriarte M, Atencia G, Wessels A, Munoz-Chapuli R (2002) Origin of coronary endothelial cells from epicardial mesothelium in avian embryos. The International journal of developmental biology 46: 1005-13

Perez-Pomares JM, de la Pompa JL (2011) Signaling during epicardium and coronary vessel development. Circulation research 109: 1429-42

Petrovic J, Formosa-Jordan P, Luna-Escalante JC, Abello G, Ibanes M, Neves J, Giraldez F (2014) Ligand-dependent Notch signaling strength orchestrates lateral induction and lateral inhibition in the developing inner ear. Development (Cambridge, England) 141: 2313-24

Puente XS, Pinyol M, Quesada V, Conde L, Ordonez GR, Villamor N, Escaramis G, Jares P, Bea S, Gonzalez-Diaz M, Bassaganyas L, Baumann T, Juan M, Lopez-Guerra M, Colomer D, Tubio JM, Lopez C, Navarro A, Tornador C, Aymerich M et al. (2011) Whole-genome sequencing identifies recurrent mutations in chronic lymphocytic leukaemia. Nature 475: 101-5

Pursglove SE, Mackay JP (2005) CSL: a notch above the rest. Int J Biochem Cell Biol 37: 2472-7

Radtke F, Wilson A, Stark G, Bauer M, van Meerwijk J, MacDonald HR, Aguet M (1999) Deficient T cell fate specification in mice with an induced inactivation of Notch1. Immunity 10: 547-58

Rampal R, Arboleda-Velasquez JF, Nita-Lazar A, Kosik KS, Haltiwanger RS (2005) HIGHLY CONSERVED O-FUCOSE SITES HAVE DISTINCT EFFECTS ON NOTCH1 FUNCTION. The Journal of biological chemistry 280: 32133-32140

Red-Horse K, Ueno H, Weissman IL, Krasnow MA (2010) Coronary arteries form by developmental reprogramming of venous cells. Nature 464: 549-53

Ritter M, Oechslin E, Sutsch G, Attenhofer C, Schneider J, Jenni R (1997) Isolated noncompaction of the myocardium in adults. Mayo Clin Proc 72: 26-31

Rivera-Feliciano J, Tabin CJ (2006) Bmp2 instructs cardiac progenitors to form the heart-valve-inducing field. Developmental biology 295: 580-8

Robinson MD, McCarthy DJ, Smyth GK (2010) edgeR: a Bioconductor package for differential expression analysis of digital gene expression data. Bioinformatics (Oxford, England) 26: 139-40

Ruiz-Villalba A, Perez-Pomares JM (2012) The expanding role of the epicardium and epicardial-derived cells in cardiac development and disease. Current opinion in pediatrics 24: 569-76

Rutenberg JB, Fischer A, Jia H, Gessler M, Zhong TP, Mercola M (2006) Developmental patterning of the cardiac atrioventricular canal by Notch and Hairy-related transcription factors. Development (Cambridge, England) 133: 4381-90

Sahlgren C, Gustafsson MV, Jin S, Poellinger L, Lendahl U (2008) Notch signaling mediates hypoxia-induced tumor cell migration and invasion. Proceedings of the National Academy of Sciences of the United States of America 105: 6392-7

Sedmera D, Pexieder T, Vuillemin M, Thompson RP, Anderson RH (2000) Developmental patterning of the myocardium. The Anatomical record 258: 319-37

Shalaby F, Rossant J, Yamaguchi TP, Gertsenstein M, Wu XF, Breitman ML, Schuh AC (1995) Failure of blood-island formation and vasculogenesis in Flk-1-deficient mice. Nature 376: 62-6

Shawber C, Boulter J, Lindsell CE, Weinmaster G (1996) Jagged2: a serrate-like gene expressed during rat embryogenesis. Developmental biology 180: 370-6

Shi S, Stanley P (2003) Protein O-fucosyltransferase 1 is an essential component of Notch signaling pathways. Proceedings of the National Academy of Sciences of the United States of America 100: 5234-9

Shou W, Aghdasi B, Armstrong DL, Guo Q, Bao S, Charng MJ, Mathews LM, Schneider MD, Hamilton SL, Matzuk MM (1998) Cardiac defects and altered ryanodine receptor function in mice lacking FKBP12. Nature 391: 489-92

Shutter JR, Scully S, Fan W, Richards WG, Kitajewski J, Deblandre GA, Kintner CR, Stark KL (2000) Dll4, a novel Notch ligand expressed in arterial endothelium. Genes & development 14: 1313-8.

Soriano P (1999) Generalized lacZ expression with the ROSA26 Cre reporter strain. Nature genetics 21: 70-1

Soufan AT, van den Berg G, Ruijter JM, de Boer PA, van den Hoff MJ, Moorman AF (2006) Regionalized sequence of myocardial cell growth and proliferation characterizes early chamber formation. Circulation research 99: 545-52

Srinivas S, Watanabe T, Lin CS, William CM, Tanabe Y, Jessell TM, Costantini F (2001) Cre reporter strains produced by targeted insertion of EYFP and ECFP into the ROSA26 locus. BMC developmental biology 1: 4

Stainier DY, Weinstein BM, Detrich HW, 3rd, Zon LI, Fishman MC (1995) Cloche, an early acting zebrafish gene, is required by both the endothelial and hematopoietic lineages. Development (Cambridge, England) 121: 3141-50

Stankunas K, Hang CT, Tsun ZY, Chen H, Lee NV, Wu JI, Shang C, Bayle JH, Shou W, Iruela-Arispe ML, Chang CP (2008) Endocardial Brg1 represses ADAMTS1 to maintain the microenvironment for myocardial morphogenesis. Developmental cell 14: 298-311

Staudt DW, Liu J, Thorn KS, Stuurman N, Liebling M, Stainier DY (2014) High-resolution imaging of cardiomyocyte behavior reveals two distinct steps in ventricular trabeculation. Development (Cambridge, England) 141: 585-93

Stollberger C, Finsterer J (2004) Left ventricular hypertrabeculation/noncompaction-don't forget the myologist!Concerning the article "Isolated myocardial noncompaction als seltene Ursache einer Synkope im Kindesalter" by Binz G. et al. Z Kardiol 92:1039-1044 (2003). Zeitschrift fur Kardiologie 93: 242-3; author reply 243-4

Sturn A, Quackenbush J, Trajanoski Z (2002) Genesis: cluster analysis of microarray data. Bioinformatics (Oxford, England) 18: 207-8

Sugishita Y, Takahashi T, Shimizu T, Yao A, Kinugawa K, Sugishita K, Harada K, Matsui H, Nagai R (2000) Expression of genes encoding vascular endothelial growth factor and its Flk-1 receptor in the chick embryonic heart. Journal of molecular and cellular cardiology 32: 1039-51

Tamura K, Taniguchi Y, Minoguchi S, Sakai T, Tun T, Furukawa T, Honjo T (1995) Physical interaction between a novel domain of the receptor Notch and the transcription factor RBP-J kappa/Su(H). Current biology : CB 5: 1416-23

Tanigaki K, Honjo T (2007) Regulation of lymphocyte development by Notch signaling. Nat Immunol 8: 451-6

Taylor P, Takeuchi H, Sheppard D, Chillakuri C, Lea SM, Haltiwanger RS, Handford PA (2014) Fringe-mediated extension of O-linked fucose in the ligand-binding region of Notch1 increases binding to mammalian Notch ligands. Proceedings of the National Academy of Sciences of the United States of America 111: 7290-5

Tian X, Hu T, Zhang H, He L, Huang X, Liu Q, Yu W, He L, Yang Z, Zhang Z, Zhong TP, Yang X, Yang Z, Yan Y, Baldini A, Sun Y, Lu J, Schwartz RJ, Evans SM, Gittenberger-de Groot AC et al. (2013) Subepicardial endothelial cells invade the embryonic ventricle wall to form coronary arteries. Cell research 23: 1075-90

Tian X, Pu WT, Zhou B (2015) Cellular origin and developmental program of coronary angiogenesis. Circulation research 116: 515-30

Timmerman LA, Grego-Bessa J, Raya A, Bertran E, Perez-Pomares JM, Diez J, Aranda S, Palomo S, McCormick F, Izpisua-Belmonte JC, de la Pompa JL (2004) Notch promotes epithelial-mesenchymal transition during cardiac development and oncogenic transformation. Genes & development 18: 99-115

Toyofuku T, Zhang H, Kumanogoh A, Takegahara N, Yabuki M, Harada K, Hori M, Kikutani H (2004) Guidance of myocardial patterning in cardiac development by Sema6D reverse signalling. Nat Cell Biol 6: 1204-11

Van de Walle I, De Smet G, Gartner M, De Smedt M, Waegemans E, Vandekerckhove B, Leclercq G, Plum J, Aster JC, Bernstein ID, Guidos CJ, Kyewski B, Taghon T (2011) Jagged2 acts as a Delta-like Notch ligand during early hematopoietic cell fate decisions. Blood 117: 4449-59

van de Weijer T, van Ewijk PA, Zandbergen HR, Slenter JM, Kessels AG, Wildberger JE, Hesselink MK, Schrauwen P, Schrauwen-Hinderling VB, Kooi ME (2012) Geometrical models for cardiac MRI in rodents: comparison of quantification of left ventricular volumes and function by various geometrical models with a full-volume MRI data set in rodents. Am J Physiol Heart Circ Physiol 302: H709-15

van den Akker NM, Molin DG, Peters PP, Maas S, Wisse LJ, van Brempt R, van Munsteren CJ, Bartelings MM, Poelmann RE, Carmeliet P, Gittenberger-de Groot AC (2007) Tetralogy of fallot and alterations in vascular endothelial growth factor-A signaling and notch signaling in mouse embryos solely expressing the VEGF120 isoform. Circulation research 100: 842-9

Wallberg AE, Pedersen K, Lendahl U, Roeder RG (2002) p300 and PCAF act cooperatively to mediate transcriptional activation from chromatin templates by notch intracellular domains in vitro. Mol Cell Biol 22: 7812-9

Waller-Evans H, Promel S, Langenhan T, Dixon J, Zahn D, Colledge WH, Doran J, Carlton MB, Davies B, Aparicio SA, Grosse J, Russ AP (2010) The orphan adhesion-GPCR GPR126 is required for embryonic development in the mouse. PLoS One 5: e14047

Walter W, Sanchez-Cabo F, Ricote M (2015) GOplot: an R package for visually combining expression data with functional analysis. Bioinformatics (Oxford, England) 31: 2912-4

Wang Y, Nakayama M, Pitulescu ME, Schmidt TS, Bochenek ML, Sakakibara A, Adams S, Davy A, Deutsch U, Luthi U, Barberis A, Benjamin LE, Makinen T, Nobes CD, Adams RH (2010) Ephrin-B2 controls VEGF-induced angiogenesis and lymphangiogenesis. Nature 465: 483-6

Wang Y, Wu B, Chamberlain AA, Lui W, Koirala P, Susztak K, Klein D, Taylor V, Zhou B (2013) Endocardial to myocardial notch-wnt-bmp axis regulates early heart valve development. PLoS One 8: e60244

Watanabe T, Koibuchi N, Chin MT (2010) Transcription factor CHF1/Hey2 regulates coronary vascular maturation. Mechanisms of development 127: 418-27

Watanabe Y, Kokubo H, Miyagawa-Tomita S, Endo M, Igarashi K, Aisaki KI, Kanno J, Saga Y (2006) Activation of Notch1 signaling in cardiogenic mesoderm induces abnormal heart morphogenesis in mouse. Development (Cambridge, England) 133: 1625-34

Weng AP, Ferrando AA, Lee W, Morris JPt, Silverman LB, Sanchez-Irizarry C, Blacklow SC, Look AT, Aster JC (2004) Activating mutations of NOTCH1 in human T cell acute lymphoblastic leukemia. Science (New York, NY) 306: 269-71

Weng AP, Millholland JM, Yashiro-Ohtani Y, Arcangeli ML, Lau A, Wai C, Del Bianco C, Rodriguez CG, Sai H, Tobias J, Li Y, Wolfe MS, Shachaf C, Felsher D, Blacklow SC, Pear WS, Aster JC (2006) c-Myc is an important direct target of Notch1 in T-cell acute lymphoblastic leukemia/lymphoma. Genes & development 20: 2096-109

Wu B, Zhang Z, Lui W, Chen X, Wang Y, Chamberlain AA, Moreno-Rodriguez RA, Markwald RR, O'Rourke BP, Sharp DJ, Zheng D, Lenz J, Baldwin HS, Chang CP, Zhou B (2012) Endocardial cells form the coronary arteries by angiogenesis through myocardial-endocardial VEGF signaling. Cell 151: 1083-96

Wu L, Aster JC, Blacklow SC, Lake R, Artavanis-Tsakonas S, Griffin JD (2000) MAML1, a human homologue of Drosophila mastermind, is a transcriptional co-activator for NOTCH receptors. Nature genetics 26: 484-9.

Xin M, Olson EN, Bassel-Duby R (2013) Mending broken hearts: cardiac development as a basis for adult heart regeneration and repair. Nature reviews Molecular cell biology 14: 529-41

Xu J, Krebs LT, Gridley T (2010) Generation of mice with a conditional null allele of the Jagged2 gene. Genesis 48: 390-3

Yang J, Bucker S, Jungblut B, Bottger T, Cinnamon Y, Tchorz J, Muller M, Bettler B, Harvey R, Sun QY, Schneider A, Braun T (2012) Inhibition of Notch2 by Numb/Numblike controls myocardial compaction in the heart. Cardiovasc Res 96: 276-85

Yang LT, Nichols JT, Yao C, Manilay JO, Robey EA, Weinmaster G (2005) Fringe glycosyltransferases differentially modulate Notch1 proteolysis induced by Delta1 and Jagged1. Mol Biol Cell 16: 927-42

Zaffran S, Kelly RG, Meilhac SM, Buckingham ME, Brown NA (2004) Right ventricular myocardium derives from the anterior heart field. Circulation research 95: 261-8

Supplementary Information

Video Legends

Video 1. Imaris 3D reconstruction of whole-mount stained E9.5 *CBF1:2HB-Venus* heart. The myocardial surface in red was built from the SMA staining. Venus (white nuclei), revealing Notch activity in CD31/Pecam1-positive cells (green), can be observed in the ventricular endocardium. Nuclei are counterstained with DAPI.

Video 2. Representative Z-stack of CMRI short axis views of hearts from 6-month-old WT and *Jag1^{flox};cTnT-Cre* mice. The mutant heart exhibits dilated ventricles and a thinner septum than the WT heart.

Video 3. Representative M-mode echocardiography analysis of the hearts of 6-month-old WT and *Jag1^{flox};cTnT-Cre* mice. The mutant heart shows contraction defects.

Video 4. Representative Z-stack of CMRI short axis views of hearts from 6-month-old WT and *Jag1^{flox};cTnT-Cre* mice. The mutant heart exhibits a remarked segmental dyskinesia in the RV free wall.

Video 5. Docking between the Notch1 extracellular domain homodimer (NECD, green and cyan) and Dll4 (yellow), Jag1 (orange) and Jag1 and Jag2 (gray).

Supplementary Table Legend

Supplementary Table 1. Excel file containing the list of deregulated genes identified by RNA-seq analysis (upregulated genes in red and downregulated genes in green). E9.5 *Dll4^{flox};Tie2-Cre* (sheet 1); E9.5 *Dll4^{flox};Nfat-Cre* (sheet 2); E9.5 *Notch1^{flox};Nfat-Cre* (sheet 3). 144 common deregulated genes from E9.5 *Dll4^{flox};Tie2-Cre, Dll4^{flox};Nfat-Cre* and *Notch1^{flox};Nfat-Cre* listed by the log fold change (logFC) of the *Dll4^{flox};Tie2-Cre* (sheet 4, related to Fig. 1k). E15.5 *Jag1^{flox};cTnT–Cre* (sheet 5); E15.5 *Jag2^{flox};cTnT–Cre* (sheet 6); E15.5 *Jag1^{flox};Jag2flox;cTnT–Cre* (sheet 7); E15.5 *MFng^{GOF};Tie2–Cre* (sheet 8). Combined analysis of E15.5 *Jag1^{flox};cTnT–Cre, Jag2^{flox};cTnT–Cre* and *Jag1^{flox};Jag2flox;cTnT–Cre* with batch correction; deregulated genes are organized according to the logFC of the *Jag1^{flox};Jag2flox;cTnT–Cre* (sheet 9). Genes represented in the circular plot of *Dll4^{flox}* and *Notch1^{flox}* mutants (sheet 11, related to Fig. 1l); genes represented in the circular plot of *Jag1^{flox};cTnT –Cre* mutants (sheet 12, related to Fig. 3b); logFC of the 319 genes shown in the heat map of Figure 7c (sheet 13).

Cover Page. Whole-mount two-photon microscopy image of an E9.5 *MFng*^{tg}*;Tie2-Cre* embryo showing MFng-GFP expression in endocardium.

Back Cover. E16.5 *MFng*^{tg}*;Tie2-Cre* heart sections stained with N1ICD (red nuclei). Myocardium was counterstained with cardiac Troponin T antiboby (blue) and endocardium with endomucin (green). Ectopic expression of *MFng* in the endocardium impairs myocardial Jag1-Jag2 signaling to Notch1 (red nuclei), inducing a severe Left Ventricular Non Compaction (LVNC) phenotype.

Your theory is crazy, but it's not crazy enough to be true.

Niels Bohr

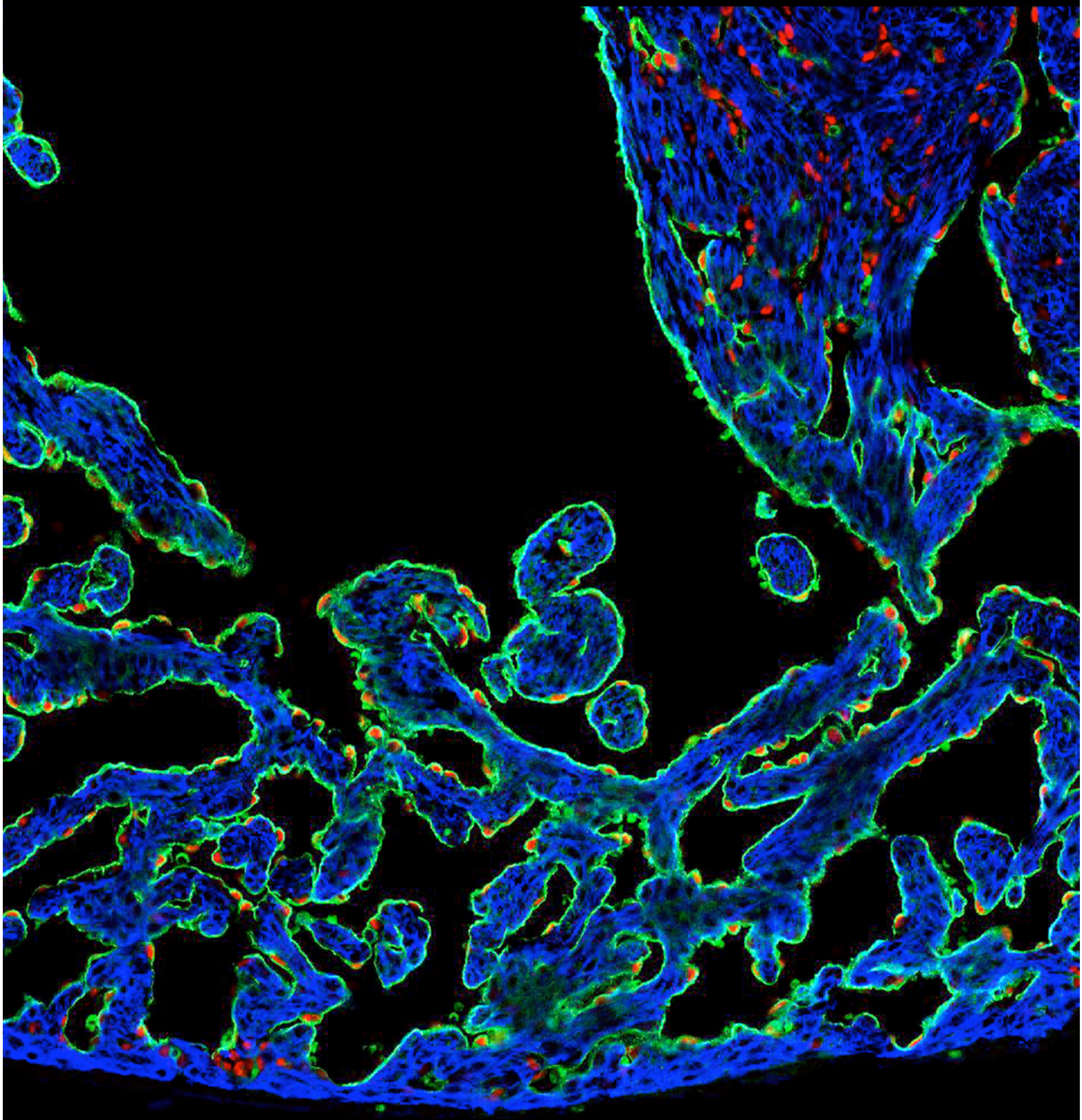

UAM UNIVERSIDAD AUTONOMA DE MADRID

cnic